THESIS FOR THE DEGREE OF LICENTIATE OF ENGINEERING

DC Distribution Systems

DANIEL NILSSON

Division of Electric Power Engineering
Department of Energy and Environment
CHALMERS UNIVERSITY OF TECHNOLOGY
Göteborg, Sweden 2005

DC Distribution Systems
DANIEL NILSSON

Technical Report at Chalmers University of Technology

Division of Electric Power Engineering
Department of Energy and Environment
Chalmers University of Technology
SE-412 96 Göteborg
Sweden
Telephone + 46 (0)31-772 1000

Chalmers Bibliotek, Reproservice
Göteborg, Sweden 2005

DC Distribution Systems
DANIEL NILSSON
Division of Electric Power Engineering
Department of Energy and Environment
Chalmers University of Technology

Abstract

In this thesis, the use of direct current for low-voltage distribution systems is investigated. Current trends in the electric power consumption indicate an increasing use of dc in end-user equipment, like computers and other electronic appliances used in households and offices, and in larger equipment used in the industry. With a dc distribution system, power conversion within the appliance can be avoided, and losses reduced. The ac/dc conversion is centralized, and by using a fully controllable power-electronic interface, high power quality for both the ac and the dc system during steady state and ac grid disturbances can be obtained. Connection of back-up energy storage and small-size generation is also easier to realize in a dc system.

To facilitate practical application, it is important that the shift from ac to dc distribution can be done with minimal changes. Results from measurements carried out on common household appliances reported in this thesis show that most loads are able to operate with dc supply without any modifications. Furthermore, the measurements are used to derive simple, yet sufficiently accurate, load models. These are used for further analysis of the dc system, both in steady state and during transients, by using the simulation software PSCAD/EMTDC.

To provide a high-quality interface between the ac and dc system, which also allows bi-directional power flow, a Voltage Source Converter (VSC) in series with a Buck converter is proposed, both with controllable output voltages. Three different controllers for the VSC output voltage are implemented and tested both in simulations and through experiments on a small laboratory system rated at 3 kVA. The effect of different capacitor sizes, bandwidths of the controllers and load types is studied. The main conclusion is that the best performance is shown by the energy-balance dc-link-voltage controller, which only relies on measuring the dc-link voltage.

In the laboratory setup, the proposed ac/dc interface is used to supply a small dc system with four loads, representing a typical office. The system is compared with an identical system supplied with ac, both during steady state and ac grid faults. Measurements show that the dc system with the proposed interface improves the power quality by balancing the three ac phase currents and removing low-order harmonics, otherwise present in the current when the loads are supplied with ac. During grid faults, the output dc voltage is maintained quite constant and the loads are not affected by the disturbance. This test setup proves that a dc system for low-voltage installations is entirely feasible and can be preferred to a conventional, 50-Hz ac system in applications where many electronic loads are used, high reliability and power quality are desired, and/or low magnetic fields are required.

Keywords: direct current (dc), ac/dc interface, Buck converter, current control, distribution systems, load modeling, power electronics, voltage control, voltage source converter (vsc).

Acknowledgements

This research project has been carried out at the Department of Energy and Environment at Chalmers University of Technology. This work has been carried out within Elektra Project no. 3395 and has been financed by Elforsk, Swedish National Energy Agency and ABB Corporate Research. The financial support is gratefully acknowledged.

I would like to thank my supervisor Dr. Ambra Sannino for all the nice discussions and all the help during this work. Especially the guidance on how to be a perfect conference delegate.

I would also like to thank my examiner Prof. Jaap Daalder.

The members of the reference group Ingemar Andersson (Göteborg Energi), Anders Lasson (Volvo), Michael Lindgren (ABB), Johan Swahn (Chalmers) and John Åkerlund (UPN) are acknowledged. Thanks for all your comments on the work.

For all the discussions and help I would like to thank Massimo Bongiorno, Stefan Lundberg, Andreas Petersson and Oskar Wallmark. Robert Karlsson and Magnus Ellsén I would like to thank for the support with the laboratory work. For the nice working environment I would like to thank the staff at Elteknik.

I would like to thank my family for their support and love during all these years I have been a student at Chalmers.

Finally, I would like to express my deepest gratitude to Lina for her love and understanding.

Table of Contents

Chapter 1

Introduction

1.1 Background and Motivation

Recent developments and trends in the electric power consumption clearly indicate an increasing use of dc in end-user equipment. Computers, TVs, and other electronic-based apparatus use low-voltage dc obtained by means of a single-phase rectifier followed by a dc voltage regulator. In factories, the same input stage is used for process-control equipment, while directly-fed ac machines have been replaced by ac drives that include a two-stage conversion process. Electrical energy production from renewable sources is at dc (as in photovoltaic systems [1] and fuel cells [2]) or requires a similar two-stage conversion as in ac drives, e.g. variable-speed wind turbines and natural-gas microturbines. By using dc for distribution systems it would thus be possible to skip one stage in the conversion in all these cases, with consequent savings and higher reliability due to a decreased number of components. Moreover, energy delivery at dc is characterized by lower losses and voltage drops in lines.

A dc distribution system also allows direct connection of battery blocks for back-up energy storage. The latter is often needed for avoiding supply interruptions in hospitals or big office buildings or in industrial complexes with high power quality demands and is presently implemented with Uninterruptible Power Supply (UPS) systems using two conversions (from ac to dc and back). A direct connection to a dc network would thus save two conversions in this case.

Another advantage of removing the conversion stage in the single pieces of equipment is that the low-quality EMC problems caused by the conversion equipment, e.g. harmonic pollution, are also removed. One could argue that the problem is only moved somewhere else, i.e. at the interface between the supplying ac network and the low-voltage dc network, where centralized power conversion is needed. However, as there are only one (or a few) supplying points in such a system, the converter interface can be made more sophisticated in order to achieve a high power quality. The design and verification of this power-electronic interface is one of the aims of this thesis. In steady state, it should absorb sinusoidal grid currents to have a high power quality. Moreover, it should be able to maintain a stable dc voltage during load variations on the dc system and disturbances on the ac system. The latter is to prevent that sensitive loads, e.g. computers, trip in case of an ac fault. Finally, in larger dc systems with local power generation, the interface should allow bi-directional power flow to inject the surplus power into the ac system during periods of high generation and low consumption in the dc system.

Designing a dc distribution system means also dealing with issues, like the choice of voltage level, voltage regulation and transformation, system protection and electrical safety, well-established in ac power systems, but little practice exists for dc systems. This in turn requires analysis tools for dc systems, among others models for steady-state and transient simulations of different operating conditions. Existing standards for short circuit calculations of dc systems, e.g. IEC 61600 [3] and IEEE Std. 946 [4], describe how to model the components in the system. However, these standards, which are intended for application to auxiliary systems in plants and power stations, which often are dc-based battery systems, give simple models that are not adequate for detailed transient studies. Furthermore, a number of modern loads, which are common in today's homes and offices, are not covered. To study dc systems, an effort is clearly needed in the field of analysis tools for dc system analysis.

1.2 Aim and Outline of the Thesis

The aim of the thesis is to design a high-quality dc distribution system for low-voltage applications. The emphasis is on system modeling and on the design of the power electronic interface with the ac system. The thesis starts with an overview in Chapter 2 of dc systems used today and their design .

Many of the existing loads today can be supplied with dc without any modification. A study in Chapter 3 presents that common loads can be supplied with dc and for what voltage range. This is a key issue regarding the selection of a system voltage level. To model the steady-state characteristic of the loads and their transient behavior, different tests were carried out. The study resulted in steady-state and transient models for the loads operating with dc voltage.

The design and control of an ac/dc interface is presented in Chapter 4 and 5 together with simulation and measurement results. In this project, an interface consisting of a Voltage Source Converter (VSC) in series with a Buck converter was chosen. Chapter 4 deals with the three-phase two-level VSC, and Chapter 5 with the VSC in series with a Buck converter. The performance of the interface during different load conditions on the dc side and different disturbances on the ac system has been evaluated, together with different control strategies.

The last part of the project was to build a small dc network and supply using an ac/dc interface. A small system with four loads representing a small office was tested both during steady state and during ac faults. The performance of the system was compared with the result when the loads were supplied directly with ac. The laboratory setup and the measurement results are presented in Chapter 6.

1.3 List of Publications

Some of the results of this work have been presented in the following publications:

1. D. Nilsson and A. Sannino, "Efficiency Analysis of Low- and Medium-Voltage dc Systems," in Proc. *IEEE Power Engineering Soc. General Meeting*, vol. 2, 2004, pp. 2315-2321.

2. D. Nilsson and A. Sannino, "Load Modelling for Steady-State and Transient Analysis of Low-Voltage dc Systems," in *Conf. Rec. IEEE-IAS Annu. Meeting*, vol. 2, 2004, pp. 774-780.

Chapter 2

DC Distribution Systems

The first electric power distribution system was built and tested at the end of the 19^{th} century. After that the electrification of the cities began and many distribution systems were built around the world. DC systems were dominating in the beginning and it took some years before ac came strong and replaced the dc systems. The last dc distribution systems in Sweden were closed in the 1970's, but dc systems can still be found in special applications. In this chapter a historical background to the "battle of the currents" is given as an introduction. An overview of existing dc systems used in special applications are also presented, with their pros and cons. Finally, the ideas around a future dc distribution system and how it can be built up are presented.

2.1 Historical Background

In the end of the 19^{th} century, the "battle of the currents" between Thomas Alva Edison and George Westinghouse took place [5]. Edison worked with direct current (dc) systems, and Westinghouse with alternating current (ac) systems. Who won the fight everybody knows, but is ac still the right choice for the 21^{st} century?

When the battle began, cities were illuminated by gas or arc light powered by dc dynamos. The arc light was produced between two carbon tips and gave a glaring light with an open flame and noxious fumes, and the tips needed periodically to be renewed. The arc light was suitable for streets and in large indoor places like train stations and factories.

Edison saw a possibility to replace the arc lighting with incandescent lamps. The problem of finding a suitable filament was solved when Edison with some ideas from Joseph Swan made the carbonized cotton filament burn for more than 13 hours. Edison and his team developed dc dynamos with constant voltage output, meters, lamp sockets, switching equipment and fuses. The first incandescent lighting system with a central dc generating station was demonstrated at Holborn Viaduct in London, England, beginning in January 1882. The more known Pearl Street Station in New York began in September 1882. The success resulted in many installed systems in cities across the continent. Edison's lighting systems had some drawbacks. They were operated with low-voltage dc, 100 or 110 V, which resulted in small isolated systems to reduce the losses. A big system would have resulted in a large amount of copper.

In 1881 the first ac system was demonstrated in London by Lucien Gaulard and John Gibbs. Westinghouse took the ideas back with him to the U.S., and William Stanley im-

proved the design. In 1886 the Westinghouse Electric Company had designed equipment for an ac lighting system. In 1887 Nikola Tesla filed for seven U.S. patents in the field of polyphase ac motors, power transmission, generators, transformers and lighting. Westinghouse purchased these patents, and employed Tesla to develop the ac system. In 1891 Westinghouse made history by setting up a 13 mile long transmission line. And many more would follow [6, 7].

At that time an ac system was a proper choice. The loads were mainly incandescent lamps and machines, and the possibility to transform the voltage from one level to another made ac suitable for transmitting electric power over long distances. Also ac machines could be made more robust with less maintenance compared with dc machines.

2.2 Existing DC Systems

DC systems can today be found in special applications. It is of interest to investigate where dc systems can be found and how dc is used before presenting a future dc distribution system. Focus of this part are high power dc systems, and key issues like grid design, operating voltage level, voltage control, energy storage, grounding and protection.

2.2.1 Telecommunication

The telecommunication system uses a low-voltage dc power system, and it was developed when the centralized battery system was built. The nominal voltage of the system is -48 V with the anode connected to ground. The dc system is supplied from the ac mains via voltage controlled rectifiers. The system uses transient limiting distribution, i.e. high impedance distribution, to limit the fault current in case of a short circuit, and to maintain the non-faulted equipment in operation. Battery back-up is installed to supply the system if a disturbance occurs on the ac mains. The size of the batteries are 3 to 8 hours of operation [8]. It is also possible to have standby generation, e.g. a diesel engine, connected to the system, which can be started if the duration of the fault is long. In the beginning the telecommunication system was using copper wire to distribute the phone calls. Today almost all backbone communication is going through optical wires. The equipment inside the stations is computer based and consumes high power. Since the system is using low voltage the currents become very high, and studies have therefore been carried out to investigate usage of a higher voltage level to reduce the currents [9–11]. A typical telecommunication power system is shown in Fig. 2.1.

2.2.2 Vehicles and Ships

High power dc systems are also used in vehicles and ships which have electric propulsion. The basic idea of hybrid electric vehicles (HEV) is to run the internal combustion engine with small power variation to minimize to environmental effects. Instead the power variations can be taken from the electric system. When the car accelerates, power to the wheels is supplied by the electric machines, and when the car decelerates the electric power generated is stored in batteries. The electric power is also used to supply the loads in the car. The system must handle high power, and a high voltage dc system is required, where a 300 V system is suited for full hybrid vehicles [12]. The power system of the HEV consists of

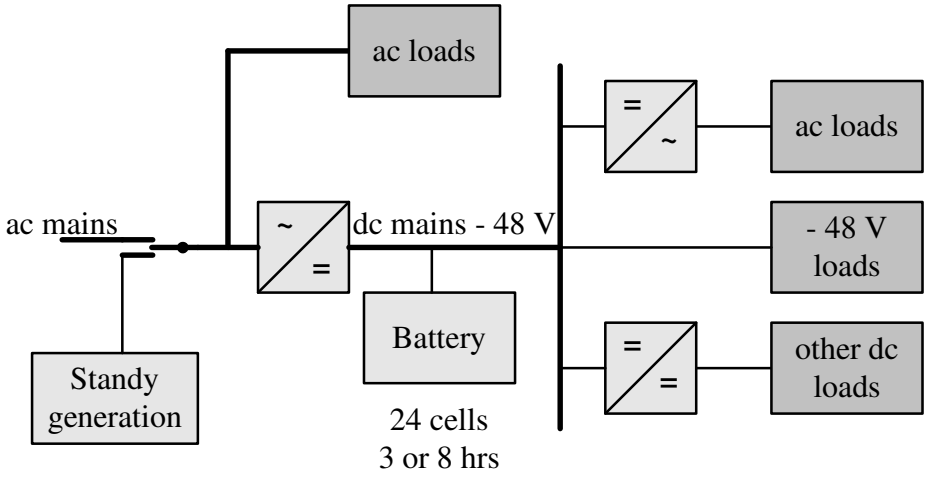

Fig. 2.1. Layout of distribution system for telecommunication.

starter/generator (engine), electric machine with associated converter, energy storage (battery or supercaps) with associated chargers, converters to adjust high voltage to required load voltage, see Fig. 2.2 [13–15].

Ships can also use an electric propulsion system [16]. The electric power is generated by diesel engines, and used for supplying electric loads and the electric machines used for propulsion. The electric system uses both ac or dc depending on the application [17]. Naval ships and submarines use also other types of power sources like stirling machines or nuclear power, which can be used underwater. Eliminating the mechanical link between the power plant and the propulsor will enable reduction of noise and vibrations, which is important to minimize the risk of detection [18–20].

2.2.3 Traction

DC has been used for a long time in traction systems, and the reason is because dc machines are very easy to speed control by simply changing the series resistance. The traction power system is supplied from the ac systems via six, 12 or 24-pulse rectifiers depending on the configuration [21]. A higher number will reduce the current ripple. Standard voltages are 600 or 750 V for urban metros and 1.5 up to 3 kV for regional systems [22]. The power is supplied to the train through a conductor rail laid on insulators on one side of the running rail, or through an overhead catenary. The return path is usually the grounded tracks. The dc power systems is protected by circuit breakers controlled by relays which will trip the breakers in case of overcurrent, ground fault and short circuits. Today ac machines are more used than dc machines due to less maintenance, and this requires inverters which are very convenient to supply with dc. AC is more economical to use for high-speed trains, which consume high power.

2.2.4 HVDC

High Voltage DC (HVDC) is a technique to transmit electric power using dc voltage instead of ac voltage. HVDC makes it possible to transmit power over a long distance or using underground cable. The absence of reactive power decreases the losses. Another advantage with HVDC is that two ac systems with different frequency can be connected. The

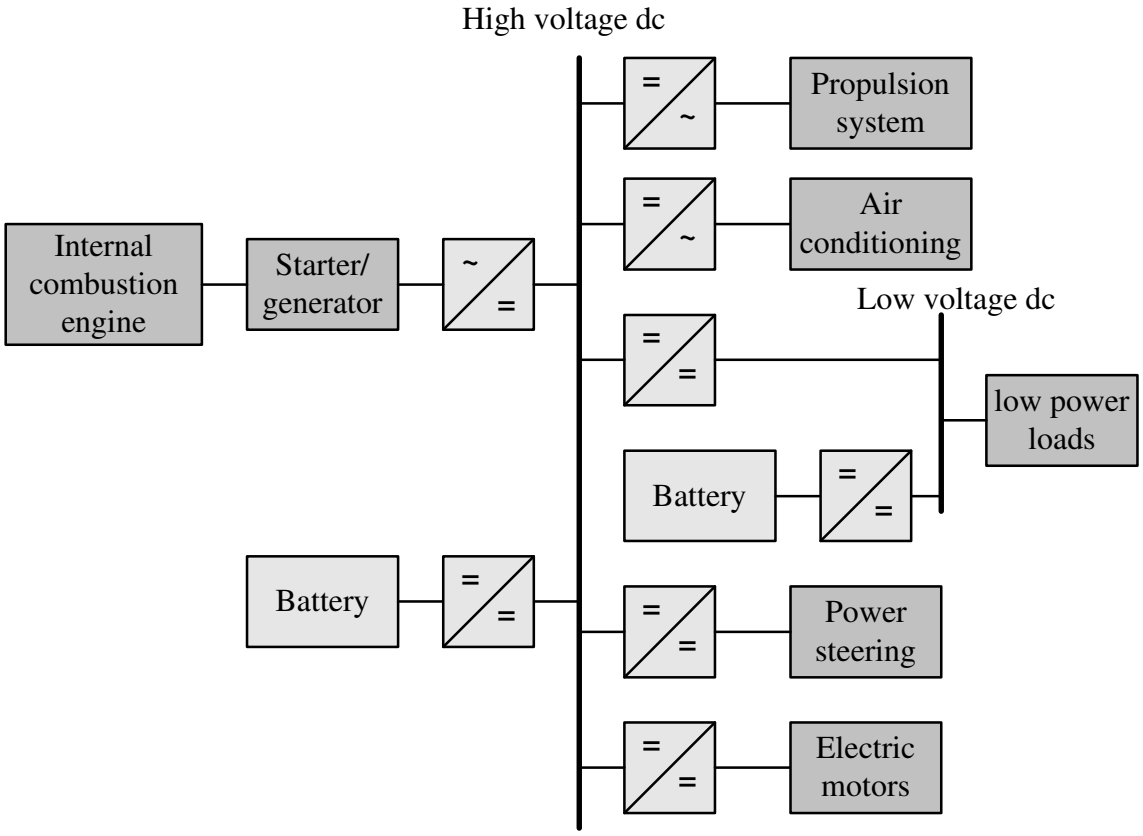

Fig. 2.2. Layout of hybrid electrical vehicle power system.

rectifier/inverter stations are using thyristors or IGBT's depending on the installation.

The thyristor based rectifier/inverter operates as a Current Source Converter (CSC), which is a line-commutated converter [23]. The CSC needs an ac voltage provided by the grid to operate. HVDC with CSC is used for high voltage, high power transmission. The dc-link voltage is determined by the transmitted power, and the polarity of the dc-link is changing with the direction of the power. Since the CSC is line-commutated there will be low-frequency harmonics present. These can be removed by using transformers, which will increase the pulse number from 6 up to 12 or 24, and tuned filters. A HVDC system with CSC has an operating dc-link voltage up to 1200 kV, and special dc circuit breakers must be used [24].

The more expensive IGBT-based rectifier/inverter operates as a VSC, which is a self-commutated converter with controllable voltage magnitude, frequency and phase. The VSC produces only current harmonics at multiples of the switching frequency and its side band, and they are easy to filter. The consumed active and reactive power of the converter can be controlled individually at both ends of the HVDC link. A HVDC system with VSC has an operating dc-link voltage ranging from 20 to 300 kV. The IGBT-based HVDC can be used for black start operation, which is not possible for the thyristor-based HVDC [23, 25]. A scheme of a HVDC system connected between two ac systems is shown in Fig. 2.3.

2.3 Low-Voltage DC Distribution System

The type of loads used in a power system today are very different from the loads used 100 years ago, when resistive loads and machines were dominating. The fast development of

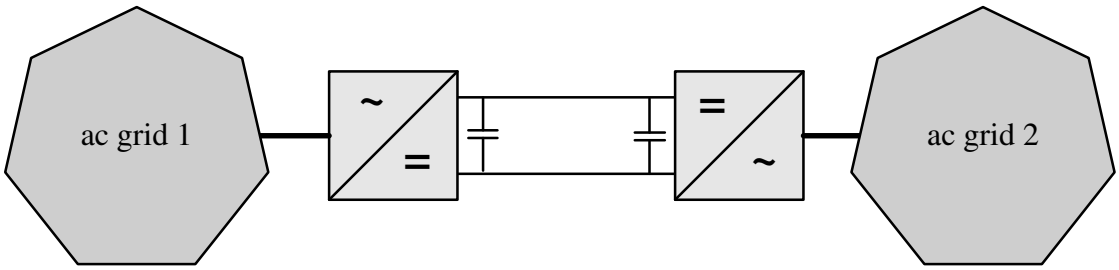

Fig. 2.3. Layout of HVDC system.

semiconductors make the power electronic loads dominate today, which are using a different voltage than the supplying grid, both in amplitude and frequency. Converting the grid voltage to the required load voltage is a problem, and efforts have to be put on the design so it fulfills the EMC standards, and this costs both energy losses and money. Since most electronic loads are utilizing a dc link, is it then possible to overcome this problem by using dc instead of ac in distribution systems?

2.3.1 Reliability

Today, after some major power disturbances in southern Sweden, reliability has become a hot issue. A power outage with a duration longer than a couple of hours has a great impact on our modern society, which is highly dependent on electric power. Most public services need computers and communication equipment to operate, but fail in case of a power outage. Some back-up systems are installed to feed the most critical loads but after a few hours they need maintenance to continue to operate. If the communication systems do not work it is difficult to arrange and perform the service.

A distribution system which could be operated either connected to the large power grid utilizing all its advantages or in island in case of disturbances, would solve the above mentioned problem. In case of a disturbance of the supplying main grid, the distribution grid is disconnected from the main grid, and all sensitive loads are supplied with the local energy storage and the local generation. This type of network design creates “microgrids”, which is a growing research issue about future power systems [26].

2.3.2 EMC and Power Quality

The number of non-linear electric loads connected to the ac system is increasing. The mismatch between the supplying ac grid and the loads, which results in a need for power conversion, is resulting in EMC and power quality problems like reactive power consumption and low-frequency current harmonics. This will result both in increased losses and malfunction of protection, and more design issues of the loads. It is necessary to meet the EMC standards which regulates the distorsion of the load current generated by the load, and to decrease the sensitivity of the loads. SS 4211811 limits the even harmonics to 1 % and odd harmonics to 4 % up to the 7^{th} harmonic [27]. EN 50160 limits the THD to 8 % and the unbalance to 2 % [28]. IEEE Std. 519-1992 limits the harmonic level for each harmonic order up to the 35^{th} and limits the THD to 5 % [29]. A dc system would not totally remove power conversion inside the loads, only the last stage from ac to dc, which creates the low-frequency EMC problems.

2.3.3 Loads

The electrical appliances today are designed to operate with ac, but many of them can run on dc without modification. All resistive loads like heaters, incandescent lamps, stoves, operate with both ac and dc, and the output power is equal if the RMS values are the same. All electronic loads like computers, fluorescent lamps with electronic ballast, flat screen TV, battery charger, which all internally use dc, have a bridge rectifier to convert ac to dc. This rectification will introduce current harmonics, which have a negative effect on the power system: neutral conductors become overloaded and protections malfunction. All these electronic loads can directly be supplied with dc. Rotating loads driven by a universal machine, or frequency controlled machines can also be supplied with dc. Problems arise with loads using a fix speed ac machine which utilizes a virtual phase created by a reactive component to get a rotating magnetic field. Loads with inductive parts cannot be supplied with dc, since dc creates a constant increasing current through it. Also loads with mechanical breakers designed for ac voltage cannot be supplied with dc. The breaker will be destroyed when breaking dc, due to no natural current zero. Loads supplied with dc are further treated in Chapter 3.

2.3.4 Power Generation

The number of alternative generation sources connected to the distribution system increases [30]. Some of them, like photovoltaic and fuel cells, produce dc, and they can easily be connected to a dc distribution system directly, or through a dc/dc-converter. Microturbines, generating high-frequency ac, which is very suitable to convert to dc due to the high frequency, is also easy to connect to a dc system. Connecting the generation to an ac system using converters generating a synchronized sinusoidal ac current is more complicated, regarding both design and control.

The electric power output of a wind turbine can be kept at a maximum if the speed of the turbine is allowed to vary. If the shaft is directly connected to the generator the frequency will vary with the wind speed, and this is not possible if the electric output has to be synchronized to the grid. To overcome this problem an ac/dc/ac-converter can be used which is an expensive solution. A cheaper and simpler solution is to connect an ac/dc-converter to a dc grid. Other types of generators operating with varying speed are hydro and tidal generators.

2.3.5 Energy Storage

UPS are used to supply sensitive loads in an ac systems. The UPS configuration for an ac system, shown in Fig. 2.4, consists of an ac/dc-converter, energy storage and a dc/ac-converter. Supplying sensitive loads with dc requires only a simple dc/dc-converter instead of two ac/dc-converters, which is shown in Fig. 2.5. Both components and losses can be reduced.

2.4 Low-Voltage DC Distribution System Layout

The idea of using low-voltage dc distribution systems has been analyzed in pre studies of dc systems [31–37]. Also some test facilities are planned to evaluate such a system. A low-

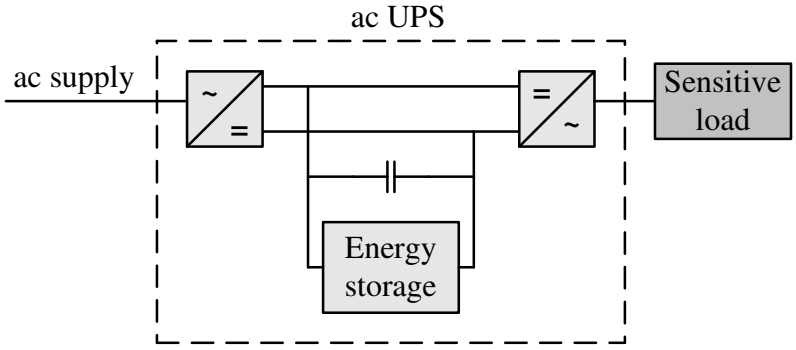

Fig. 2.4. UPS configuration for ac system.

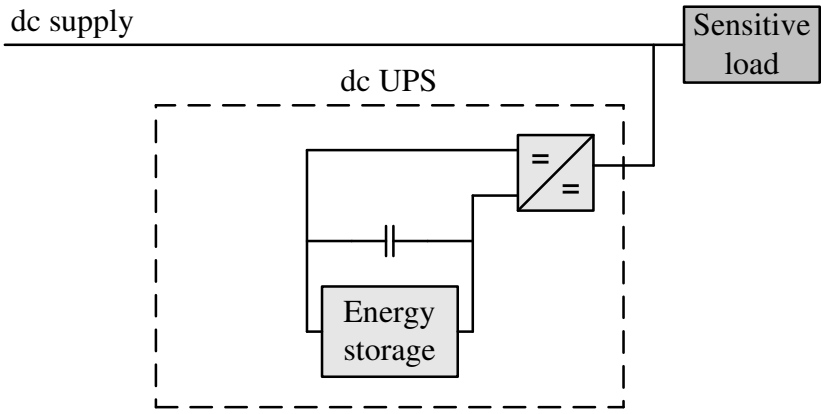

Fig. 2.5. UPS configuration for dc system.

voltage dc distribution system with ac/dc interface, loads, energy storage and generation is shown in Fig. 2.6. The design of the ac/dc interface plays a big role in the interaction of the ac and dc systems. Different types of interface are described and analyzed in Section 2.4.3. Other components in the dc system which are of interest are cables and breakers. These will be discussed in the following sections.

2.4.1 Cables

Low-voltage power cables have different voltage ratings depending on the size. Larger power cables are rated 1 kV, single wire installation cables are rated 450/750 V and polywire installation cables are rated 300 V phase-to-ground and 500 V phase-to-phase [38]. A three-phase ac system requires five wires: three phase conductors, one neutral and one ground. A dc system require three wires: two phase conductors and one ground. An existing five-wire ac cable in a retrofit dc system can be used in two different configurations. The first is to use two wires for each pole and one for ground. The other alternative is to use one for each pole, two for neutral and one for ground, where the idea is to have the load connected between one pole and ground. This will result in twice the load voltage between the poles, and therefore twice the power. The different configurations are shown in Fig. 2.7. The two retrofit dc configurations are compared with an ac case for a five single-wire installation with 1.5 mm^2 wire rated 450/750 V and 10 A. The ac load is assumed to have a power factor of 0.95, and the dc load voltage equals the peak value of the ac voltage. The power transmitted in each cable configuration is shown in Table 2.1.

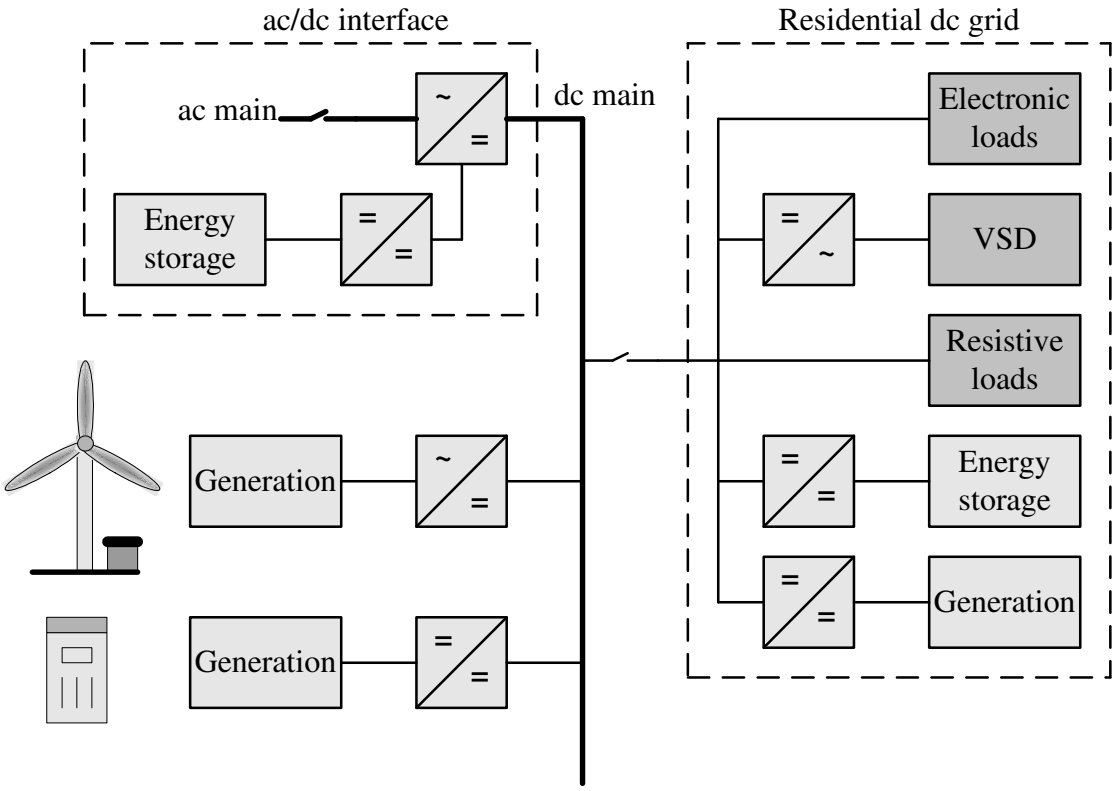

Fig. 2.6. Layout of a low-voltage dc system. VSD denotes variable speed drive.

TABLE 2.1
COMPARISON OF DIFFERENT CONFIGURATIONS.

	ac case (a)	dc case (b)	dc case (c)
U_{rms} [V]	230	325	650
I_{rms} [A]	10	20	20
P [W]	6555	6500	13000

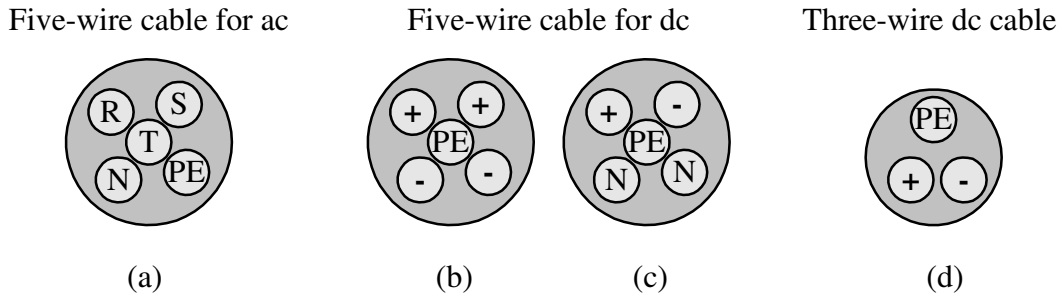

Fig. 2.7. Use of cables in retrofit or new dc systems.

2.4.2 Fuses and Circuit Breakers

Fuses and circuit breakers are components in the power system that can open the circuit during a fault. Both components work in the same way to open the circuit. First an arc is created, and this is achieved by either melting metal or open contacts. Then the dielectric strength across the arc has to be increased so the arc extinguishes when the current becomes zero, which it becomes every half cycle in an ac system. If the voltage over the extinguished arc, the *recovery voltage*, builds up slower than the dielectric strength, the arc cannot re-ignite. The X/R-ratio determines how fast the recovery voltage builds up. The higher the X/R-ratio, the faster the recovery voltage builds up. The dielectric strength can be increased by cooling the arc, pressurizing the arc, stretching the arc and introducing fresh air [39].

However, dc has no natural current zero. One possibility to interrupt dc is to create a larger distance between the contacts in the circuit breaker. Existing three-phase ac circuit breakers, where the three contact pairs are connected in series, can be used for dc applications. A standard three-phase ac circuit breaker rated 690 V can be used up to 600 V dc [40–42]. Another way to accomplish a larger distance is to use a magnetic field to stretch the arc. The size of the breaker is reduced but at a higher cost. This type of breaker can be found in dc machine systems and traction systems [43].

The other possibility to interrupt dc is to use a breaker together with a resonant circuit. The resonant circuit creates a voltage zero, and if the breaker then opens at zero voltage no arc will be generated. This type of breaker can be found in HVDC systems [44]. The two variants are shown in Fig. 2.8.

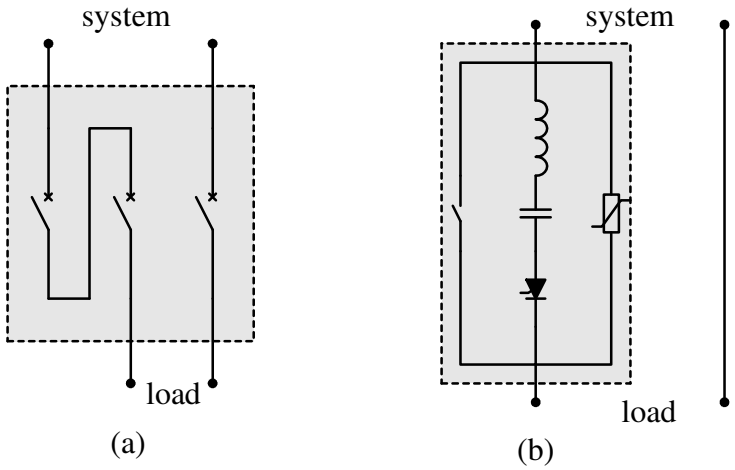

Fig. 2.8. Circuit breakers for dc: (a) three poles in series, (b) zero volt switching hybrid dc circuit breaker.

2.4.3 AC/DC Interface

The interface between the ac and dc systems has a great significance on the operation of the dc system. Different topologies have different possibilities to control the power flow. The more the power can be controlled, the higher the cost. A proper ac/dc interface for a future dc distribution system shall provide a controllable dc-link voltage, high power quality, bi-directional power flow, and high transient performance during faults and disturbances. Moreover, it must have low losses and low costs. Bi-directional power flow capability is

necessary if it shall be possible to transfer power from the dc system to the ac system during low-load, high-generation condition in the dc system. Galvanic isolation prevents having a path between the ac and dc systems in case of a fault. Five different topologies of ac/dc interfaces from no control to full control are presented in this section.

Diode rectifier

A diode bridge is a very cheap device for rectification of ac to dc, and it can be designed for both single-phase and three-phase connection. The schemes of a single-phase and a three-phase diode rectifier are shown in Fig 2.9 [45]. The diode rectifier has many disadvantages. The output dc-link voltage is uncontrolled and the maximum dc-link voltage is equal to the peak value of the phase-to-ground voltage for a single-phase rectifier, and equal to the peak value of the phase-to-phase voltage for a three-phase rectifier. The dc-link voltage decreases if the load current increases. The rectifier consumes symmetrical ac currents and produces a high amount of odd low-frequency harmonics. Finally, the power can flow only from the ac side to the dc side and the diode rectifier obviously provides no galvanic isolation.

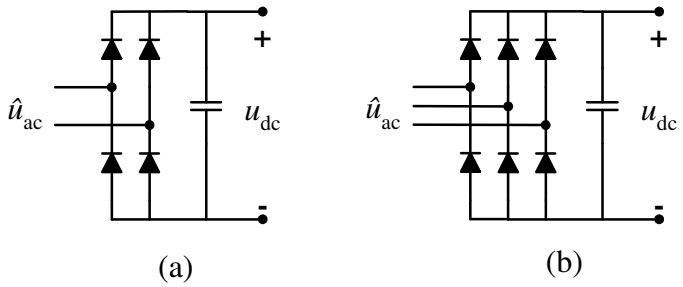

Fig. 2.9. Diode rectifier: (a) single phase, (b) three phase.

Diode Rectifier + Power Factor Correction

The diode bridge can be modified by adding some components, as shown in Fig. 2.10, which will give it buck or boost characteristics with controllable dc-link voltage and power factor correction (PFC) [46]. This is obtained by controlling the current through the inductor by opening and closing the transistor. The current waveform is set to be sinusoidal and the amplitude is set by the dc-link reference voltage. The diode rectifier with PFC has no galvanic isolation [47]. For high power applications three single-phase rectifiers can be connected to each phase and with their dc-links in series.

Transformer and Voltage Source Converter

A three-phase VSC utilizes six switches instead of three, as a three-phase diode rectifier with PFC has. The scheme of the VSC with a transformer is shown in Fig. 2.11. The three additional switches make it possible to have bi-directional power flow [45]. The VSC is a hard-switched converter utilizing high-frequency switching, and it is necessary to filter the grid currents. This is done by connecting an L- or an LCL-filter between the converter and the grid [48]. The three phase currents through the filter are set to be sinusoidal in average, with an amplitude given by dc-link voltage controller. The VSC operated as a rectifier has a boost output characteristic. The lower level of the output dc link voltage is determined

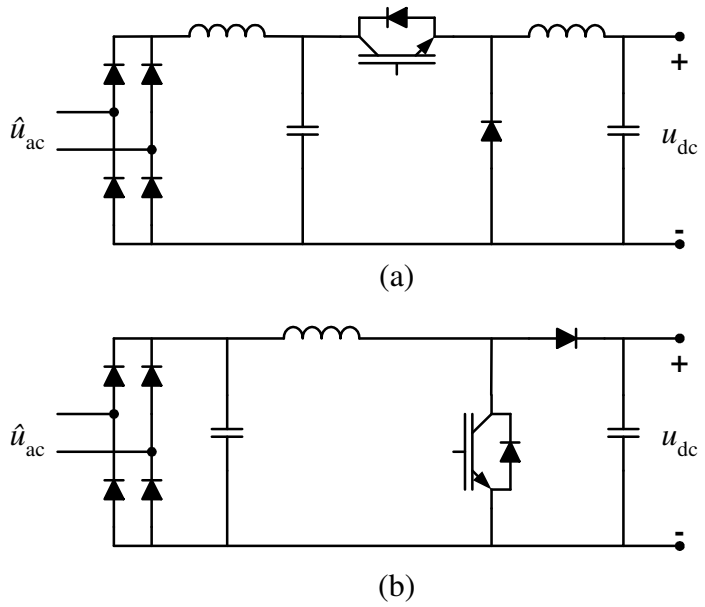

Fig. 2.10. Single-phase diode rectifier with PFC: (a) Buck, (b) Boost.

by the ac voltage, and equals twice the peak value of the phase-to-ground voltage [49]. To be able to adjust the minimum dc output a transformer can be connected between the VSC and the ac grid. The transformer will serve for three things: step down ac voltage, galvanic isolation between ac and dc, and serve as a grid filter (using the leakage inductance of the transformer). A VSC also has a controllable power factor [48].

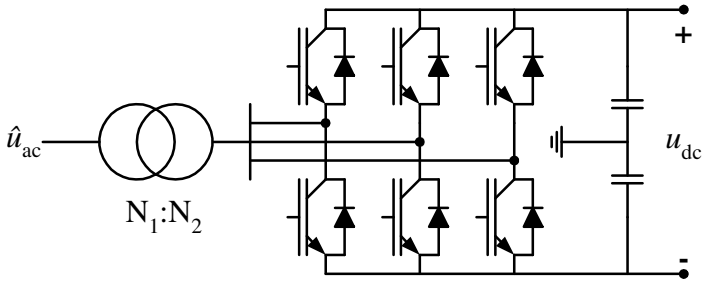

Fig. 2.11. VSC connected to the ac grid via a transformer.

Three-Level VSC

The configuration of a three-level VSC, shown in Fig. 2.12 uses 12 switches instead of six [50]. Compared with the two-level VSC it results in two, instead of one, controlled dc links from the same ac supply. The two dc-link voltages u_{dc1} and u_{dc2} can be controlled individually. In a dc system application, it means that loads can be connected to either of the two dc links, and it is still possible to maintain balanced dc-link voltage, which would not be possible with a two-level VSC.

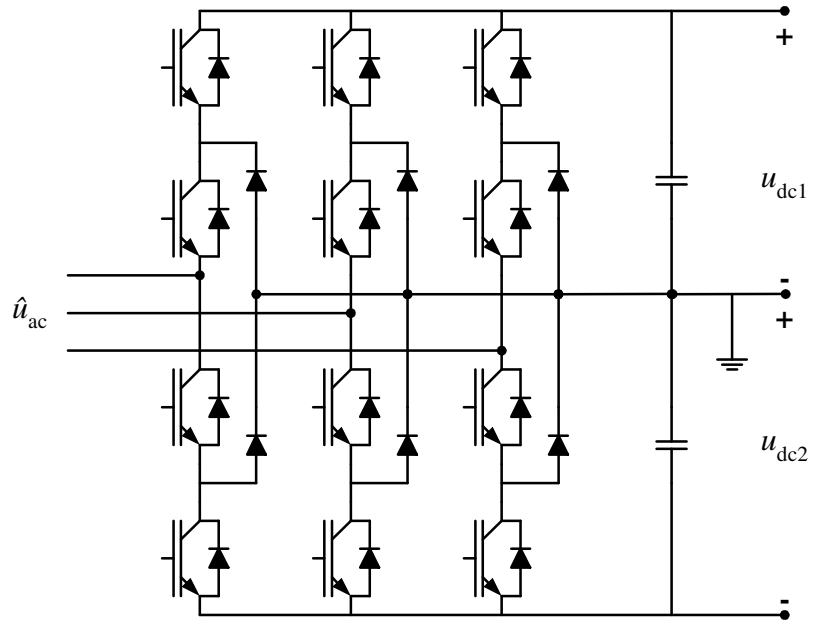

Fig. 2.12. Three-level VSC.

VSC and Buck

A combination of a VSC and a dc/dc Buck converter [46] is shown in Fig. 2.13. Combining two converters by connecting them in series gives increased controllability of the output dc-link voltage. The voltage of the dc link between the VSC and the Buck converter is allowed to vary in a wider range since the output dc-link voltage is controlled by the Buck converter. In case of faults in the ac system, a VSC is not capable to maintain the dc-link voltage at the reference value. Using a two converter interface increases the possibility. However, the configuration uses eight switches instead of six, which increases the losses. The configuration has bi-directional power flow but no galvanic isolation.

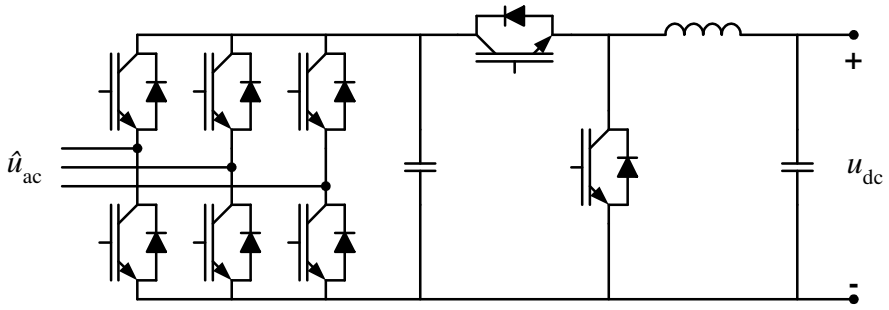

Fig. 2.13. VSC in series with a Buck converter.

TABLE 2.2
AC/DC INTERFACES.

Interface type	Output dc-link voltage u_{dc}		Number of switches	Bi-directional power flow	Galvanic isolation
	Min	Max			
Diode	-	$\hat{u}_{\text{ac}}$	0	No	No
Diode PFC (Buck)	0	$\hat{u}_{\text{ac}}$	3	No	No
Diode PFC (Boost)	$\hat{u}_{\text{ac}}$	∞	3	No	No
Transformer and VSC	$2\frac{N_2}{N_1}\hat{u}_{\text{ac}}$	∞	6	Yes	Yes
Three-level VSC	$\hat{u}_{\text{ac}}$	∞	12	Yes	No
VSC and Buck	0	∞	8	Yes	No

Conclusions

All five described configurations are possible choices as an ac/dc interface. The trade-off is as usual price and performance. Depending on the system configuration, different interfaces can be more or less proper. Table 2.2 gives, for the different types, range of dc-link voltage output, number of switches, if the interface allows bi-directional power flow and if the interface gives galvanic isolation. The VSC and Buck configuration is chosen as the ac/dc interface in this project since it has a wide range output dc voltage, and can be designed to have a high transient performance during faults and disturbances, which will be shown later in Chapter 4 and 5.

2.5 Conclusions

In this chapter, the history of dc distribution systems has been presented together with applications where dc systems can be found today. The key issues of a future dc distribution system and its components have been highlighted and discussed.

Today, dc systems can be found in many different applications with different voltage and power ratings. The systems can have a simple structure, with two converters and one dc link connecting them like a HVDC system, or a complex structure with parallel connected converters, used both for connecting generation and supplying loads, like in a car or on a ship.

A low-voltage dc distribution system has a potential to be used in future power systems. A dc systems with a suitable voltage is more adjusted to today's load situation. The design of electronic loads would be simpler if they were supplied with dc since less components are needed for the power conversion, and less non-linear currents would be present in the grid. Connection of energy storage and sources would also be easier since simpler converters are required.

The interface between the ac and dc systems plays a big role for the performance of the two systems. An interface shall provide a stable dc-link voltage and be able to handle load variations, and faults and disturbances in the ac grid. The ac grid currents shall be sinusoidal with no low-frequency harmonics for a good power quality. The VSC with a Buck converter is chosen for the project. It has a controllable dc-link voltage which can be varied in a wide range, and it has a good performance during faults and disturbances on the ac system, which will be further analyzed. However, the topology violates the low cost and low losses demand, at least with the components available today.

Chapter 3

Load Modeling

This chapter will describe load modeling for steady-state and transient analysis of low-voltage dc systems. There are two reasons for this investigation. The first is to determine whether existing low-voltage ac loads can be supplied with dc without being modified, and if 'yes', within which voltage range. The second reason is to develop models which can be used for steady-state and transient studies of dc systems using software like PSCAD/EMTDC and MatLab. The measurement results presented here can be found in [51, 52].

3.1 Introduction

A wider use of dc for power distribution calls for suitable calculation methods and models of system components to analyze the operation of the dc grid. Chapter 16 in the IEEE Brown Book [53] and IEC 61660 [3] describe how to calculate load flow/voltage drop and short-circuit currents in dc auxiliary systems in power plants and substations. In these two standards, models of sources, branches and cables for both steady-state and transient analysis are given. However, loads are only modeled as constant resistance (CR), constant current (CC) or constant power (CP), and no further description is given. An interesting question that arises with a wider use of dc is if existing loads can be used without any changes and, if so, how they will operate in steady state and in response to voltage variations. Finally, it is also of interest to find out what is the most suitable voltage level for the loads.

To investigate all existing loads used in a low-voltage ac system was not possible, due to financial issues. Instead all existing loads were categorized into groups, and then one or more sample loads were investigated. A view of all loads used in offices and households gives a basis for the choice of the load groups. The different groups together with an example from [51], where 51 different loads were tested, are listed in Table 3.1.

3.2 Measurement and Analysis

The aim of the measurement was two-fold: to determine the load characteristic in steady state; and to determine the transient response. Both 230 V dc and 325 V dc have been mentioned as possible rated values for a low-voltage dc grid [34]. 230 V and 325 V equal the rms-value and the peak value, respectively, of a 230 V ac voltage. Moreover, a deviation of e.g. $\pm 10\%$ should be allowed and the loads should still operate correctly. Therefore, it

TABLE 3.1
TESTED LOAD TYPES.

Load type	Example
Resistive lighting	Incandescent lamp
Resistive heaters	Coffee maker
Induction machine	Refrigerator
Universal machine	Vacuum cleaner
Electronic lighting	Fluorescent lamp with HF ballast
Electronic load	Computer power supply

was of interest to test the loads at least in the range of 200-360 V dc, but where possible a wider voltage range was considered.

The load can be characterized as CR, CC, CP or a mix of these. The mathematical expression for the three different power characteristic as a function of the voltage becomes [54]

$$P(U) = A_{\text{CR}}U^2 + A_{\text{CC}}U + A_{\text{CP}} \tag{3.1}$$

where A_{CR} is the constant resistance coefficient, A_{CC} is the constant current coefficient, and A_{CP} is the constant power coefficient. Normalizing (3.1) with respect to nominal voltage, U_0, and nominal power, P_0, gives

$$\frac{P(U)}{P_0} = a_{\text{CR}}\left(\frac{U}{U_0}\right)^2 + a_{\text{CC}}\frac{U}{U_0} + a_{\text{CP}} \tag{3.2}$$

where a_{CR} gives the constant resistance characteristic in per unit (p.u.), a_{CC} the constant current characteristic in p.u., and a_{CP} the constant power characteristic in p.u.. The measurement results show that not all loads can be categorized into these three groups, and more characteristics are derived when necessary.

The measurement setup is shown in Fig. 3.1. The test object was supplied from a dc generator with controllable voltage. The dc voltage was stabilized by connecting a capacitor C = 3300 μF in parallel with the source. The voltage at the load terminals and the load current were measured and recorded. The voltage was applied for a sufficient time to be sure that the current was constant and the test object was not damaged. However, no long-term tests were carried out, because the aim was to develop a model of the load, and not to investigate how the voltage level affects the lifetime of the test object.

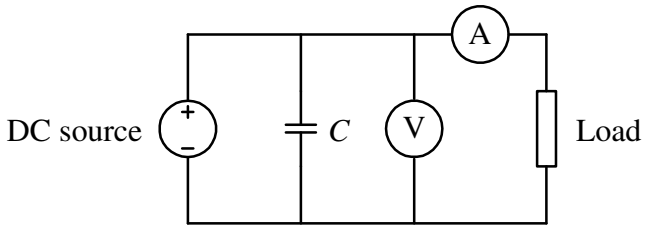

Fig. 3.1. Scheme of the test setup for steady-state measurement.

The loads were also subjected to a fast voltage reduction to determine their transient behavior. Each load was tested with four different step magnitudes with retained voltage equal to 0.88, 0.76, 0.62 and 0.47 p.u.. For each magnitude, the test was repeated ten times to decrease the influence of noise. The voltage step was done with the “step device” shown

in Fig. 3.2, consisting of one transistor, one resistor, zener diodes, RC-filters and a switch. When the switch is open, the load is supplied with the nominal voltage. When the switch is closed, the load is supplied with a reduced voltage, whose magnitude is determined by the zener diodes. The resistor in parallel with the transistor is used for bypassing the load current, thus preventing the transistor to get too warm. The RC-filters are used to reduce the voltage transients that may arise when the transistor is opened. The measured quantities

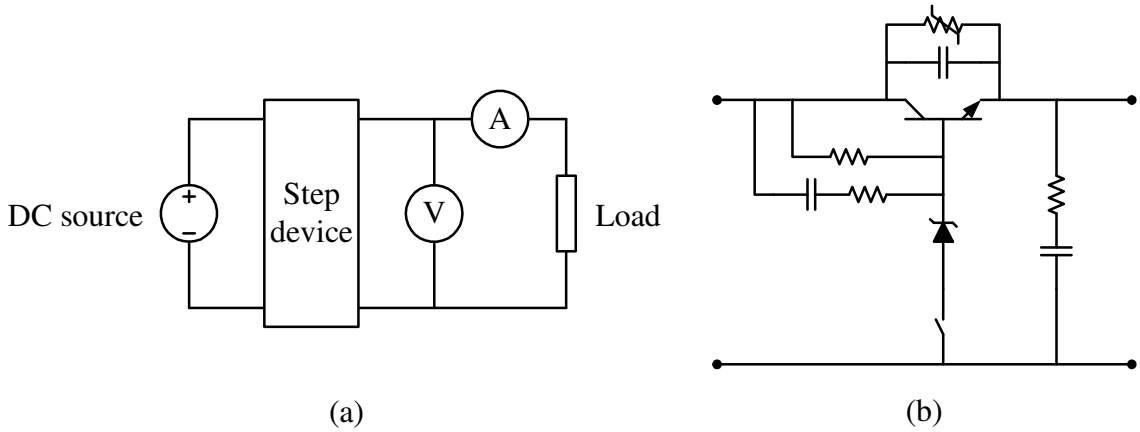

Fig. 3.2. Scheme of the test setup for transient measurement: (a) measurement setup, (b) step device.

are voltage at the load terminals and current absorbed by the load. Based on these, load power and resistance are calculated. The accuracy of the voltage and current measurement is reported in Table 3.2.

From the measurement results, steady-state and transient models of the tested objects are derived. The steady-state model is useful for voltage drop calculations and for calculating power/current variations due to slow voltage variations. The transient model is useful for simulations of disturbances in the grid.

TABLE 3.2
MEASUREMENT ACCURACY FOR THE INSTRUMENTS USED.

Instrument	Accuracy	Range
Fluke 87	$\pm 0.2\%$	-
Fluke 77	$\pm 0.3\%$	-
LeCroy Differential Probe AP032	$\pm 2\%$	dc - 15 MHz
LeCroy Current Probe AP011	$\pm 1\%$	dc - 120 kHz

3.3 Resistive Loads

Resistive loads use, as the name indicates, the resistance to emit electromagnetic energy, which can be both in the frequency range of thermal radiation, visible light or a combination. Loads emitting thermal energy are denoted heaters, and loads emitting light are denoted lighting. The electric characteristic of a resistive load is given by Ohm's law

$$U = RI \tag{3.3}$$

where U is the voltage, I the current and R the resistance, which can be calculated as

$$R = \frac{\rho l}{A} \tag{3.4}$$

where ρ is the resistivity, l is the length of the conductor, and A is the cross-section area of the conductor. The resistivity ρ is temperature dependent and can be calculated as

$$\rho = \rho_0(1 + \alpha(T - T_0)) \tag{3.5}$$

where ρ_0 is the resistivity at 300 K, α is the temperature coefficient, T_0 is 300 K, and T is the operating temperature. The conductor temperature T is proportional to I, $T \sim I$, if it changes with the current. The resistivity as function of the current can then be written as

$$\rho = \rho_0(1 + \beta I) \tag{3.6}$$

where β is the current coefficient. Finally, the conductor resistance is calculated as

$$R = \frac{\rho_0(1 + \beta I)l}{A} = \frac{\rho_0 l}{A} + \frac{\rho_0 \beta I l}{A} = R_0 + R_1 I \tag{3.7}$$

which gives that the resistance is linearly dependent on the current. Rewriting (3.3) using (3.7) gives

$$U = (R_0 + R_1 I)I = R_0 I + R_1 I^2. \tag{3.8}$$

The instantaneous power, P, is given by UI, and using (3.8) to calculate the power as a function of the voltage, yields

$$P(U) = U\left(\pm \sqrt{\frac{U}{R_1} + \frac{R_0^2}{4R_1^2}} - \frac{R_0}{2R_1} \right). \tag{3.9}$$

3.3.1 Heaters

As the name indicates, heaters are used for producing heat energy which can be used in many applications. Tested heaters are coffee maker, curling brush, kettles, sandwich makers, and a stove. The steady-state measurement results show that heaters all have a constant resistance behavior, i.e. the terms a_{CR} in (3.2) and R_0 in (3.8) dominate. The relation between A_{CR} and R_0 for heaters is

$$A_{\text{CR}} = \frac{1}{R_0}. \tag{3.10}$$

The value obtained from the measurements can be compared with the calculated value using the nominal power given for each load. The steady-state model of the heaters is a pure resistance calculated from the nominal power, if it is given. Otherwise, the value obtained from the measurements is used. The resulting models of the steady-state measurements are reported in Table 3.3. An average error between model and measurement in the measured voltage range can also be found in the table. The steady-state measurement result for a coffee machine (Butler), which will represent a typical heater load, is shown in Fig. 3.3. It shows that the voltage is a linear function of the current, and the power is a quadratic function of the voltage.

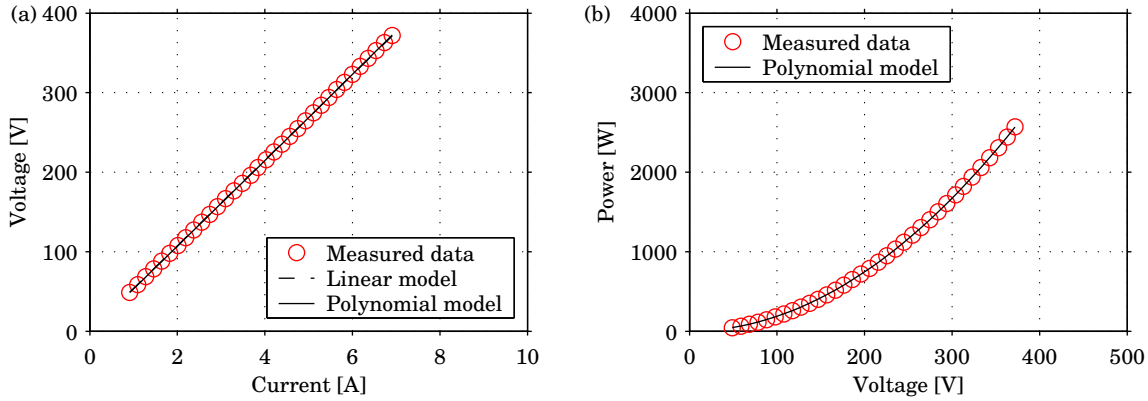

Fig. 3.3. Steady-state measurement of a coffee maker (Butler): (a) resistance characteristic, (b) power characteristic.

TABLE 3.3
MODEL PARAMETERS OF HEATER LOADS.

Heater load	P_{rated} [W]	Model $R = [\Omega]$	Error [%]
Coffee Maker (Butler)	1000	52.90	$\pm$ 1.62
Coffee Maker (Philips)	850	62.24	$\pm$ 3.13
Curling Brush (XL Concept)	11	4809.1	$\pm$ 2.45
Kettle (Elram)	2000	26.45	$\pm$ 6.1
Kettle (Solingmüller)	2025	26.12	$\pm$ 2.48
Sandwich Maker (Mirabella)	800	66.13	$\pm$ 2.48
Sandwich Maker (AFK)	700	75.57	$\pm$ 0.86
Stove (Siemens)	-	40.26	$\pm$ 4.67

The transient measurements of the heater loads show as expected that a fast reduction of the voltage will result in a fast reduction of the current, independently of the magnitude of the voltage step. This shows that the model in (3.8) can be used, with R_0 calculated from the nominal power and R_1 = 0. The voltage recorded during the transient measurement is used together with the obtained model parameters to verify the model in PSCAD/EMTDC. The simulated result of the coffee maker model is plotted together with the measurement in Fig. 3.4, which shows a 0.12 p.u. voltage step. The simulated current agrees well with the measured current.

3.3.2 Lighting

A common electric device used for lighting is the incandescent lamp, or light bulb. It consists of a filament of tungsten inside a glass bulb filled with argon. Twenty-six incandescent lamps from five different manufacturers, and with five different power ratings, were tested. Also two tungsten halogen lamps were tested. The steady-state measurements for the lighting loads show that they do not act as a constant resistance load. The term R_1 in (3.8) is not insignificant, i.e., the resistance changes with the current. This means that (3.9) must be used to calculate $P(U)$. The measurement result for a 60 W incandescent lamp is shown in Fig. 3.5. The steady-state measurements show that the lighting loads have temperature-dependent resistance and can be modeled as in (3.8). The resistance increases when the current increases, and it can be seen in Fig. 3.5(a) that the voltage increases faster than the

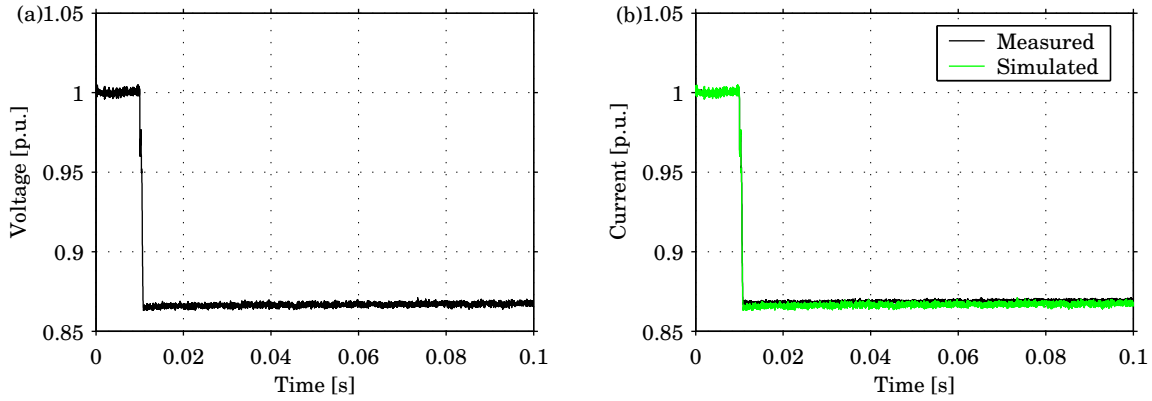

Fig. 3.4. Transient measurement and modeling of coffee maker (Butler): (a) voltage, (b) current during voltage step.

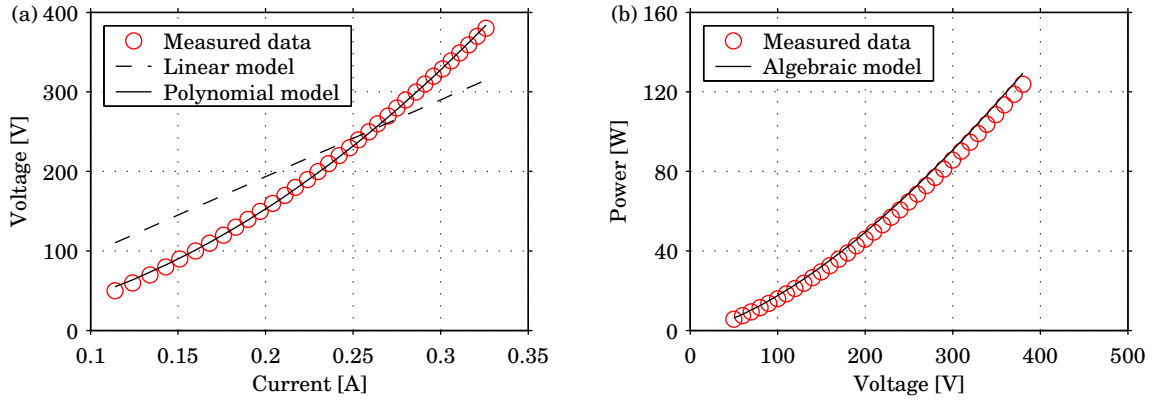

Fig. 3.5. Steady-state measurement of 60 W incandescent lamp: (a) resistance characteristic, (b) power characteristic.

current. The resistance value must stabilize before recording the current for each tested voltage value in order to get the correct measurement data. However, after a fast voltage step the situation is a bit different. Directly after the voltage step the resistance is unchanged, and the current is reduced proportionally. But, when the current decreases, the resistance decreases according to (3.7), so the current starts to increase exponentially. A discrete function of the resistive transient is given by

$$\hat{R}(k+1) = \hat{R}(k) + \frac{\tau}{\Delta t}(R(k+1) - \hat{R}(k)) \tag{3.11}$$

where τ is the time constant, Δt the time step of the simulation, k the discrete time and $R(k)$ is the steady-state resistance value corresponding to the given voltage value, obtained from the load characterization. In [51] it is shown that the estimated time constant of the filament, τ_{est}, is linked to the rated power as

$$\tau_{\text{est}} = 0.0151 \ln P - 0.0112. \tag{3.12}$$

The transient measurement result for a 60 W incandescent lamp when a 0.12 p.u. voltage step is applied is plotted together with the simulated result in Fig. 3.6. It clearly shows the temperature dependency of the filament. First the current follows the sudden voltage reduction and then the current starts to increase. To model an incandescent lamp it is necessary to

TABLE 3.4
MODEL PARAMETERS FOR LIGHTING.

Lighting load	P_{rated} [W]	Model $R = R_1 I + R_0$ [Ω]	τ_{est} [s]	Error [%]
Incandescent Lamp	25	$16966.2I + 128.4$	0.0375	±1.59
Incandescent Lamp	40	$7010.2I + 133.7$	0.0446	±1.42
Incandescent Lamp	60	$2925.8I + 113.5$	0.0508	±1.27
Incandescent Lamp	75	$1709.5I + 106.7$	0.0541	±1.23
Incandescent Lamp	100	$994.5I + 87.6$	0.0585	±1.12
Tungsten Halogen Lamp	150	$435.9I + 74.7$	0.0564	±1.68

know R_0, R_1 and τ_{est}. From the nominal power R_0 and τ_{est} can be calculated. However, R_1 can only be obtained through measurements. The obtained models for lighting are reported in Table 3.4.

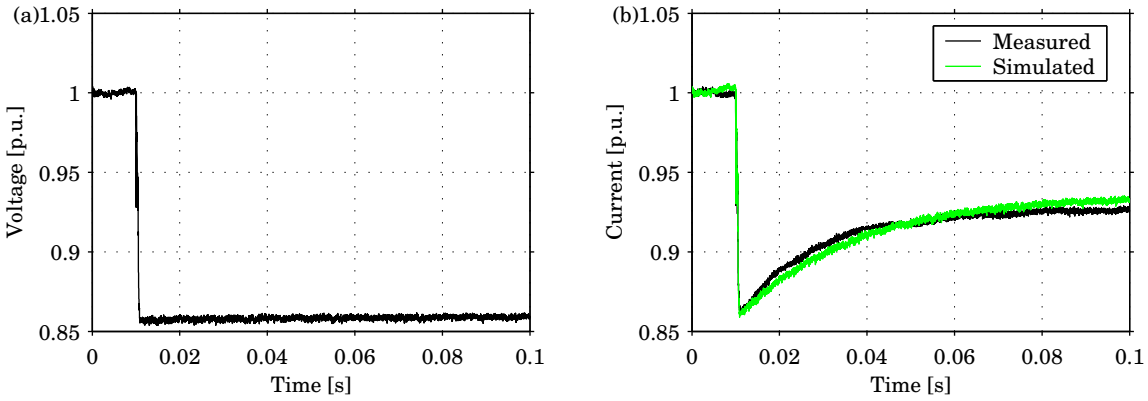

Fig. 3.6. Transient measurement and modeling of incandescent lamp: (a) voltage, (b) current during voltage step.

3.4 Rotating Loads

Many different types of machines are used for household appliances. The size varies from very small up to very big. Small machines are usually universal machines. They can be built very compact and have a high rotational speed. Bigger machines can be both universal or induction machines. For instance, vacuum cleaners use universal machines, whereas refrigerators normally use single-phase induction machines. Modern loads as washing machines and refrigerators use three-phase induction machines together with power electronics to control the speed. These loads can be supplied with low-voltage dc if they use single-phase ac supply, but not if they use a three-phase ac supply. Then the dc-link voltage becomes higher than 325 V.

Single phase ac machines, e.g. used in old refrigerators, use a virtual phase shifted 90° by a capacitor, to get a rotating magnetic field. Two different types exists: capacitive start induction run, and capacitive start capacitive run [55]. These machines cannot be operated with dc since they use reactive components.

The universal machine has the same configuration as a series magnetized dc machine, and it works as the name indicates with both ac and dc [55]. A scheme of the universal machine is shown in Fig. 3.7.

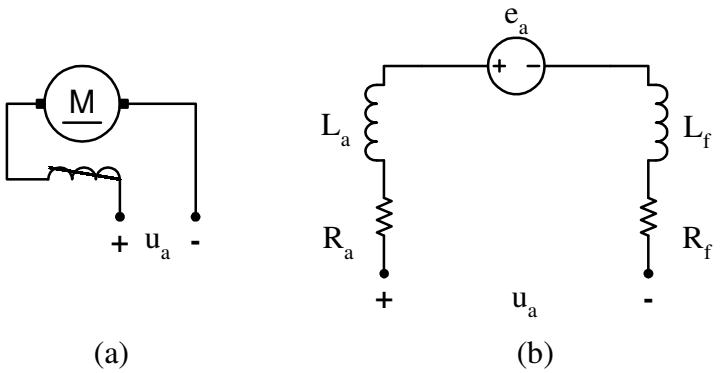

Fig. 3.7. Series magnetized dc machine: (a) principle scheme, (b) electrical scheme.

The electrical dynamics of the universal machine is given by

$$u_{\mathrm{a}} = e_{\mathrm{a}} + R_{\mathrm{eq}} i_{\mathrm{a}} + L_{\mathrm{eq}} \frac{\mathrm{d}i_{\mathrm{a}}}{\mathrm{d}t} \tag{3.13}$$

where u_{a} is the applied voltage, e_{a} is the back emf, i_{a} is the current, R_{eq} is the equivalent resistance, which is the sum of the resistance of the armature R_{a} and that of the field winding R_{f}, L_{eq} is the equivalent inductance of the machine, which is the sum of the inductance of the armature L_{a} and that of the field winding L_{f}. The back emf, e_{a}, is proportional to the rotational speed, ω_{r}, of the machine, which is expressed as [55]

$$e_{\mathrm{a}} = k_{\mathrm{E}} \omega_{\mathrm{r}}. \tag{3.14}$$

The torque of the machine, τ_{e}, is proportional to the current, i_{a}, [55]

$$\tau_{\mathrm{e}} = k_{\mathrm{T}} i_{\mathrm{a}}. \tag{3.15}$$

The constant k_{E}, equal to k_{T}, is given by the physical design of the machine as

$$k_{\mathrm{E}} = k_{\mathrm{T}} = \frac{n_{\mathrm{a}} l r}{2 a \phi_{\mathrm{f}}} \tag{3.16}$$

where n_{a} is the number of conductors on the armature, l is the length of each conductor, r is the radius, a is the cross sectional area of the conductor and ϕ_{f} is the uniform flux in the stator [55]. Since the machine is series magnetized, (3.14) and (3.15) can be rewritten as

$$e_{\mathrm{a}} = k_{\mathrm{e}} \phi_{\mathrm{f}} \omega_{\mathrm{r}} \tag{3.17}$$

and

$$\tau_{\mathrm{e}} = k_{\mathrm{t}} \phi_{\mathrm{f}} i_{\mathrm{a}}. \tag{3.18}$$

The magnetic flux, ϕ_{f}, is directly proportional to the current, which gives

$$e_{\mathrm{a}} = k_{\mathrm{m}} i_{\mathrm{a}} \omega_{\mathrm{r}} \tag{3.19}$$

and

$$\tau_{\mathrm{e}} = k_{\mathrm{m}} i_{\mathrm{a}}^2. \tag{3.20}$$

The mechanical dynamics of the machine is given by

$$J_{\text{eq}}\frac{\mathrm{d}\omega_{\text{r}}}{\mathrm{d}t} = \tau_{\text{e}} - \tau_{\text{l}} \tag{3.21}$$

where J is the inertia of the motor, τ_{e} is the electric torque and τ_{l} is the load torque.

The steady-state electrical model of the universal machine is

$$U_{\text{a}} = E_{\text{a}} + R_{\text{eq}}I_{\text{a}} = k_{\text{t}}\phi_{\text{f}}\omega_{\text{r}} + R_{\text{eq}}I_{\text{a}}. \tag{3.22}$$

The steady-state current as a function of the voltage can be found from (3.22) as

$$I_{\text{a}} = \frac{U_{\text{a}}}{R_{\text{eq}}} - \frac{k_{\text{t}}\phi_{\text{f}}\omega_{\text{r}}}{R_{\text{eq}}}. \tag{3.23}$$

Five different universal machines were tested: three vacuum cleaners, one blender and one mixer. The measurement result for a vacuum cleaner (from LG) is shown in Fig. 3.8, which shows that the current increases linearly with the voltage. The universal machine can be modeled as a variable current source, which also can be seen from (3.23). The model is of the form $I = Y_0U + I_0$, and the model parameters obtained from the measurements and the related error are reported in Table 3.5.

TABLE 3.5
MODEL PARAMETERS FOR ROTATING LOADS AND ESTIMATED ERROR.

Load	P_{rated} [W]	Model $I = Y_0U + I_0$ [A]	Error [%]
Blender (Melissa)	300	$1.13 \cdot 10^{-3}U + 0.371$	± 1.61
Mixer (Ide Line)	220	$8.4 \cdot 10^{-4}U + 0.316$	± 1.05
Vacuum cleaner (Electrolux)	unknown	$0.0156U + 0.562$	± 3.07
Vacuum cleaner (Euroline)	1400	$0.0150U + 1.054$	± 0.59
Vacuum cleaner (LG)	1300	$0.0172U + 0.616$	± 1.25

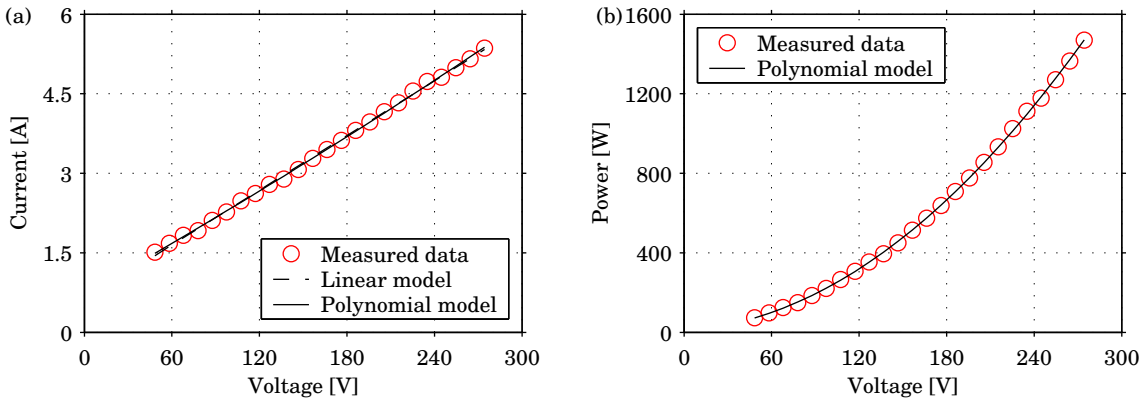

Fig. 3.8. Steady-state measurement of vacuum cleaner (LG): (a) resistance characteristic, (b) power characteristic.

The transient response of a universal machines has two parts: one electric transient which is fast, and one mechanical transient which is approximately one decade slower. A mathematical model has to be used to be able to reproduce both the electrical and the mechanical transient from the measured voltage and current. The derivation of the mathematical model

taking into account the mechanical transient is further described in [51]. The high rotational speed of the machine made it impossible to measure the rotor speed, which is used in the dynamic model described in (3.13) and (3.14). The transient measurement result and the mathematical model for a vacuum cleaner are shown in Fig. 3.9 where a 0.12 p.u. voltage step is applied. This plot shows the mechanical transient, where the current first drops and then starts to increase. Fig. 3.10 shows the electrical transient, where the current decreases with a time constant due to the inductive parts in the machine.

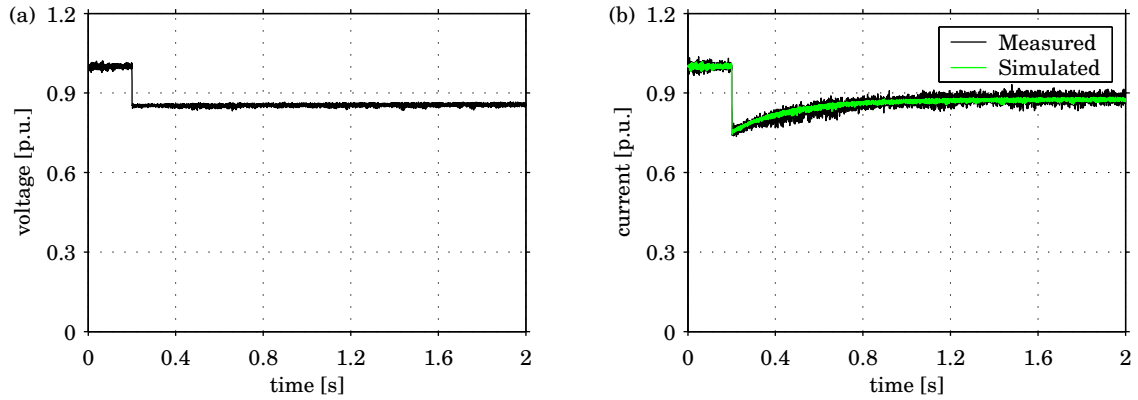

Fig. 3.9. Transient measurement and modeling of vacuum cleaner (LG): (a) voltage, (b) current during voltage step.

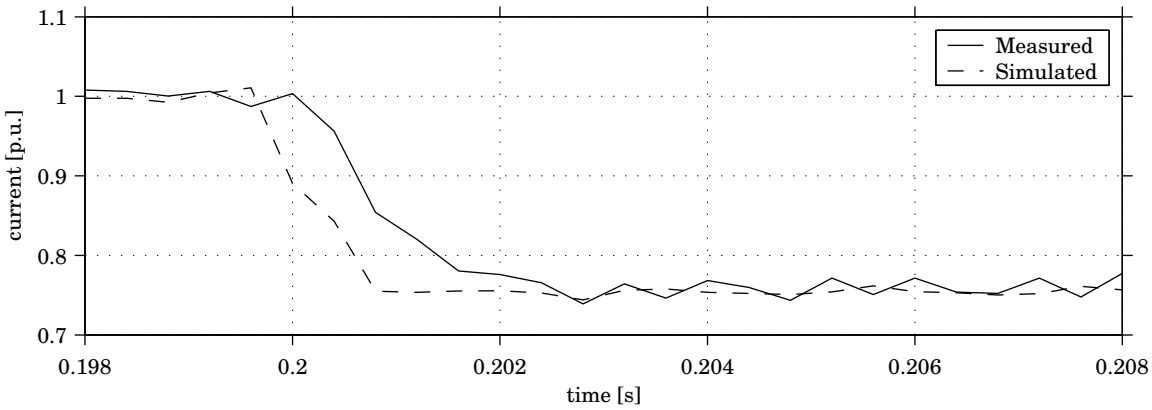

Fig. 3.10. Zoom of transient current measurement and modeling of vacuum cleaner during voltage step.

3.5 Electronic Loads

Electronic loads can today be found everywhere: computer equipment, battery chargers and lighting. Electronic loads use a different voltage amplitude and frequency than the supplying grid. To convert the supplying ac voltage it must first be rectified, and then converted to the desired voltage waveform. Old electronic loads use a low-frequency transformer to step down the voltage, which is then rectified using a diode bridge. This type works only with a certain voltage amplitude and frequency. Today it is important that a load can work properly with both 230 V/50 Hz and 110 V/60 Hz, i.e., the load must have a wide range input. This

is accomplished by using a switch mode power supply (SMPS) [46]. The input voltage is first rectified by a diode bridge and then adjusted to the load using a dc/dc-converter, which is shown in Fig. 2.10. The SMPS can be equipped with PFC to decrease the amount of low-frequency current harmonics. All electronic loads with a low-frequency transformer cannot operate with dc due to the inductance. However, SMPS can be operated with dc without any design modifications as long as the dc voltage is in the same range as the ac input. Electronic loads can be divided into two groups with respect to their main function: power supply or lighting appliance.

3.5.1 Power Supply

Electronic power supplies can be found in various types of loads. Eleven different electronic power supplies of different loads were tested: computer power supplies, monitors, battery chargers, IP telephone and a satellite receiver. As an example, the steady-state measurement of a computer power supply is shown in Fig. 3.11. The steady-state measurements showed that these loads behave as constant power loads, which is not difficult to understand since they use a dc/dc-converter to adjust the load voltage, and therefore the load consumes the same power regardless of the input voltage. However, the voltage range in which the loads could operate was different for different loads.

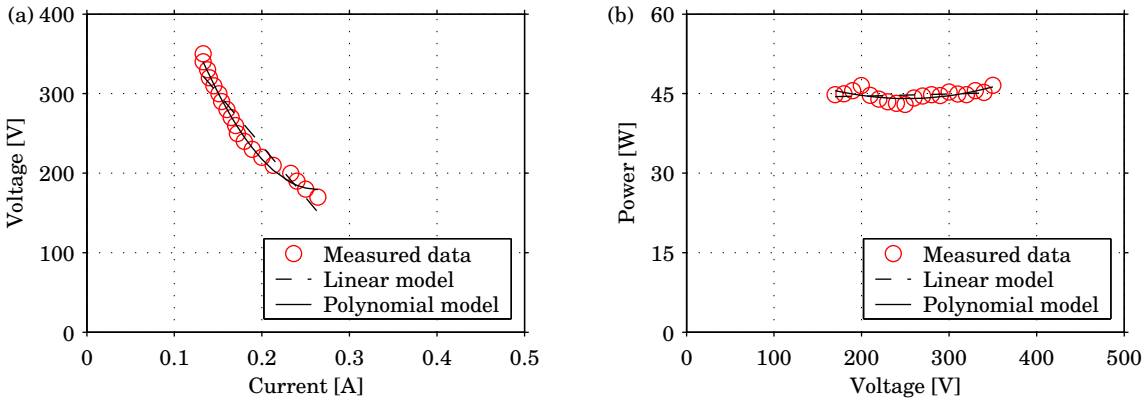

Fig. 3.11. Steady-state measurement of computer power supply (Dell): (a) resistance characteristic, (b) power characteristic.

The transient measurements of the electronic power supplies show that when the voltage decreases the current drops to zero during a short while and then it increases to a new steady-state value. This is shown by the transient measurement for a computer power supply in Fig. 3.12. From the electric scheme in Fig. 3.13 it can be seen that when the supply voltage becomes lower than the voltage over the capacitor the diodes block the supply current and the load takes energy from the capacitor. When the capacitor voltage becomes less than the supply voltage, the supply current starts to increase to the new steady-state value. Since the voltage now is lower, the current must be higher since the load has CP characteristic. The time during which the supply current is zero and the rise time of the current are determined by the values of the components. The steady-state model can be calculated from the rated power of the load. For computer power supplies, which are not always operating at nominal power, measurement data can be used instead. Measurements must be done to determine the value of R, L and C in Fig. 3.13. The values of the components are chosen from standard

E-series. The resulting model parameters together with the operating range for electronic power supplies are reported in Table 3.6.

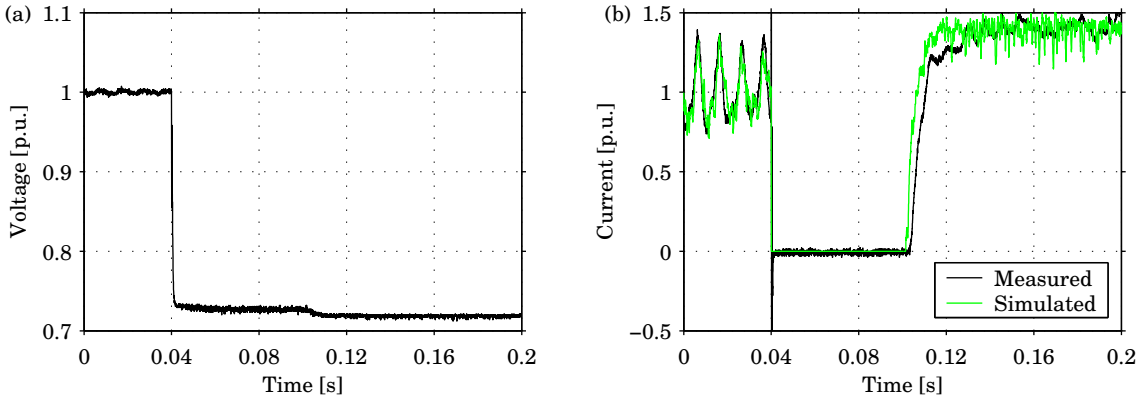

Fig. 3.12. Transient measurement and modeling of computer power supply (Dell): (a) voltage, (b) current during voltage step.

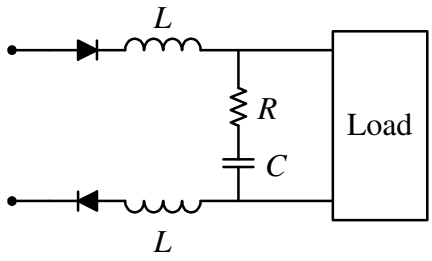

Fig. 3.13. Electric model of a power supply load.

3.5.2 Lighting Appliances

Electronics is more and more used in lighting appliances to increase the controllability of the lamp [56]. Dimmable fluorescent lamps and fluorescent lamps for emergency lighting for mentioning two examples. Two different types of lighting appliance using electronic power supply were tested: compact fluorescent lamps and fluorescent tubes with HF ballast. The compact fluorescent lamps have a simple electronic control compared with the HF ballast. The HF ballast can be designed to operate with both ac and dc (emergency lighting) [57]. Some HF ballast are designed to keep the light output at a constant level regardless of the voltage input, and others are designed to be dimmable; the light output is decreased when the supply voltage is decreased [58]. The load characteristic of the HF ballast may also change with the supply voltage level. All these controller designs make it very difficult to model the HF ballast with a simple model.

Eight compact fluorescent lamps were tested and the steady-state measurements show that they behave as constant current loads. The value of the current drawn by the lamp cannot be calculated from the nominal power, but must be determined by measurements. The operating range differs between the lamps. The resulting steady-state measurement of a compact fluorescent lamp (IKEA) is shown in Fig. 3.14.

Three different HF ballasts were tested. The steady-state measurements show that two of them have CP load characteristic and one has CC characteristic in the lower voltage interval

TABLE 3.6
MODEL PARAMETERS OF ELECTRONIC POWER SUPPLIES.

Load	P_{rated} [W]	Range [V]	Model $R = U^2/I_0$ [Ω]	Error [%]	Parameters
Chieftech computer power supply	350	200-380	$U^2/40$	20	$R = 7\ \Omega$ $L = 25$ mH $C = 350$ µF
Dell computer power supply	unknown	170-380	$U^2/43.5$	1.5	$R = 10\ \Omega$ $L = 1$ mH $C = 230$ µF
Macintosh computer power supply	87	150-380	$U^2/43.5$	4	$R = 10\ \Omega$ $L = 0.1$ mH $C = 230$ µF
Sirtech computer power supply	235	180-380	$U^2/37.9$	20	$R = 10\ \Omega$ $L = 25$ mH $C = 350$ µF
Ericsson battery charger	unknown	100-300	$U^2/6.7$	8.0	$R = 100\ \Omega$ $L = 2$ mH $C = 10$ µF
Ericsson battery charger	unknown	100-300	$U^2/6.9$	4.3	$R = 100\ \Omega$ $L = 2$ mH $C = 10$ µF
Ericsson battery charger	unknown	100-300	$U^2/8.05$	2.0	$R = 100\ \Omega$ $L = 2$ mH $C = 10$ µF
IP telephone (Grandstream)	unknown	100-380	$U^2/2.76$	24	$R = 150\ \Omega$ $L = 1$ mH $C = 11$ µF
LCD monitor (AOC)	32	130-330	$U^2/30$	1.2	$R = 100\ \Omega$ $L = 1$ mH $C = 70$ µF
Monitor (NCD)	unknown	200-350	$U^2/84$	3.8	$R = 1\ \Omega$ $L = 0.2$ mH $C = 300$ µF
Satellite receiver (Triasat)	unknown	200-350	$U^2/16.6$	4.8	$R = 50\ \Omega$ $L = 2$ mH $C = 50$ µF

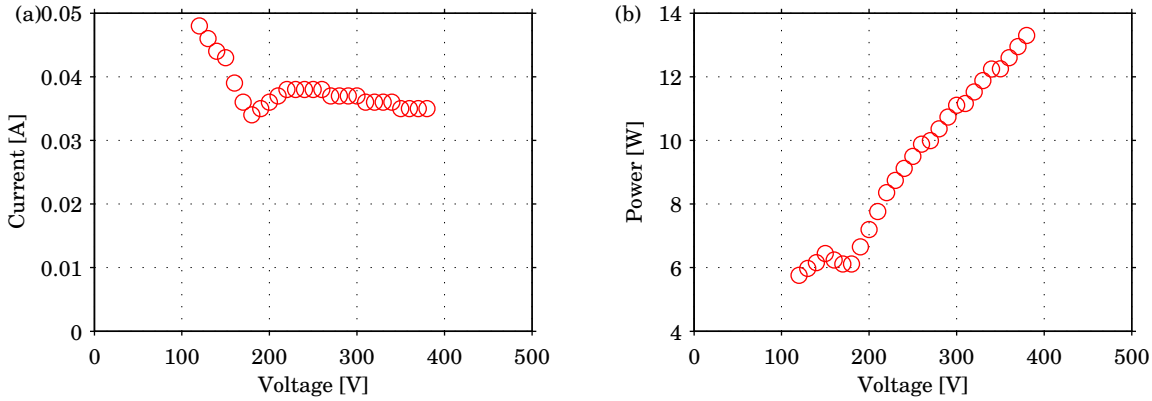

Fig. 3.14. Steady-state measurement of compact fluorescent lamp (IKEA): (a) resistance characteristic, (b) power characteristic.

and CP characteristic in the higher voltage range. The steady-state measurement of two HF ballasts are shown in Figs. 3.15 and 3.16.

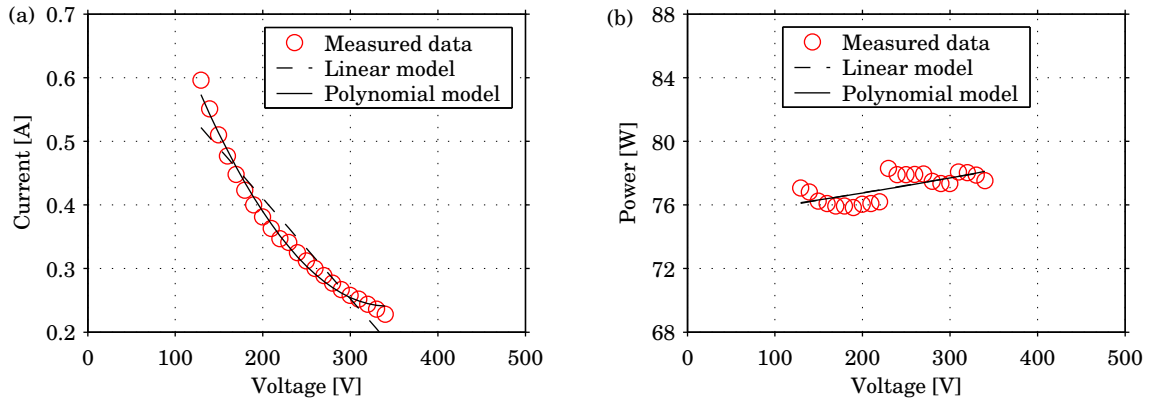

Fig. 3.15. Steady-state measurement of HF ballast (Tridonic) with CP load characteristic: (a) resistance characteristic, (b) power characteristic.

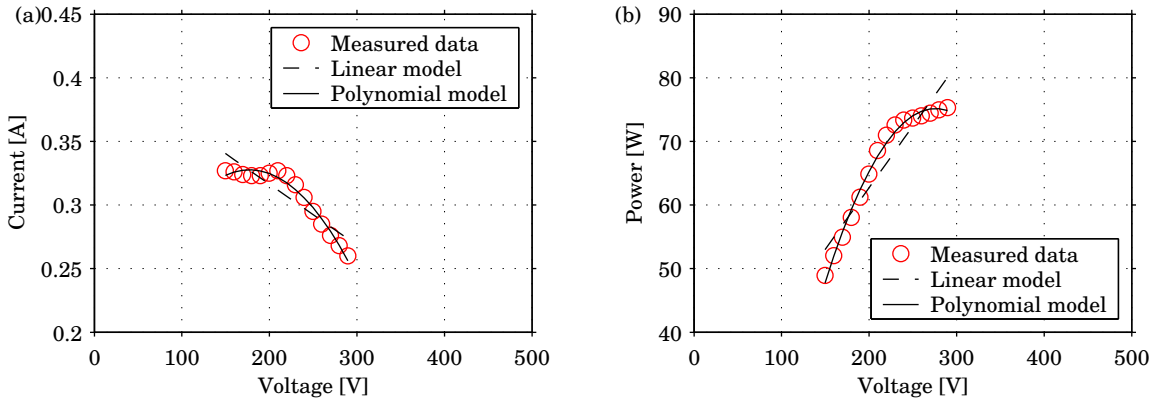

Fig. 3.16. Steady-state measurement of HF ballast (Philips) with CC and CP load characteristic: (a) resistance characteristic, (b) power characteristic.

The transient measurement of a compact fluorescent lamp (IKEA) is shown in Fig. 3.17. It shows how simple the design of the electronic is. When the voltage decreases the current

becomes zero during a short while and then it returns to the same value. The time the supply current is zero is determined by the size of the capacitor, and the rise time of the current is set by the resistor. There is no oscillation present in the current when it comes back, which indicates that there are no inductive components present.

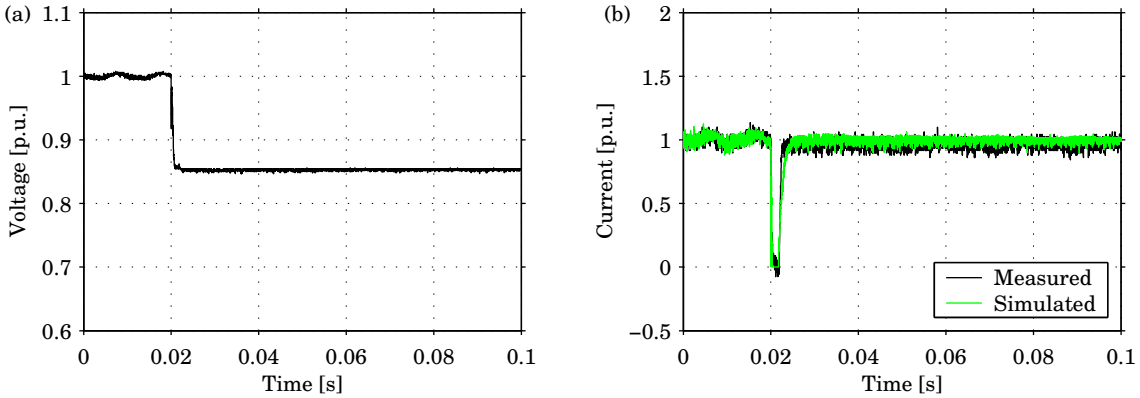

Fig. 3.17. Transient measurement and modeling of compact fluorescent lamp (IKEA): (a) voltage, (b) current during voltage step.

The HF ballasts seemed to have a more complicated transient responses, which were difficult to realize with standard electrical components. The complicated step response is due to the control circuit and its design. One of the HF ballast (Philips) can be modelled with an RLC-circuit together with the steady-state model extended with a time constant. The transient measurement of the Philips ballast and the resulting model is shown in Fig. 3.18, and the fast current transient is shown in Fig. 3.19. The measurement of the other two ballasts can only be reproduced by using a mathematical model of a second-order system with a damped oscillation. The transient measurement of the Tridonic ballast and its mathematical model are shown in Fig. 3.20. The model parameters obtained for lighting appliances are reported in Table 3.7. The characteristic and design of the ballasts vary from model to model, and measurements are required to determine the steady-state and transient model parameters.

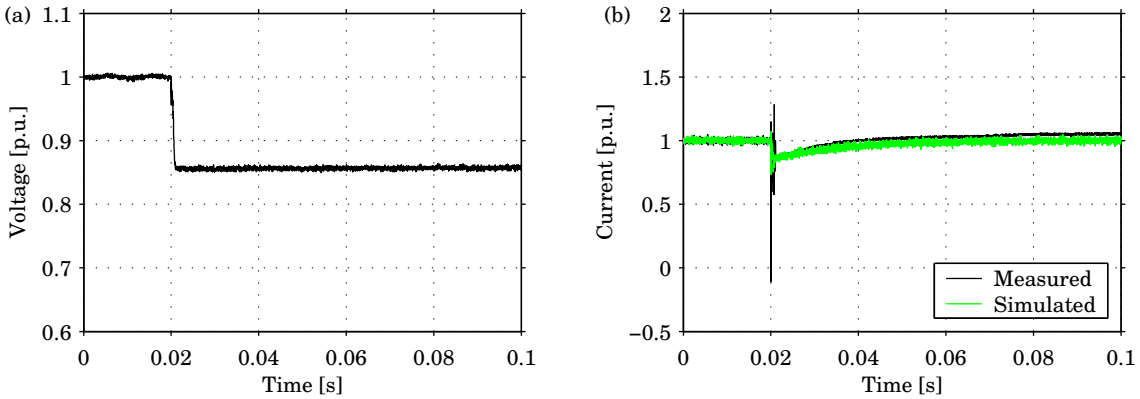

Fig. 3.18. Transient measurement and modeling of HF ballast (Philips): (a) voltage, (b) current during voltage step.

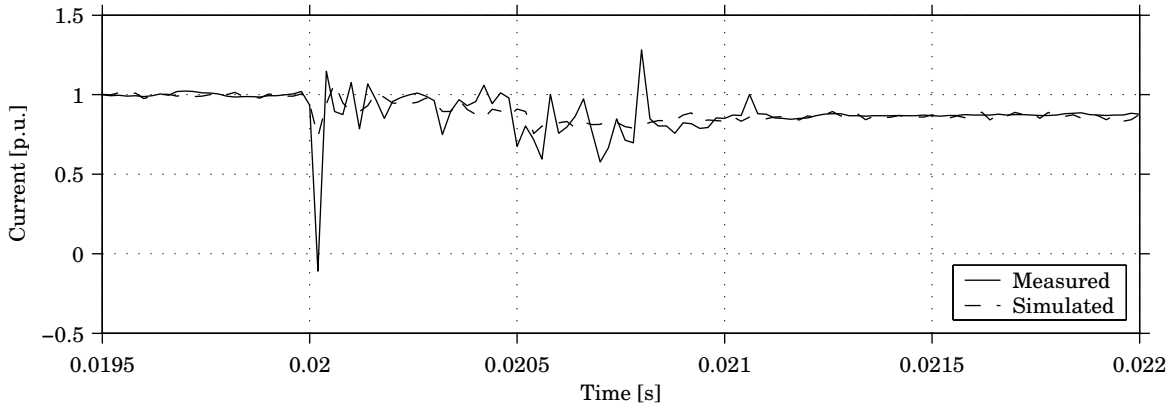

Fig. 3.19. Zoom of transient current measurement and modeling of HF ballast (Philips) during voltage step.

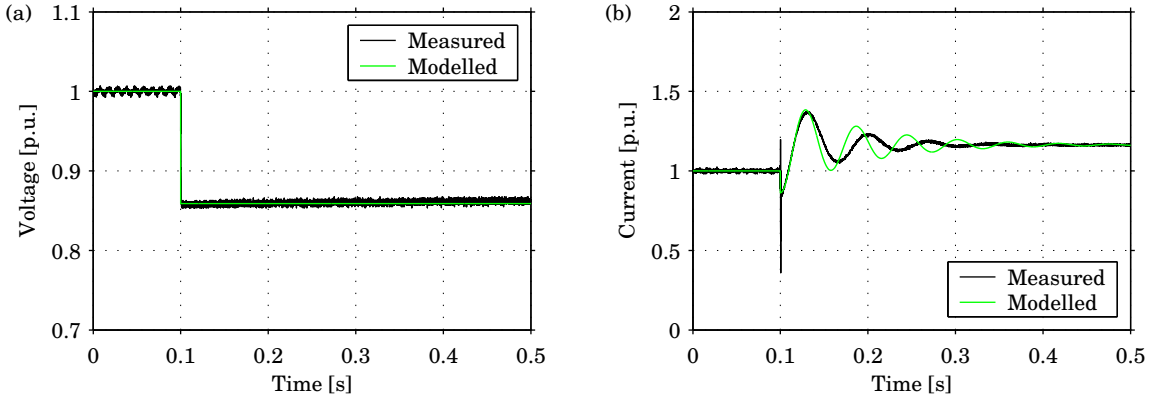

Fig. 3.20. Transient measurement and modeling of HF ballast (Tridonic): (a) voltage, (b) current during voltage step.

3.6 Conclusions

In this chapter, load modeling for transient and steady-state analysis of low-voltage dc systems has been carried out. The aim was to investigate whether it is possible to supply existing low-voltage ac loads with dc, and within which range. The second part was, if possible, to develop models of the loads to be used for dynamic studies of low-voltage dc systems.

The resistive loads were divided into two groups: heaters and lighting. Heater loads worked with dc in the tested range, and can be modeled as a pure resistance. The value of the resistance can be calculated from the nominal power. Lighting loads work also well with dc. The resistance of the lighting loads are dependent of the current, so they can be modeled as a current-dependent resistance with a time constant. To model a lighting load measurements are required, since it is not possible to determine the current-dependent resistance from the nominal power.

Rotating loads work also well with dc if the machine is a universal machine or a single phase supplied variable speed drive. A universal machine will run a little bit faster if it is supplied with dc instead of ac, since the impedance is lower. A steady-state model of the universal machine is a voltage-dependent current source, which is calculated from measurements. To model the transient, a mathematical model based on measurements can be used.

TABLE 3.7
MODEL PARAMETERS FOR ELECTRONIC LOADS USED FOR LIGHTING.

Load	P_{rated} [W]	Range [V]	Model $R = U^2/I_0$ or $R = U/I_0$ [Ω]	Error [%]	Parameters
Eurolight	9	100-300	$U/0.029$	7.5	$R = 200\ \Omega$ $L = 0$ mH $C = 3.5$ µF
Ikea	11	190-380	$U/0.038$	2.1	$R = 300\ \Omega$ $L = 0$ mH $C = 2.7$ µF
Osram	23	120-300	$U/0.067$	10	$R = 300\ \Omega$ $L = 0$ mH $C = 4.7$ µF
Philips	9	120-300	$U/0.035$	1.2	$R = 100\ \Omega$ $L = 0$ mH $C = 3.3$ µF
Philips	11	120-300	$U/0.041$	4.3	$R = 100\ \Omega$ $L = 0$ mH $C = 3.3$ µF
Philips	15	140-280	$U/0.057$	15	$R = 100\ \Omega$ $L = 0$ mH $C = 12$ µF
Sylvania	10	100-300	$U/0.046$	1.1	$R = 200\ \Omega$ $L = 0$ mH $C = 4.7$ µF
Philips	72	150-220 220-280	$U/0.325$ $U^2/70.5$	1.2 6.8	$\tau = 0.15$ s $R = 100\ \Omega$ $C = 0.5$ µF
Tridonic	72	130-340	$U^2/75$	-	-
Tridonic (Dimmable)	70.4	110-380	$U^2/58.1$	-	-

TABLE 3.8
SUMMARY OF STEADY-STATE LOAD MODELS.

	Load	Model	Parameters
Resistive loads	Heating	$R = R_0$	R_0 from rated power
	Lighting	$R = R_1 I + R_0$	R_0 from rated power R_1 from measurements
Rotating loads	Universal machines	$I = Y_0 U + I_0$	I_0 from measurements Y_0 from measurements
Electronic loads	Power supply	$R = U^2/I_0$	I_0 from measurements
	Lighting	$R = U/I_0$	I_0 from measurements

The electronic loads were divided into two groups: power supply and lighting. The power supplies showed a CP characteristic. They operate with dc, but the range in which they do varies. The transient model of power supplies is a diode rectifier, an RLC circuit and the load characteristic. The load characteristic can in most cases be determined from the nominal power, but the RLC circuit requires measurements. The compact fluorescent lamps showed CC characteristic, which together with the RC circuit must be calculated from measurements. The steady-state characteristic of the HF ballast varied from design to design and can only be determined from measurements. For some HF ballasts it was not possible to realize a transient model with an electric circuit, but the transient response could be mathematically described from measurements. Finally, an overview of the steady-state models are presented in Table 3.8.

Chapter 4

Voltage Source Converter and its Control

In this project, the two-level three-phase VSC connected in series with a Buck converter was chosen as the ac/dc interface. It can have a wide range of dc output voltage, which makes it suitable in a laboratory setup. In this chapter, the control of the VSC is presented.

4.1 Introduction

A two-level three-phase VSC, described earlier in Section 2.4.3, is used to convert dc to ac voltage with variable magnitude, frequency and phase, or ac to dc voltage with variable magnitude. The advantages with a VSC compared with other types of rectifiers described in Section 2.4.3 are controllable dc voltage, sinusoidal grid currents and bi-directional power flow. The VSC connected to the ac system through an L-filter, shown in Fig. 4.1, consists of six IGBT valves and a dc-link capacitor. Seen from the ac side, a VSC can be considered as

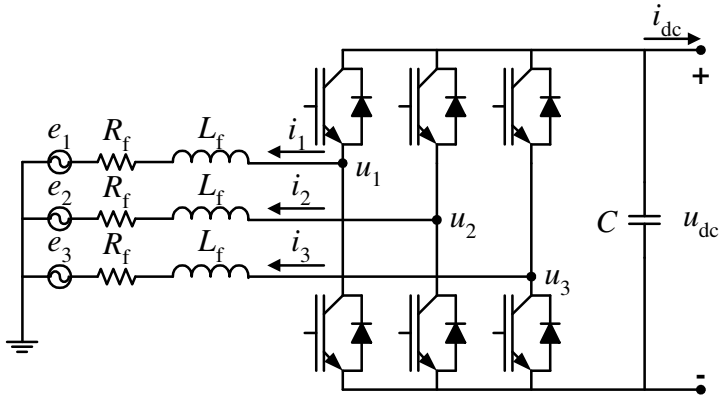

Fig. 4.1. A three-phase VSC connected through an L-filter to an ac grid.

a voltage source with variable frequency, magnitude and phase. A single-line diagram of a VSC connected to the ac grid is shown in Fig. 4.2. By controlling the output voltage of the VSC, u, the transmitted active power p and reactive power q can be individually controlled

according to

$$\begin{aligned} p &= \frac{|u|^2}{|Z|}\cos\epsilon - \frac{|u||e|}{|Z|}\cos(\epsilon+\varphi) \\ q &= \frac{|u|^2}{|Z|}\sin\epsilon - \frac{|u||e|}{|Z|}\sin(\epsilon+\varphi) \end{aligned} \tag{4.1}$$

where e is the grid voltage, R_f is the filter resistance, L_f is the filter inductance, $Z = R_\mathrm{f} + \mathrm{j}2\pi f_\mathrm{g} L_\mathrm{f}$ is the line impedance, f_g is the frid frequency, ϵ is $\arg(Z^*)$ and φ is the transmission angle.

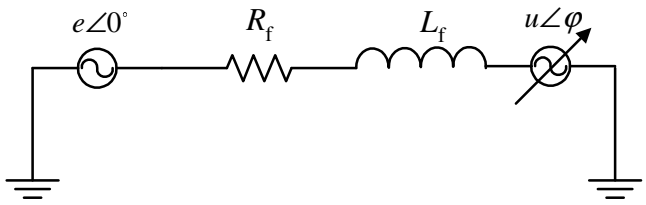

Fig. 4.2. Single-phase equivalent scheme of a VSC connected to an ac grid.

The following sections describe how to calculate and generate the necessary output voltage of the VSC to transfer the demanded active and reactive power. In a digital control system, the reference values for the output phase voltages are calculated from the input reference values, which can be active and reactive power transfer demand. The aim of the control system of the VSC used as a rectifier is to maintain high power quality on the ac side, and a stable voltage on the dc side under both steady state operation and disturbances. The control system measures the three phase voltages and currents, and the dc-link voltage and current. The reference phase voltages to the analogue system are calculated from the sampled values together with the reference value to the *Pulse Width Modulation* (PWM) [59]. In the first controller step, the dc-link voltage controller (DCC) calculates a current reference which is used by the vector current controller (VCC) which in turn calculates the voltage references. The control system is shown in Fig. 4.3. The measured quantities are sampled with a constant frequency f_s. The sampled ac quantities are transformed to $\alpha\beta$- and dq-components, using Clarke and Park transformation, respectively. The transformation angle θ is determined by using a phase-locked loop (PLL) [60]. In Section 4.2 PWM, is explained; in Section 4.3, the vector current controller is analyzed; in Section 4.4, the three dc-link-voltage controllers are analyzed.

4.2 Pulse Width Modulation

A two-level three-phase VSC has three phase legs, where each phase leg has two IGBT valves. One valve is connected to the plus pole and the other is connected to the minus pole of the dc link. Having three phase legs results in eight different switching states. The eight switching states can be visualized as a hexagon in the $\alpha\beta$-plane, as shown in Fig. 4.4 [49]. Each switching state is denoted by the state of each phase leg (‘1’ means that the switch connected to plus is on and ‘-1’ means that the switch connected to minus is on). Switching states 0 (-1,-1,-1) and 7 (1,1,1), which both results in a zero output voltage vector, are the origin.

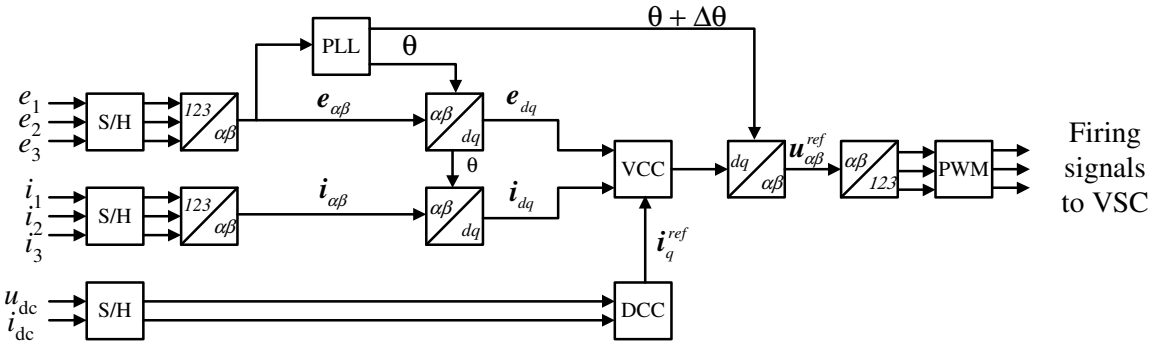

Fig. 4.3. Block scheme of VSC control system.

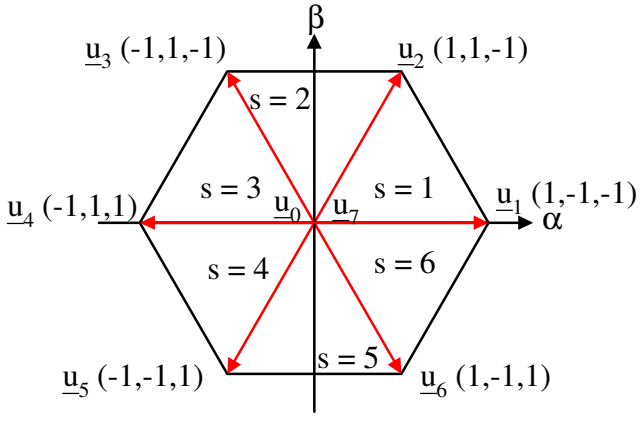

Fig. 4.4. The eight switching states of a two-level three-phase VSC.

An output ac voltage with fixed magnitude can be generated by utilizing the eight switching states. All six switches have a duty ratio equal to 0.5, and the magnitude of the ac voltage can be changed by changing the dc-link voltage. The disadvantages with a converter operating in *square wave*, which this operation mode is called, are that the output voltage contains low-frequency harmonics [61]. A variable output ac voltage is obtained by controlling the time each of the six IGBT valves is on during one switching period. This will result in a voltage vector inside the hexagon. By combining the eight switching states, any voltage vector inside the hexagon can be generated. A voltage vector inside each sector of the hexagon can be generated by controlling the time during which the two vectors limiting the sector, together with zero vector are on. For example, a voltage vector inside sector $s = 4$ is obtained by utilizing state $\underline{u}_4$, $\underline{u}_5$ and $\underline{u}_0$. This is called *state space modulation*. It is possible with state space modulation to reduce the low-order harmonics [46]. A simpler way to determine the on time of the switch is to compare the reference voltage signal for each phase with a triangular wave, which has its peak value equal to half the dc-link voltage. By comparing the three reference signals and the triangular signals, three pulse patterns are obtained, which are used to control the IGBTs in the three phase legs of the VSC. When the voltage reference value is lower than the triangular wave, the IGBT connected to the plus pole conducts, and when the reference value is higher than the triangular wave, the IGBT connected to the minus pole conducts. The output voltage for each leg reproduces the pulse pattern, and its fundamental component is equal to the reference signal. By changing the width of the pulses to the IGBTs, the output voltage is varied, and therefore this is called Pulse Width Modulation [62].

The dc-link voltage and the reference values are sampled and used to generate the triangular wave and the reference signals, which are compared to determine the firing pulses. The sampling can be done once per switching period (this is called *regular-sampled symmetric PWM*) or twice per switching period (this is called *regular-sampled asymmetric PWM*). Fig. 4.5 shows an example of how the switching pattern is generated for a sinusoidal reference signal using asymmetric regular sampled voltages [63].

The fundamental component of the PWM signal equals the desired ac voltage. The modulation technique and the switching frequency influence the harmonic content of the obtained output voltage. Using PWM reduces the low-order harmonics: harmonic components are concentrated at the switching frequency and its side bands, and at multiples of the switching frequency [46]. High switching frequency allows smaller filters to filter the harmonics, but increases the switching losses in the converter. Therefore, moderate switching frequency are chosen for high-power applications [59].

The maximum output voltage is a vector inside the hexagon, and if the voltage vector becomes larger this is called *overmodulation* (OVM). By limiting the voltage vector inside a circle inscribed in the hexagon, it is possible to reduce the low-order harmonics in the output voltage. This will give a maximum sinusoidal phase-to-phase voltage with a magnitude equal to $u_{\mathrm{dc}}\sqrt{1/2}$ using power invariant Clarke-transformation [64]. Using the technique which compares the reference signal with the triangular wave will limit the maximum sinusoidal voltage to $\frac{u_{\mathrm{dc}}}{2}\sqrt{3/2}$. By choosing the right modulation technique 0.15 p.u. can be gained. Adding a zero sequence to the reference signals, which decreases the peak value of the reference signal makes it possible to use the additional 0.15 p.u.. This modulation technique is called *optimized PWM* [62]. This zero sequence must be prevented to flow in the system and there are two ways to block it; the first way is to have the dc-link ungrounded, and the second way is to prevent the zero sequence to flow on the ac side. One method is to use a delta-wye transformer, which blocks the zero sequence.

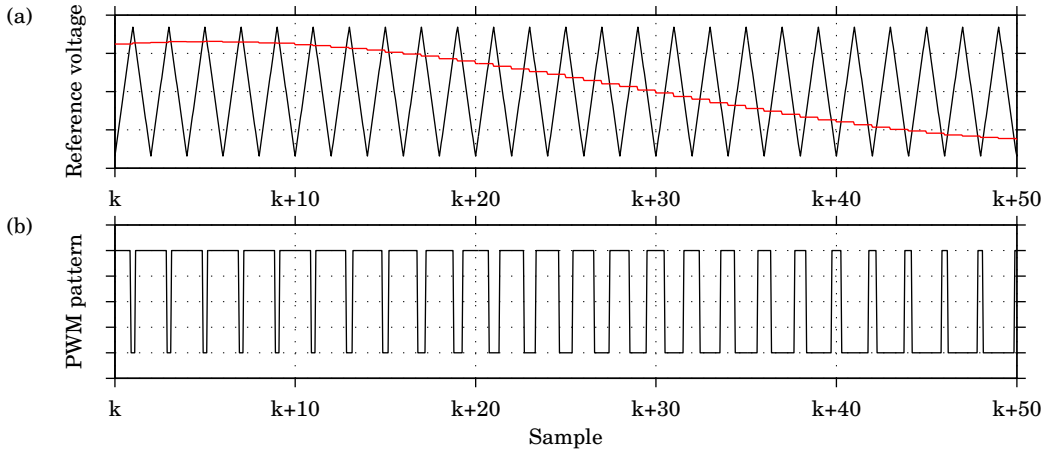

Fig. 4.5. Pulse width modulation (PWM): (a) regular sampled reference signal and triangular wave, (b) corresponding PWM pattern.

4.3 Vector Current Control

The current control system adopted here uses a vector controller implemented in the synchronous dq-coordinate system, where the symmetrical ac quantities appear as dc quantities [49]. From Fig. 4.1, the following equations can be derived

$$\begin{aligned} u_1(t) - e_1(t) - R_\mathrm{f} i_1(t) - L_\mathrm{f}\frac{\mathrm{d}i_1(t)}{\mathrm{d}t} &= 0 \\ u_2(t) - e_2(t) - R_\mathrm{f} i_2(t) - L_\mathrm{f}\frac{\mathrm{d}i_2(t)}{\mathrm{d}t} &= 0 \\ u_3(t) - e_3(t) - R_\mathrm{f} i_3(t) - L_\mathrm{f}\frac{\mathrm{d}i_3(t)}{\mathrm{d}t} &= 0. \end{aligned} \tag{4.2}$$

These three equations can be transformed into the $\alpha\beta$- and dq reference frame. The $\alpha\beta$-transformation is power invariant and the dq-transformation is made in a flux oriented system. After these two transformations, (4.2) becomes

$$L_\mathrm{f}\frac{\mathrm{d}\boldsymbol{i}_{dq}(t)}{\mathrm{d}t} = \boldsymbol{u}_{dq}(t) - (R_\mathrm{f} + \mathrm{j}\omega L_\mathrm{f})\boldsymbol{i}_{dq}(t) - \boldsymbol{e}_{dq}(t). \tag{4.3}$$

The calculation time of the digital control system is one sample, which means that the digital controller will be one sample after the real system. To run the system with high gain without having instability, the delay time must be compensated. One method is to use a state observer which can predict the grid currents for the next sample. Using a Smith Predictor [65], the predicted current $\hat{\boldsymbol{i}}_{dq}$ is calculated by using Forward Euler Method

$$\hat{\boldsymbol{i}}_{dq}[k+1] = \left(1 - \frac{R_\mathrm{f} T_\mathrm{s}}{L_\mathrm{f}} - \mathrm{j}\omega T_\mathrm{s}\right)\hat{\boldsymbol{i}}_{dq}[k] + \frac{T_\mathrm{s}}{L_\mathrm{f}}(\boldsymbol{u}_{dq}[k] - \boldsymbol{e}_{dq}[k]) + K(\boldsymbol{i}_{dq}[k] - \hat{\boldsymbol{i}}_{dq}[k]) \tag{4.4}$$

where K is the observer gain and T_s is the sampling time. From (4.3), a discrete time PI-controller can be derived with the following expression [49]

$$\begin{aligned} u_d^{\mathrm{ref}}[k] &= e_d[k] + R_\mathrm{f} i_d[k] - \frac{\omega L_\mathrm{f}}{2}(i_q[k] + i_q^{\mathrm{ref}}[k]) \\ &\quad + k_\mathrm{p}(i_d^{\mathrm{ref}}[k] - i_d[k] - \hat{i}_d[k-1] + \hat{i}_d[k]) + \Delta u_{\mathrm{i}d}[k] \\ u_q^{\mathrm{ref}}[k] &= e_q[k] + R_\mathrm{f} i_q[k] + \frac{\omega L_\mathrm{f}}{2}(i_d[k] + i_d^{\mathrm{ref}}[k]) \\ &\quad + k_\mathrm{p}(i_q^{\mathrm{ref}}[k] - i_q[k] - \hat{i}_q[k-1] + \hat{i}_q[k]) + \Delta u_{\mathrm{i}q}[k] \end{aligned} \tag{4.5}$$

and the integral error is equal to

$$\begin{aligned} \Delta u_{\mathrm{i}d}[k] &= \Delta u_{id}[k-1] + k_\mathrm{i}(i_d^{\mathrm{ref}}[k-2] - i_d[k] - \hat{i}_d[k-1] + \hat{i}_d[k]) \\ \Delta u_{\mathrm{i}q}[k] &= \Delta u_{iq}[k-1] + k_\mathrm{i}(i_q^{\mathrm{ref}}[k-2] - i_q[k] - \hat{i}_q[k-1] + \hat{i}_q[k]) \end{aligned} \tag{4.6}$$

where k_p is the proportional gain and k_i the integral gain. To obtain dead-beat gain, which means that the sampled current at time $k+2$ equals the reference current at time k, the controller parameters have to be selected as [49]

$$\begin{aligned} k_\mathrm{p} &= \frac{L_\mathrm{f}}{T_\mathrm{s}} + \frac{R_\mathrm{f}}{2} \\ k_\mathrm{i} &= \frac{k_\mathrm{p} T_\mathrm{s} R_\mathrm{f}}{L_\mathrm{f}}. \end{aligned} \tag{4.7}$$

The feed-forward voltage terms in (4.5) can be written as

$$\begin{aligned} u_d^{\mathrm{ff}}[k] &= e_d[k] + R i_d[k] - \frac{\omega L_\mathrm{f}}{2}(i_q[k] + i_q^{\mathrm{ref}}[k]) \\ u_q^{\mathrm{ff}}[k] &= e_q[k] + R i_q[k] + \frac{\omega L_\mathrm{f}}{2}(i_d[k] + i_d^{\mathrm{ref}}[k]). \end{aligned} \tag{4.8}$$

A scheme of the current controller is shown in Fig. 4.6. The performance of the controller

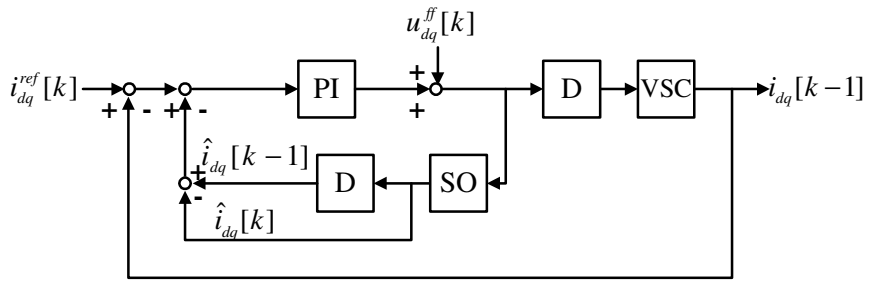

Fig. 4.6. Current control system with a state observer. $\boldsymbol{u}_{dq}^{\mathrm{ff}}[k]$ is the feed-forward term, D denotes one sample delay, and VSC denotes the system.

was simulated in PSCAD/EMTDC, and tested in a laboratory setup, which is described in Chapter 6. The VSC is connected to a stiff ac grid and supplied with a stiff dc source. The parameters of the laboratory system in Table 4.1 were used in the simulations.

TABLE 4.1
PARAMETERS OF A VSC SYSTEM.

Grid voltage	E	325 V	1.0 p.u.
Grid current	I	5.8 A	1.0 p.u.
DC-link voltage	U_{dc}	650 V	1.0 p.u.
Filter resistance	R_{f}	0.213 Ω	0.0038 p.u.
Filter inductance	L_{f}	15 mH	0.0841 p.u.
Grid frequency	f_{g}	50 Hz	
Sampling frequency	f_{s}	5 kHz	

The vector current controller with a Smith Predictor was tested both with a step in the active current i_q and the reactive current i_d. The observer gain K was set to 0.1. The simulation of a step in i_q from 0 to -0.7 p.u. is shown in Fig. 4.7, which shows that the current reference value is reached after two samples. The corresponding measurement is shown in Fig. 4.8. The measured values contain noise with an amplitude of 0.03 p.u., which results in a longer time before the current reaches the reference value. The response of the system due to the step in i_d from 0 to 0.56 p.u. is shown in Figs. 4.9 and 4.10. Also here the influence of the noise is visible.

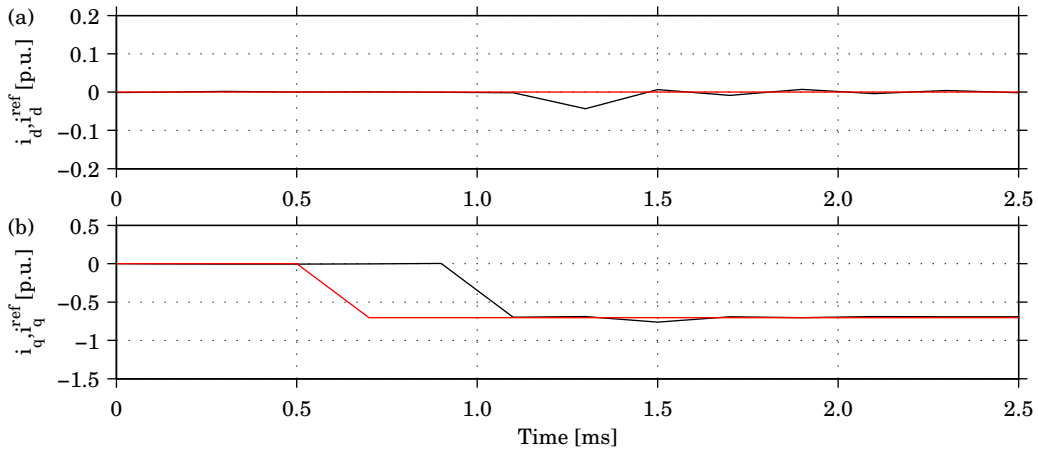

Fig. 4.7. Simulation result current controller with Smith predictor: step i_q from 0 to -0.7 p.u..

The maximum output voltage of the VSC is determined by the hexagon in the $\alpha\beta$-plane. If the output reference voltage $u_{\alpha\beta}^{\mathrm{ref}}$ is limited to $\bar{u}_{\alpha\beta}^{\mathrm{ref}}$, which stays inside the circle inside the hexagon, shown in Fig. 4.11, low-frequency harmonics can be reduced [65]. Different strategies to limit the voltage vector have been discussed in [64]. The size of the hexagon, and thereby the radius of the circle, is determined by the dc-link voltage. A current control system with voltage limitation is shown in Fig. 4.12. During voltage limitation the integral error of the current is limited to avoid wind up of the integral part of the controller. Using back calculation of the integral error will increase the performance of the controller, and is described by [65]

$$\Delta\hat{\boldsymbol{i}}_{dq}[k] = \boldsymbol{i}_{dq}^{\mathrm{ref}}[k] - \hat{\boldsymbol{i}}_{dq}[k] + \hat{\boldsymbol{i}}_{dq}[k-1] - \boldsymbol{i}_{dq}[k-1] + \frac{1}{k_{\mathrm{p}}}(\overline{\boldsymbol{u}}_{dq}^{\mathrm{ref}}[k] - \boldsymbol{u}_{dq}^{\mathrm{ref}}[k]) \tag{4.9}$$

A step in i_q from 0 to 0.7 p.u., which results in OVM, was applied to test the performance of the current controllers, both with simulation and measurement. Using a current controller

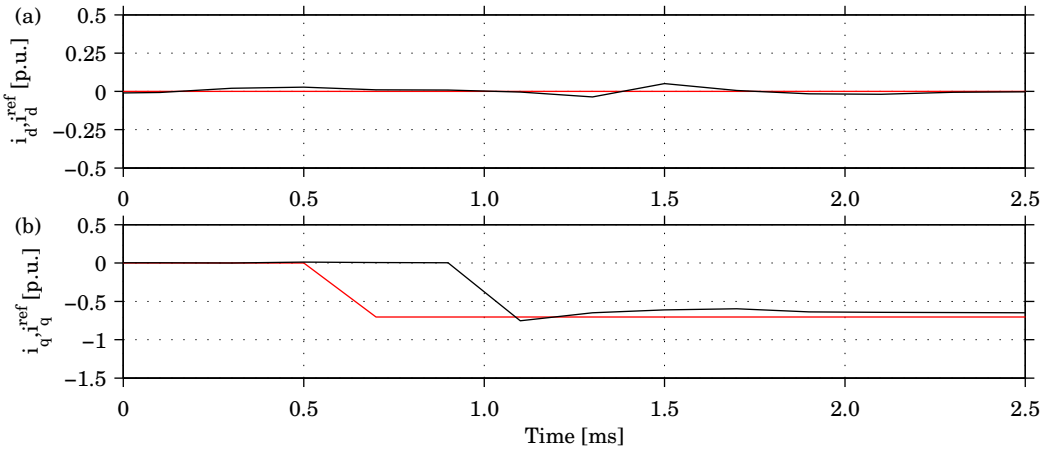

Fig. 4.8. Measurement result current controller with Smith predictor: step i_q from 0 to -0.7 p.u..

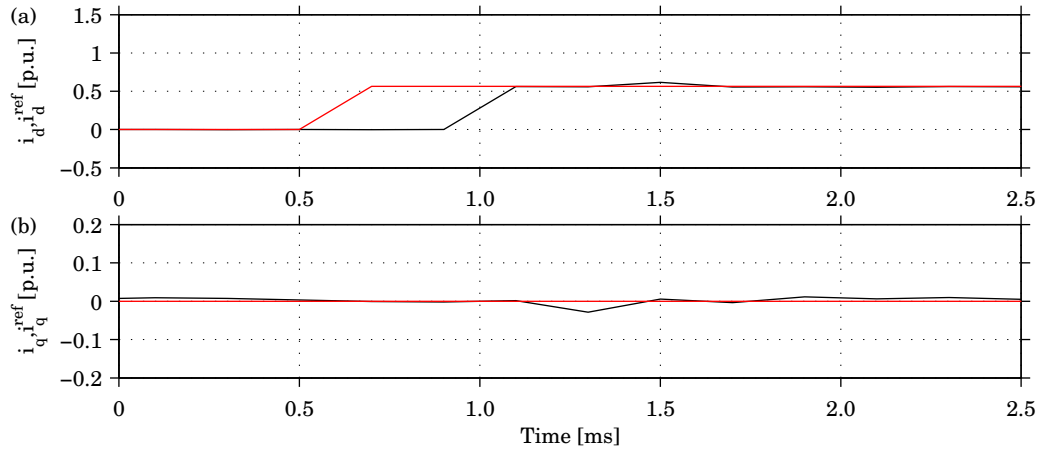

Fig. 4.9. Simulation result current controller with Smith predictor: step i_d from 0 to 0.56 p.u.

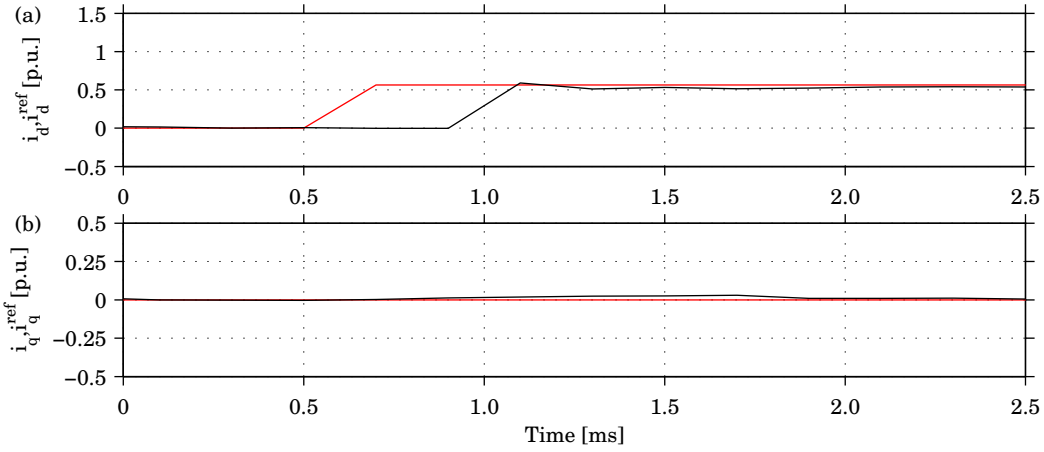

Fig. 4.10. Measurement result current controller with Smith predictor: step i_d from 0 to 0.56 p.u.

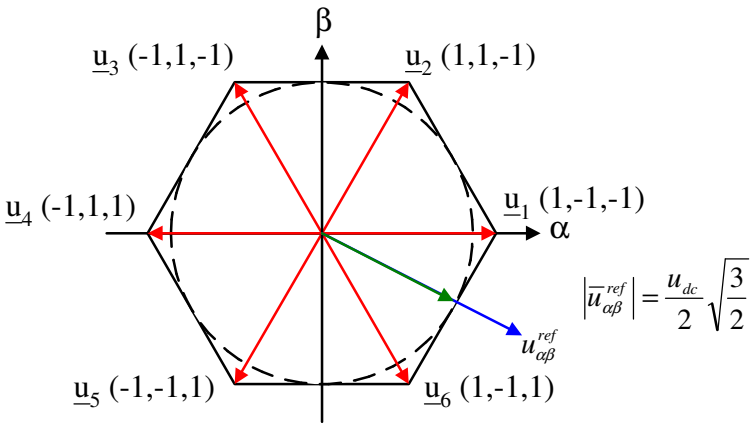

Fig. 4.11. Reference voltage $\boldsymbol{u}^{\text{ref}}_{\alpha\beta}$ and limited reference voltage $\bar{\boldsymbol{u}}^{\text{ref}}_{\alpha\beta}$ to avoid OVM.

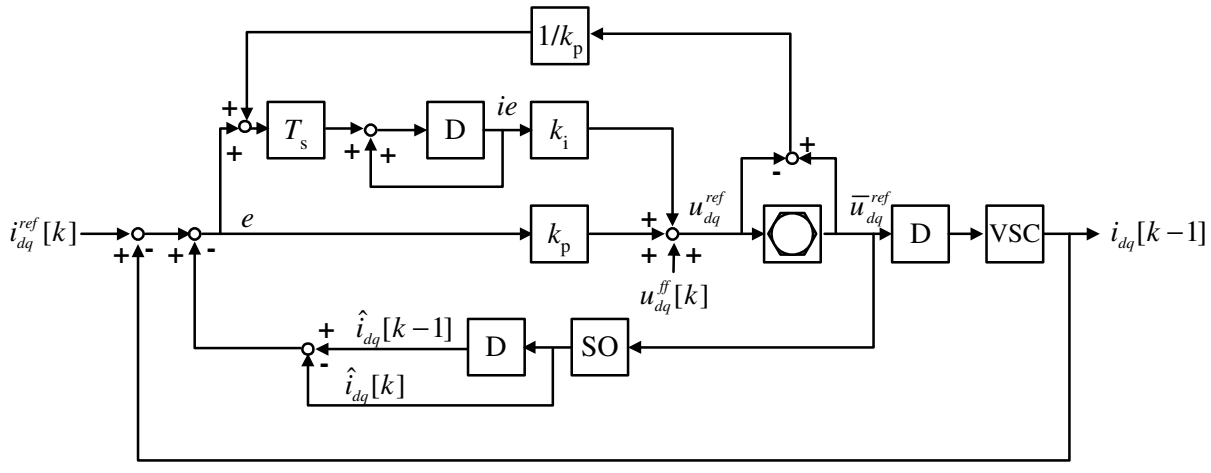

Fig. 4.12. Current control system improved by a Smith Predictor (SO), voltage limitation and back calculation. $\boldsymbol{u}^{\text{ff}}_{dq}[k]$ is the feed-forward term, D denotes one sample delay, and VSC denotes the system.

with a Smith Predictor has a slow response, an overshoot and a large cross coupling, which can be seen in Figs. 4.13 and 4.14. The second current controller with Smith predictor, voltage limitation and back calculation has a faster response, no overshoot and no cross coupling. The simulation and measurement results are shown in Figs. 4.15 and 4.16. The simulation results for the two current controllers are compared in Fig. 4.17, which shows that extending the current controller with voltage limitation and back calculation improves its transient performance.

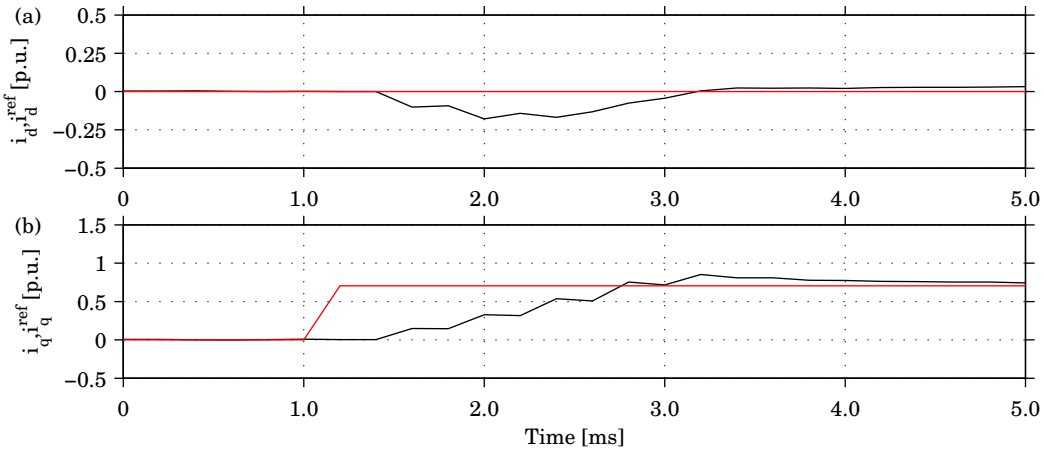

Fig. 4.13. Simulation result of current controller with Smith Predictor: step i_q from 0 to 0.7 p.u.

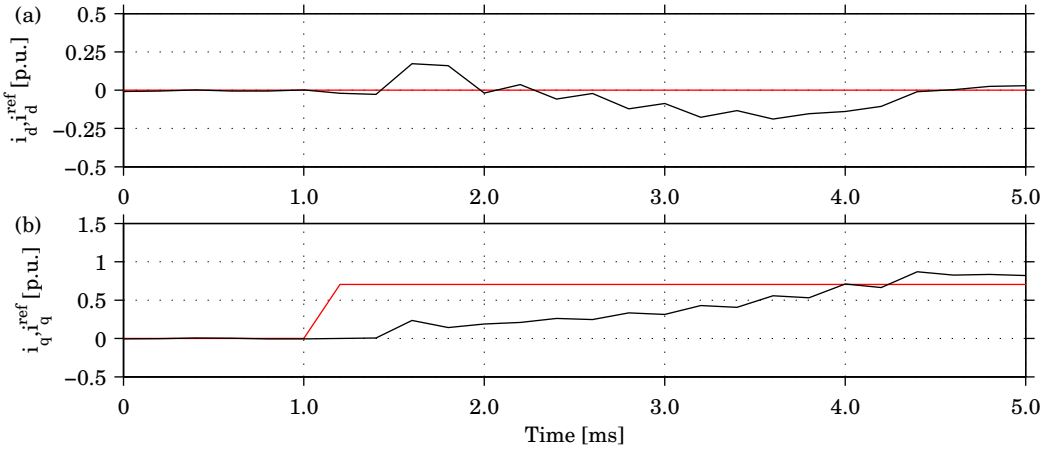

Fig. 4.14. Measurement result of current controller with Smith Predictor: step i_q from 0 to 0.7 p.u.

4.4 DC-Link-Voltage Control

When using the VSC as a rectifier the dc-link voltage is not stiff, but it must be controlled and this is achieved by controlling the active current i_q. The dc-link-voltage controller calculates the reference value of the active current i_q^{ref} which is forwarded to the current controller. In this section, three different types of dc-link voltage controllers are analyzed; one using the dc-link voltage only, one using the dc-link voltage and the measured dc load current, and one using the dc-link voltage and an observer for the dc load current.

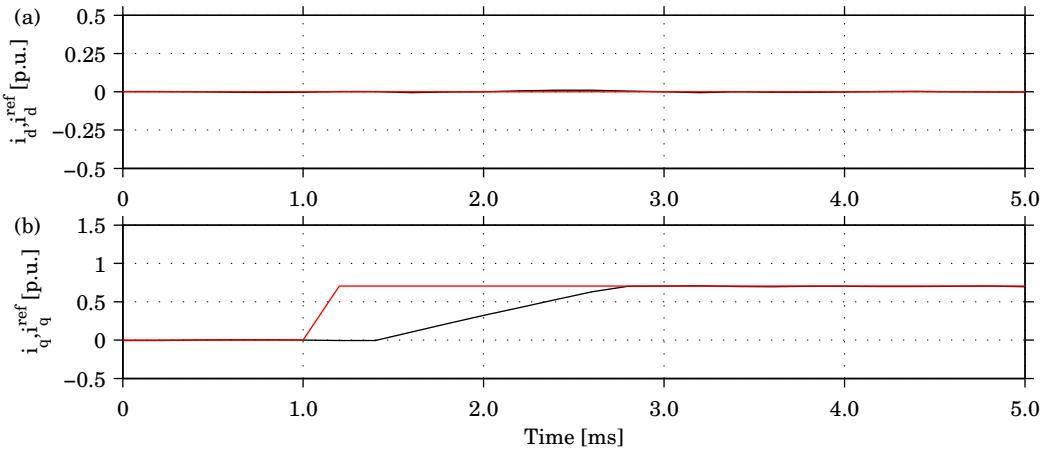

Fig. 4.15. Simulation result of current controller with Smith predictor, voltage limitation and back calculation: step i_q from 0 to 0.7 p.u.

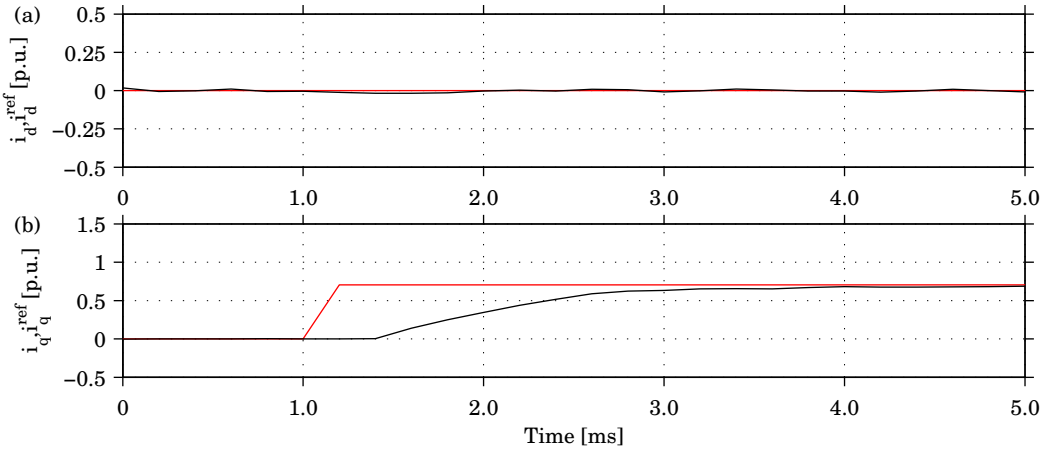

Fig. 4.16. Measurement result of current controller with Smith Predictor, voltage limitation and back calculation: step i_q from 0 to 0.7 p.u.

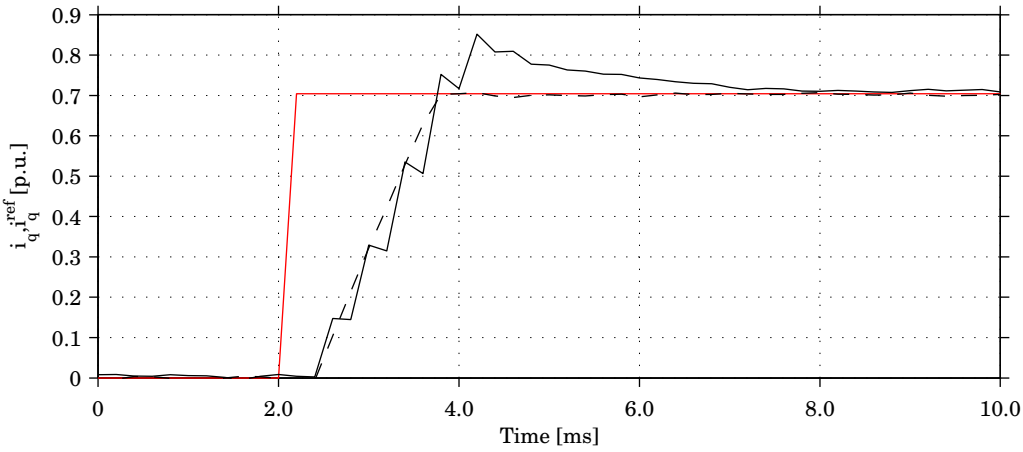

Fig. 4.17. Simulation result for current controller with Smith Predictor (solid) and current controller with Smith Predictor, voltage limitation and back calculation (dashed).

4.4.1 Energy-Balance DC-Link-Voltage Controller

The energy-balance dc-link voltage controller (EB) origins from the relation between energy change and voltage of a capacitor [66]. The sum of the power flowing out of the dc link must equal the change of energy stored in the capacitor $w_{\mathrm{c}}(t)$, which is described by

$$\frac{\mathrm{d}w_{\mathrm{c}}(t)}{\mathrm{d}t} = -p_{\mathrm{ac}}(t) - p_{\mathrm{dc}}(t) \tag{4.10}$$

where p_{ac} is the ac power, and p_{dc} is the dc power, both flowing out from the capacitor. The energy in a capacitor is equal to

$$w_{\mathrm{c}}(t) = \frac{1}{2} C u_{\mathrm{dc}}^2(t). \tag{4.11}$$

Substituting u_{dc}^2 with W gives

$$\frac{1}{2} C \frac{\mathrm{d}W(t)}{\mathrm{d}t} = -p_{\mathrm{ac}}(t) - p_{\mathrm{dc}}(t). \tag{4.12}$$

The power p_{ac} is equal to $e_q i_q$ and the transfer function from i_q to W then becomes

$$G(s) = -\frac{2e_q}{sC}. \tag{4.13}$$

The process has a pole in the origin, which makes it stable but undamped. This motivates adding a virtual resistance G_{a}, which will give an active damping and modifies the current to

$$i_q = i_q' + G_{\mathrm{a}} W. \tag{4.14}$$

The transfer function from i_q' to W becomes

$$G'(s) = -\frac{2e_q}{sC + 2e_q G_{\mathrm{a}}}. \tag{4.15}$$

The system can be represented by Fig. 4.18. If the closed loop system is chosen to be a first order system with bandwidth α, and the dc load is treated as a disturbance D with the same bandwidth as the closed loop system, the control parameters can be selected as in

$$\begin{aligned} k_{\mathrm{p}} &= -\frac{\alpha C}{2e_q} \\ k_{\mathrm{i}} &= -\frac{\alpha^2 C}{e_q} \\ G_{\mathrm{a}} &= \frac{\alpha C}{e_q}. \end{aligned} \tag{4.16}$$

The bandwidth of the dc-link-voltage controller shall be selected to be at least one decade slower than the inner current controller, which has a 5 kHz bandwidth. Fig. 4.19 shows how the poles move on the real axis, which results in a well damped system, when the bandwidth is increased from 100 to 500 Hz.

The VSC has a maximum current rating determined by the IGBT valves. To prevent the reference current to exceed the maximum current $i_q^{\max}$, the controller is extended with

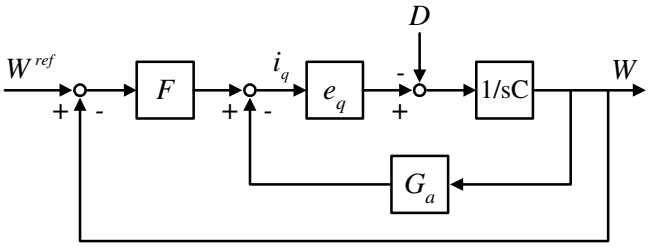

Fig. 4.18. Scheme of EB in continuous time domain.

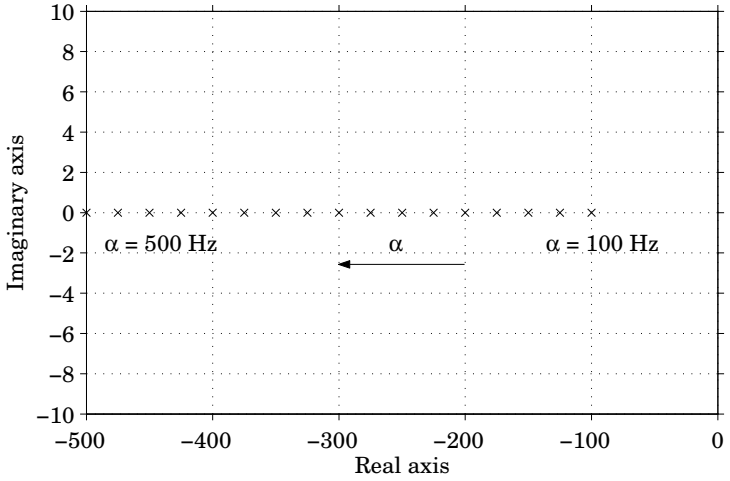

Fig. 4.19. Pole loci of the EB when the bandwidth $100 < \alpha < 500$ Hz.

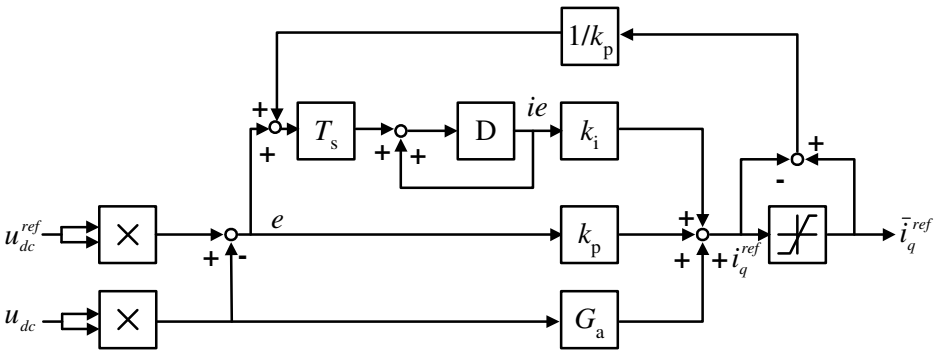

Fig. 4.20. Scheme of the discrete EB with current limitation and active damping. D denotes one sample delay.

current limitation. To avoid wind up of the integral error when the current is limited, the controller utilizes back calculation. Also, if the reference voltage is limited by the current controller, i.e. OVM, the integral error is freezed the sample after to avoid wind up. The scheme of the discrete controller used for digital implementation is shown in Fig. 4.20 and can be summarized by the expressions

$$\begin{aligned} e[k] &= (u_{\text{dc}}^{\text{ref}}[k])^2 - u_{\text{dc}}^2[k] \\ i_q^{\text{ref}}[k] &= k_{\text{p}} \cdot e[k] + k_{\text{i}} \cdot ie[k] + G_{\text{a}} \cdot u_{\text{dc}}^2[k] \\ \bar{i}_q^{\text{ref}}[k] &= \text{sgn}(i_q^{\text{ref}}[k]) \cdot \min(\text{abs}(i_q^{\text{ref}}[k]), i_q^{\text{max}}) \\ ie[k] &= ie[k-1] + T_{\text{s}} \cdot \left(e[k] + \frac{1}{k_{\text{p}}} (\bar{i}_q^{\text{ref}}[k] - i_q^{\text{ref}}[k]) \right). \end{aligned} \tag{4.17}$$

The performance of the dc-link voltage controller is investigated using both simulations and measurements. It is of interest to investigate which parameters affect the controller. The performance of the controller can be seen by how much the dc-link voltage deviates from the reference value when a load is connected and disconnected to the dc side. It is of interest to see how different designs of the dc link, selection of parameters of the controller and different load types affect the dc-link voltage. The parameters of the system are reported in Table 4.2.

TABLE 4.2
PARAMETERS OF VSC SYSTEM.

Grid voltage	E	325 V	1.0 p.u.
Grid current	I	5.8 A	1.0 p.u.
Maximum reference current	i_q^{max}	10.65 A	1.5 p.u.
DC-link voltage	u_{dc}	650 V	1.0 p.u.
DC-link capacitance	C	165 µF	2.9 p.u.
Filter resistance	R_{f}	0.213 Ω	0.0038 p.u.
Filter inductance	L_{f}	15 mH	0.0841 p.u.
Grid frequency	f_{g}	50 Hz	
Sampling frequency	f_{s}	5 kHz	

The parameters selected as the base case for the performance test of the DCC are the following: 250 Hz bandwidth of the dc-link-voltage controller, 2.9 p.u. dc-link capacitance and a 0.92 p.u. resistive load. The corresponding simulation and measurement results when connecting the load are shown in Figs. 4.21 and 4.22. The simulated dc-link voltage reaches a minimum voltage of 0.94 p.u.. The dc-link voltage shows the first order characteristic of the voltage controller. The grid currents are sinusoidal, which was one of the criteria of a good interface. The results of load disconnection are shown in Figs. 4.23 and 4.24. The simulated system has a maximum voltage of 1.06 p.u., but the measurement has a much slower voltage rise compared with the simulation result when the load is disconnected. This is because in reality it is not possible to bring the dc current to zero instantaneously.

The dc-link voltage controller was also tested with different types of loads: CR, CC and CP. Only simulation results are presented for the CC and CP case. Fig. 4.25 shows the influence of load type when connecting and disconnecting a 0.92 p.u. load. The result shows that the CP load gives the lowest dc-link voltage (0.94 p.u.) and this is due to its characteristic; when the voltage decreases the current increases, and this has a negative effect

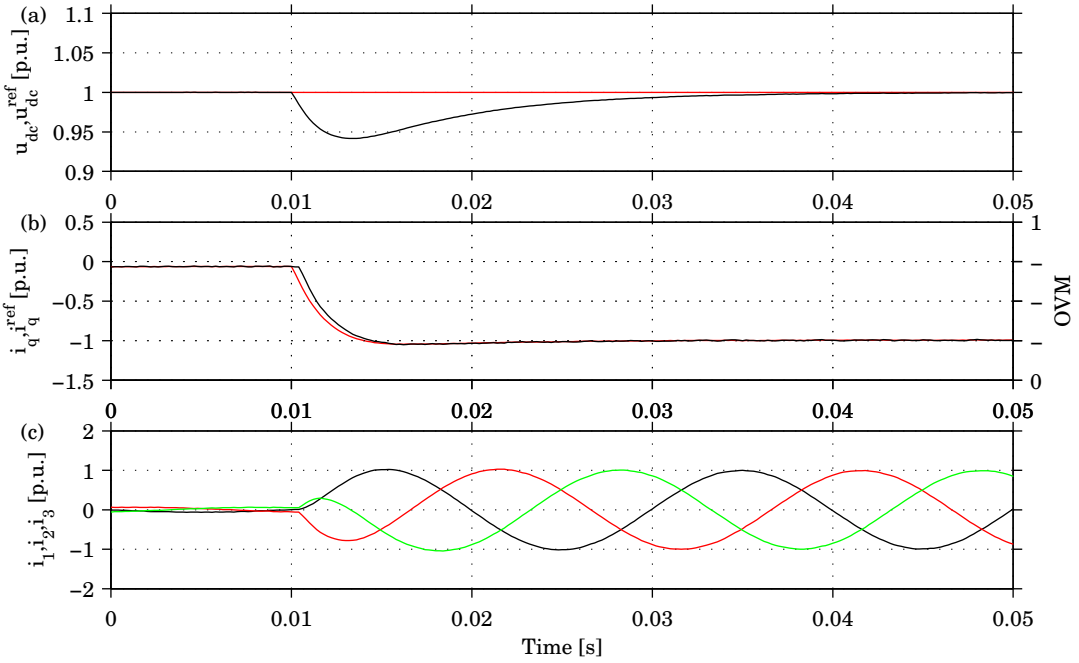

Fig. 4.21. Simulation results for EB with a 250 Hz bandwidth and a 2.9 p.u. dc-link capacitance. Connection of a 0.92 p.u. resistive load: (a) dc-link voltage, (b) active grid current and OVM signal and (c) three-phase currents.

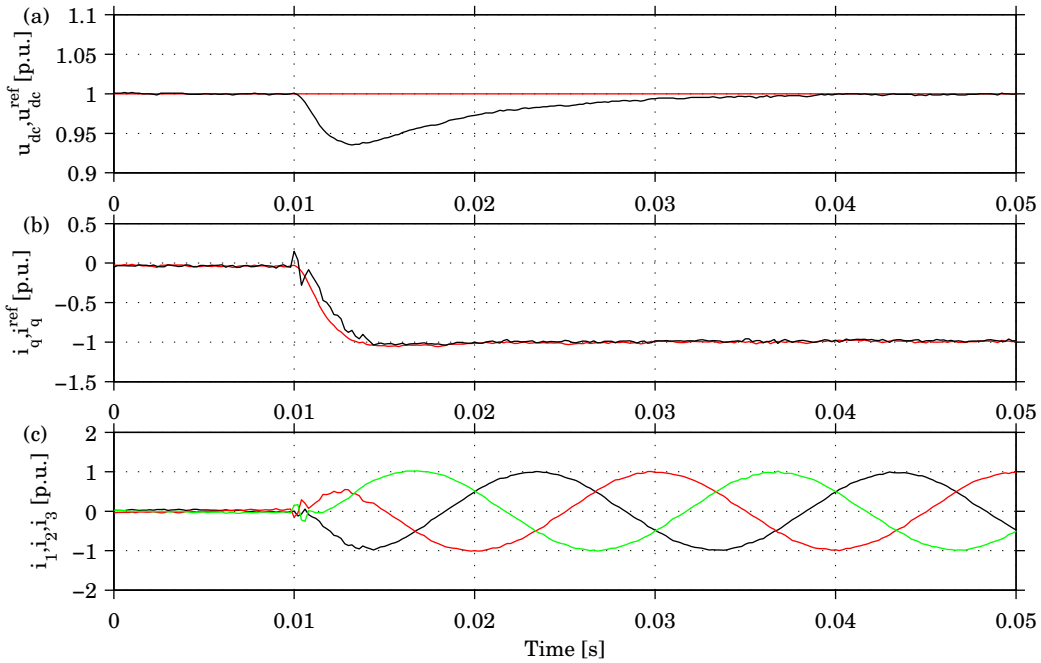

Fig. 4.22. Measurement results for EB with a 250 Hz bandwidth and a 2.9 p.u. dc-link capacitance. Connection of a 0.92 p.u. resistive load: (a) dc-link voltage, (b) active grid current and (c) three-phase currents.

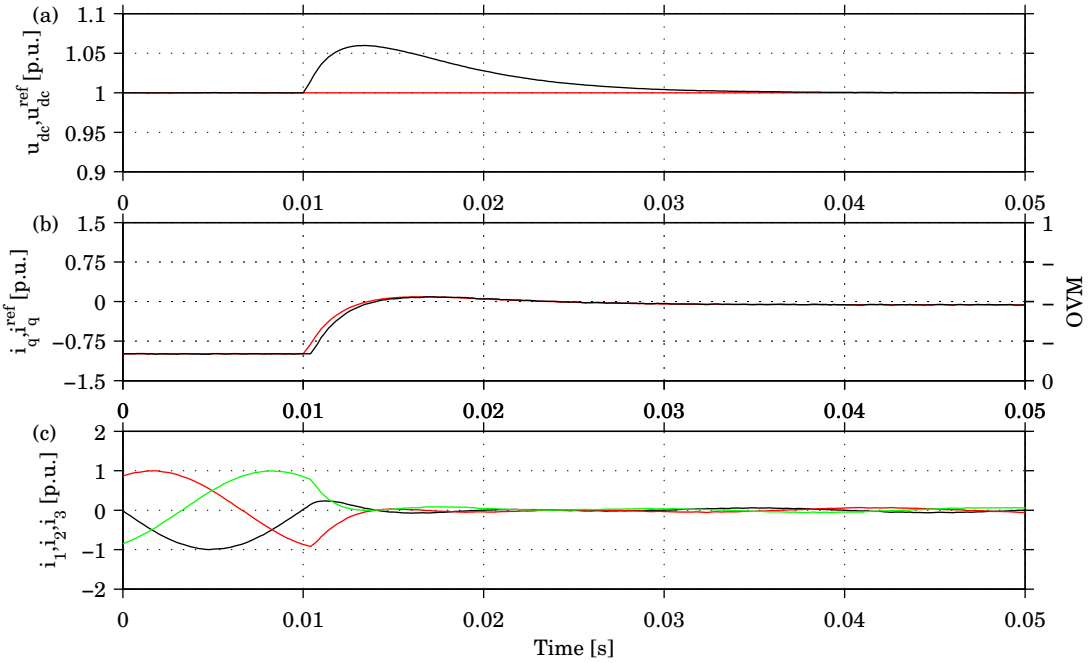

Fig. 4.23. Simulation results for EB with a 250 Hz bandwidth and a 2.9 p.u. dc-link capacitance. Disconnection of a 0 92 p.u. resistive load: (a) dc-link voltage, (b) active grid current and OVM signal and (c) three-phase currents.

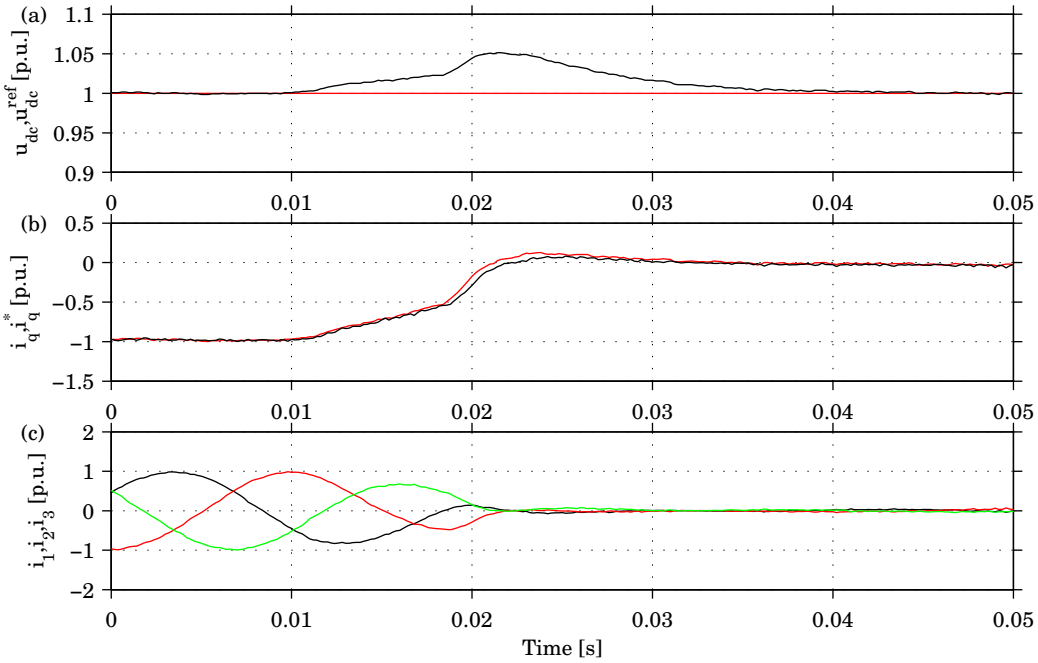

Fig. 4.24. Measurement results for EB with a 250 Hz bandwidth and a 2.9 p.u. dc-link capacitance. Disconnection of a 0.92 p.u. resistive load: (a) dc-link voltage, (b) active grid current and (c) three-phase currents.

on the system. When disconnecting a load, the type does not affect the system since the load is not connected.

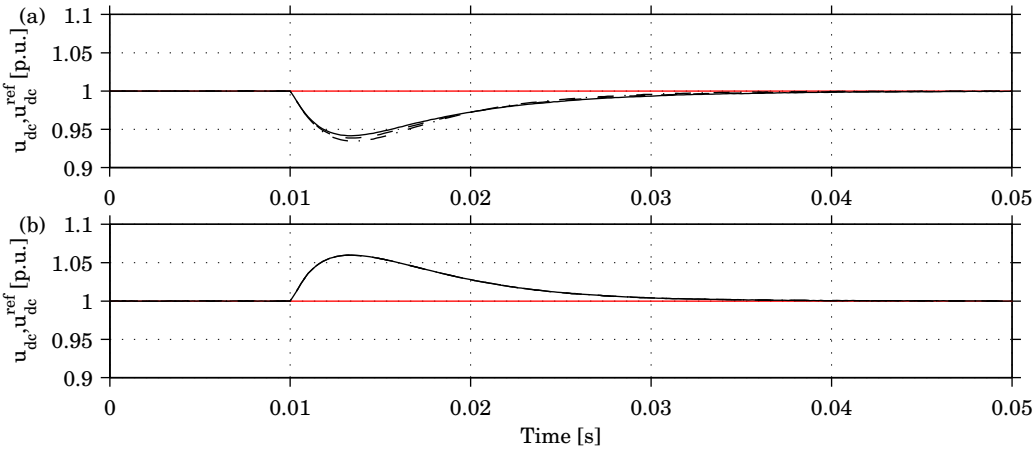

Fig. 4.25. Simulation result for EB with a 250 Hz bandwidth and a 2.9 p.u. dc-link capacitance. Connection (a) and disconnection (b) of different types of loads: CR (solid), CC (dashed) and CP (dashed dotted).

The size of the dc-link has a great impact on the performance of the system. A bigger capacitor does not require a fast voltage controller since the transient energy can be taken from it without the voltage being affected. However, a bigger capacitor will lead to a higher cost. Fig. 4.26 shows the simulation result where different sizes of the dc-link capacitance have been tested. Capacitances of 1.45, 2.9 and 5.8 p.u. have been used when connecting and disconnecting a 0.92 p.u. resistive load. The minimum value of the dc-link voltage when connecting the load was 0.89, 0.94 and 0.97 p.u. for 1.45, 2.9 and 5.8 p.u. dc-link capacitance, respectively, and the maximum value was 1.12, 1.06 and 1.03 p.u. for the same capacitors. A bigger capacitor will reduce the deviation from the reference value.

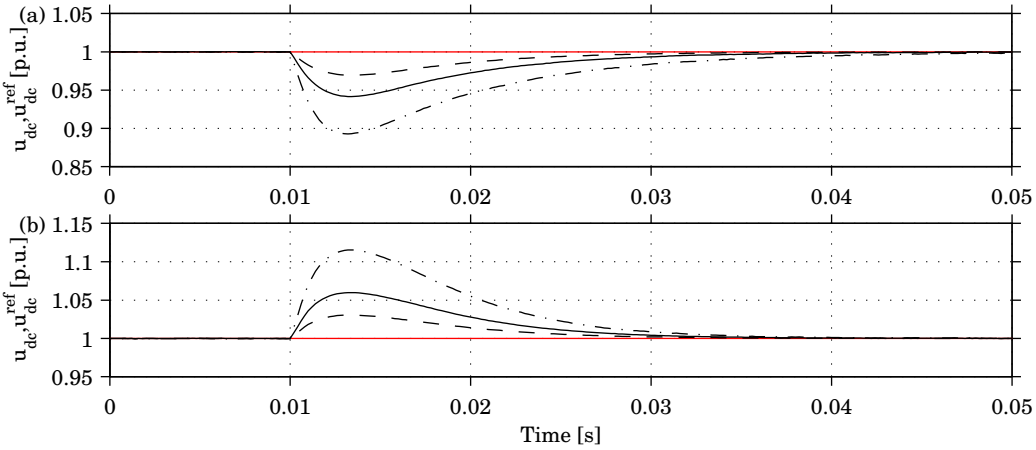

Fig. 4.26. Simulation result EB with a 250 Hz bandwidth. Connection (a) and disconnection (b) of a 0.92 p.u. resistive load, with 1.45 (dashed dotted), 2.9 (solid) and 5.8 p.u. (dashed) dc-link capacitance.

The bandwidth of the controller also determines the performance of the system. A faster controller can result in a smaller size of capacitance. Bandwidths of 250 and 500 Hz have

been tested, which equals to 10 respectively 20 times slower than the current controller. The result is shown in Fig. 4.27. Using 250 Hz results in 0.94 p.u. minimum dc-link voltage when connecting the load, and 1.06 p.u. maximum dc-link voltage when disconnecting the load. Using 500 Hz results in 0.96 and 1.04 p.u. A faster dc-link-voltage controller will reduce the magnitude of the transient when connecting and disconnecting a load, as expected.

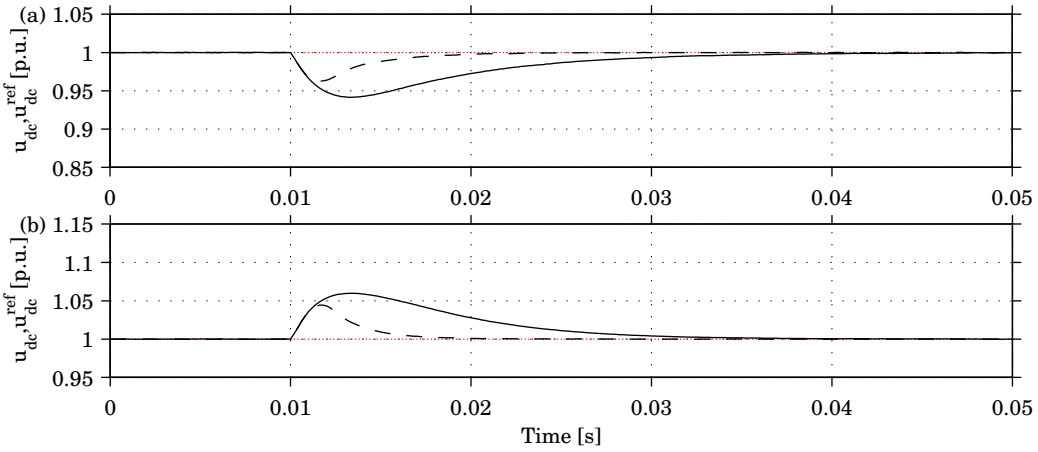

Fig. 4.27. Simulation result for EB with a 2.9 p.u. dc-link capacitance. Connection (a) and disconnection (b) of a 0.92 p.u. resistive load with 250 (solid) and 500 Hz (dashed) bandwidth of the dc-link voltage controller.

4.4.2 Load-Current-Feed-Forward DC-Link Voltage Controller

The load-current-feed-forward dc-link-voltage controller (LC) origins from the relation between the voltage and current of a capacitor

$$i(t) = C\frac{\mathrm{d}u_{\mathrm{dc}}(t)}{\mathrm{d}t}. \tag{4.18}$$

The Laplace transformation of (5.5) gives the transfer function of the process, $G(s)$, as

$$G(s) = \frac{U_{\mathrm{dc}}(s)}{I(s)} = \frac{1}{sC}. \tag{4.19}$$

The controller is chosen to be a PI-controller described by

$$F(s) = k_{\mathrm{p}} + \frac{k_{\mathrm{i}}}{s}. \tag{4.20}$$

The transfer function of the closed-loop system becomes

$$\frac{FG}{1+FG} = \frac{\frac{k_{\mathrm{p}}}{C}s + \frac{k_{\mathrm{i}}}{C}}{s^2 + \frac{k_{\mathrm{p}}}{C}s + \frac{k_{\mathrm{i}}}{C}} \tag{4.21}$$

and its denominator has the characteristic of a double-pole system, given by

$$s^2 + 2\zeta\omega_0 s + \omega_0^2,$$

where ζ is the damping constant, and ω_0 is the frequency of the undamped oscillation. Identification gives the control parameters as in

$$\begin{aligned} k_\mathrm{p} &= -4\alpha C\zeta^2 \\ k_\mathrm{i} &= -4\alpha^2 C\zeta^2 \\ k_\mathrm{ff} &= -\frac{u_\mathrm{dc}^\mathrm{ref}}{e_q} \end{aligned} \tag{4.22}$$

where α determines the bandwidth of the system. To increase the speed of the dc-link-voltage controller the measured dc load current is fed forward which is denoted *FF* in Fig. 4.28. The feed-forward term is used to mitigate the load which is denoted as D. A disadvantage is that all frequency components of the dc load current are directly fed into the reference current. Oscillation in the dc current will result in harmonics in the grid currents. One way to overcome this problem is to low-pass filter the dc current.

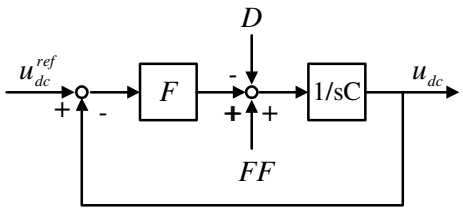

Fig. 4.28. Scheme of LC in continuous time domain.

The poles of the closed loop system when the bandwidth is increased from 100 to 500 Hz are shown in Fig. 4.29. When the bandwidth is 100 Hz, the poles lay close to the limit of a well damped system. Increasing the bandwidth moves the poles more from the area, which will give a well damped system. LC is also extended with current limitation, back calculation

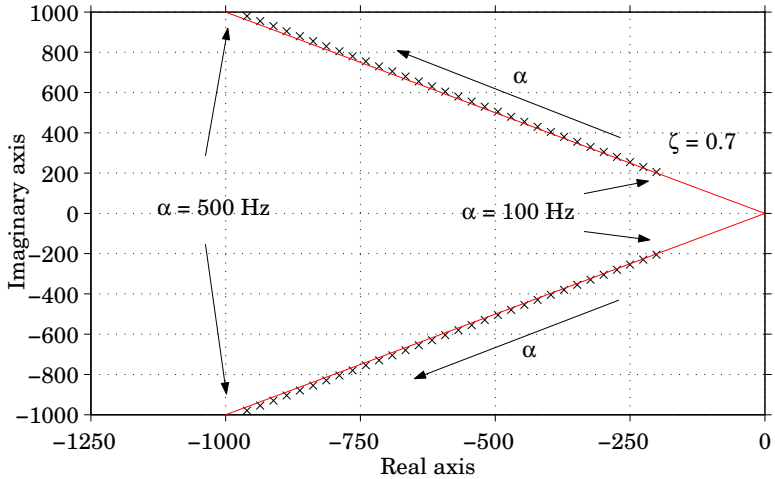

Fig. 4.29. Pole loci of the LC when the bandwidth $100 < \alpha < 500$ Hz.

and feed forward of the OVM signal. The discrete controller which can be implemented in a

digital control system is shown in Fig. 4.30, and can be summarized by

$$\begin{aligned} e[k] &= u_{\text{dc}}^{\text{ref}}[k] - u_{\text{dc}}[k] \\ i_q^{\text{ref}}[k] &= k_{\text{p}} \cdot e[k] + k_{\text{i}} \cdot ie[k] + k_{\text{ff}} \cdot i_{\text{dc}}[k] \\ \overline{i}_q^{\text{ref}}[k] &= \text{sgn}(i_q^{\text{ref}}[k]) \cdot \min(\text{abs}(i_q^{\text{ref}}[k]), i_q^{\text{max}}) \\ ie[k] &= ie[k-1] + T_{\text{s}} \cdot \left(e[k] + \frac{1}{k_{\text{p}}} (\overline{i}_q^{\text{ref}}[k] - i_q^{\text{ref}}[k] \right). \end{aligned} \tag{4.23}$$

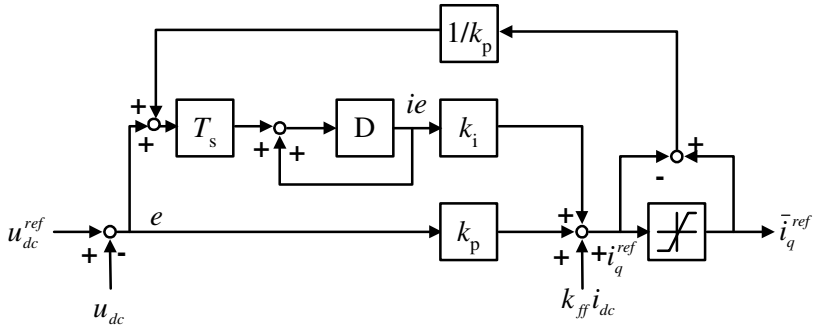

Fig. 4.30. Scheme of the discrete LC with current limitation and measured dc load current feed forward. D denotes one sample delay.

The same base case is used for LC as for EB, and simulation and measurement results of connecting a 0.92 p.u. resistive load are shown in Figs. 4.31 and 4.32. The dc-link voltage has a faster transient compared with EB, but also an oscillation is present due to the controller is close to the limit of a well-damped system. The simulated minimum dc-link voltage becomes 0.98 p.u., and the overshoot 0.013 p.u. Figs. 4.33 and 4.34 show disconnection of the same load. In the simulation the reference current i_q^{ref} has a step to zero when the load is disconnected due to the feed-forward term. This will cause the VSC into overmodulation, which is shown in Fig. 4.33(b), and the integral error in the LC will be freezed. The current controller looses track of the reference current during a short time, which causes an overshoot in the dc-link voltage. The simulation results in a maximum dc-link voltage of 1.04 p.u., and a decrease of 0.01 p.u. The high overshoot in the voltage is not present in the measurement due to the interruption of the dc current.

Like for the EB, it is interesting to see how different load types affect the performance of the system. The simulation result of connecting and disconnecting different load types is shown in Fig. 4.35. In this case, the difference between the three loads is smaller compared with the EB case in Fig. 4.25 due to fact that the LC uses the measured dc current.

The performance of the system with different sizes of dc-link capacitors has been simulated and the result is shown in Fig. 4.36. The minimum voltage when connecting a 0.92 p.u. resistive load was 0.95, 0.98 and 0.99 p.u. using 1.45, 2.9 and 5.8 p.u. dc-link capacitance, respectively. When disconnecting the load the voltage was maximum 1.08, 1.04 and 1.02 p.u. using the same sizes of capacitors. A bigger capacitor improves the performance of the system.

The last parameter to analyze for the LC is the bandwidth of the dc-link voltage controller. The same bandwidths as for the EB were tested, but it was not possible to use 500 Hz since the system became not well damped when connecting the resistive load. From Fig. 4.29 it can be seen that the poles are moving from the area were the system is well damped. The

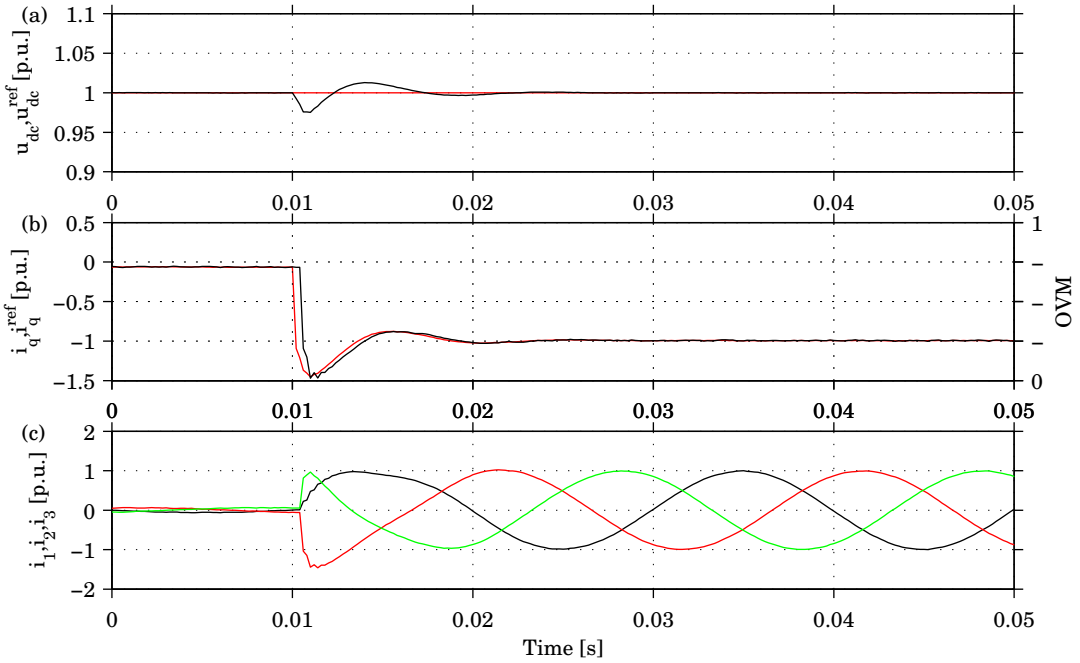

Fig. 4.31. Simulation results for LC with a 250 Hz bandwidth and a 2.9 p.u. dc-link capacitance. Connection of a 0.92 p.u. resistive load: (a) dc-link voltage, (b) active grid current and OVM signal and (c) three-phase currents.

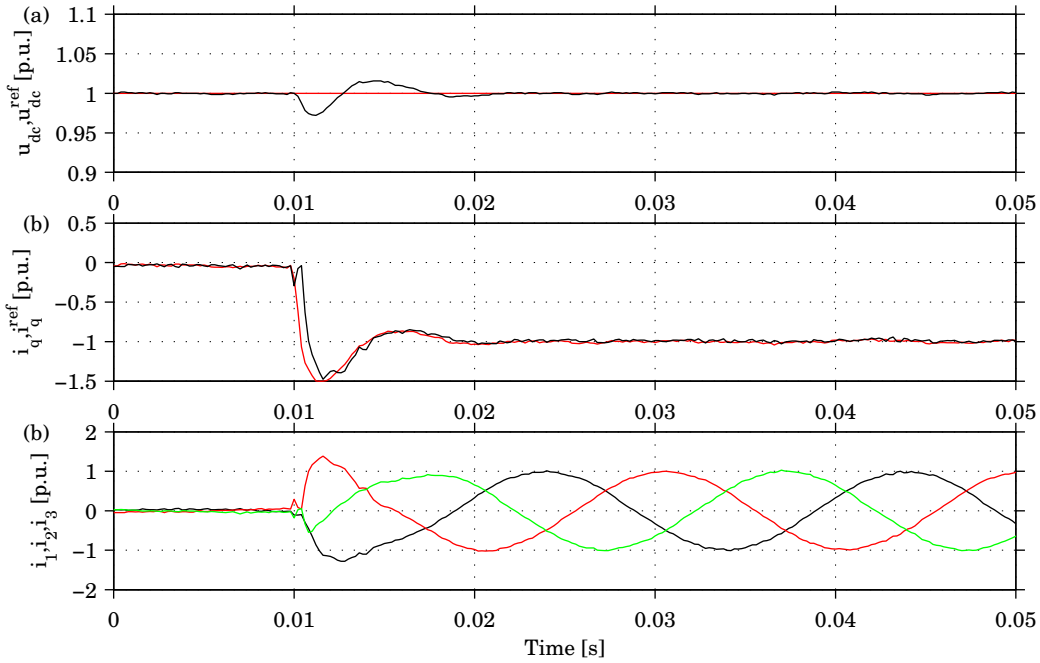

Fig. 4.32. Measurement results for LC with a 250 Hz bandwidth and a 2.9 p.u. dc-link capacitance. Disconnection of a 0.92 p.u. resistive load: (a) dc-link voltage, (b) active grid current and (c) three-phase currents.

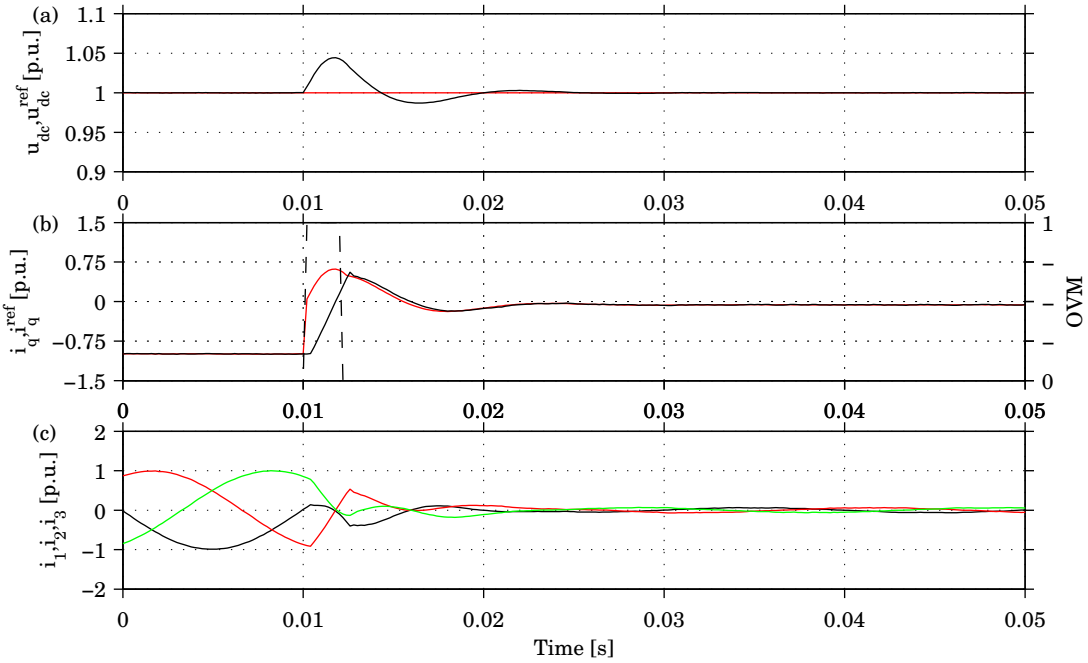

Fig. 4.33. Simulation results for LC with a 250 Hz bandwidth and a 2.9 p.u. dc-link capacitance. Connection of a 0.92 p.u. resistive load: (a) dc-link voltage, (b) active grid current and OVM signal and (c) three-phase currents.

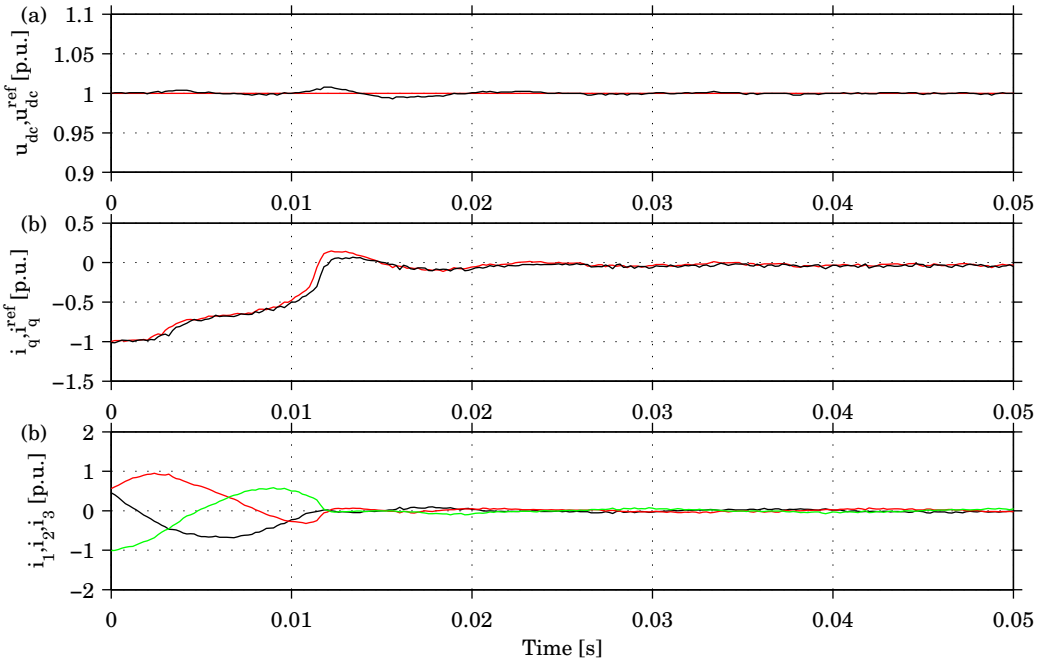

Fig. 4.34. Measurement results for LC with a 250 Hz bandwidth and a 2.9 p.u. dc-link capacitance. Disconnection of a 0.92 p.u. resistive load: (a) dc-link voltage, (b) active grid current and (c) three-phase currents.

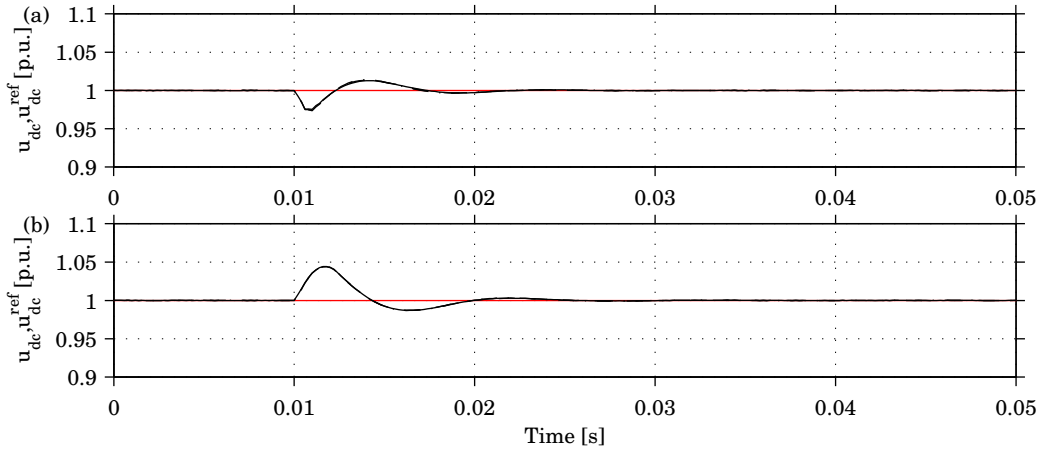

Fig. 4.35. Simulation results for LC with a 250 Hz bandwidth and a 2.9 p.u. dc-link capacitance. Connection (a) and disconnection (b) of different types of loads: CR (solid), CC (dashed) and CP (dashed dotted).

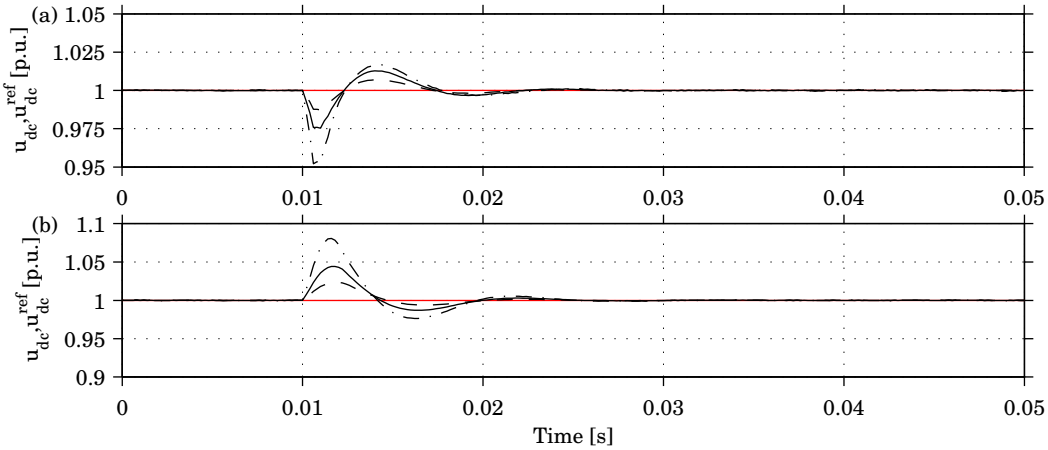

Fig. 4.36. Simulation result LC with a 250 Hz bandwidth. Connection (a) and disconnection (b) of a 0.92 p.u. resistive load, with 1.45 (dashed dotted), 2.9 (solid) and 5.8 p.u. (dashed) dc-link capacitance.

maximum bandwidth possible was 389 Hz. The result is shown in Fig. 4.37. Using 250 Hz resulted in 0.98 as minimum and 1.04 p.u as maximum dc-link voltage when connecting and disconnecting the load. Using 389 Hz resulted in the same values, but with more dc-link voltage oscillations.

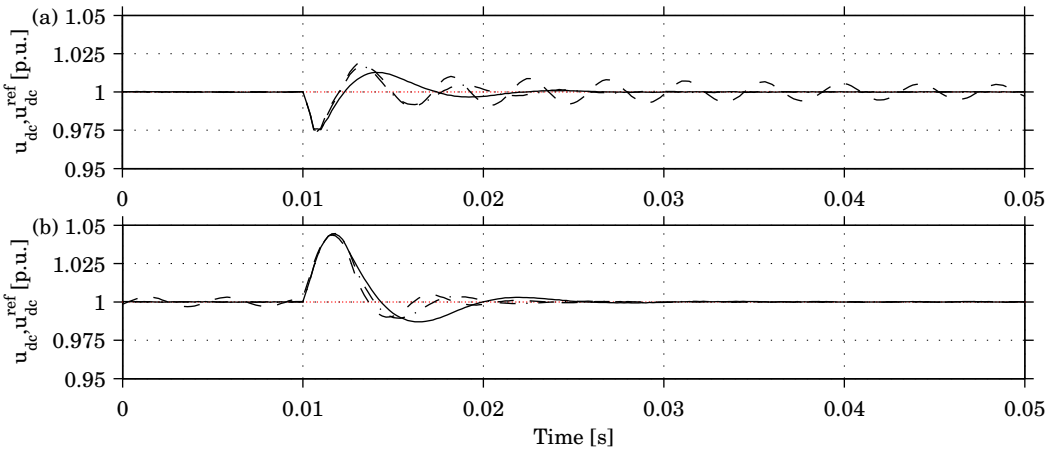

Fig. 4.37. Simulation results for LC with a 2.9 p.u. dc-link capacitance. Connection (a) and disconnection (b) of a 0.92 p.u. resistive load with 250 (solid), 389 (dashed dotted) and 500 Hz (dashed) bandwidth of the dc-link voltage controller.

4.4.3 Observer-Load-Current-Feed-Forward DC-Link-Voltage Controller

The observer-load-current-feed-forward dc-link-voltage controller (OLC) uses the same controller as LC, but with the exception that the dc load current is not measured. A dc load current observer is used to calculate the dc load current from the measured ac currents [67]. This will save costs due to reduced number of current measurement modules. The observer calculates the power flowing into the converter from the ac grid and assumes that the power is consumed by either the dc-link capacitor or the load connected to the dc link. The power losses of the converter are neglected. The scheme of the load current observer is shown in Fig. 4.38.

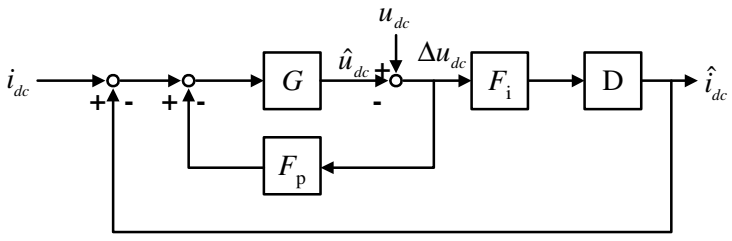

Fig. 4.38. Scheme of load current observer. D denotes one sample delay.

The process G represents the dc-link capacitor. The observer compares the calculated dc-link voltage with the measured and uses the voltage difference to calculate how much current is flowing into the capacitor and how much is going to the load.

The current observer is a second order system, and if the observer is assumed to have a real double pole in λ, which must satisfy $\lambda < 1$ to be stable, the observer gain can be

calculated as [67]

$$\begin{aligned} h_1 &= 2 - 2\lambda \\ h_2 &= \frac{C_{\mathrm{dc}}}{T_{\mathrm{s}}}(1 - h_1 - \lambda^2) \end{aligned} \tag{4.24}$$

where h_1 and h_2 are the gains of the current observer.

The discrete controller is shown in Fig. 4.39 and can be summarized by the expressions

$$\begin{aligned} i_{\mathrm{dc}}[k] &= \frac{e_q[k] \cdot i_q[k]}{u_{\mathrm{dc}}[k]} \\ \Delta u_{\mathrm{dc}}[k] &= u_{\mathrm{dc}}[k] - \hat{u}_{\mathrm{dc}}[k] \\ \hat{u}_{\mathrm{dc}}[k] &= \hat{u}_{\mathrm{dc}}[k-1] + \frac{T_{\mathrm{s}}}{C_{\mathrm{dc}}}\left(\frac{C_{\mathrm{dc}}}{T_{\mathrm{s}}} \cdot h_1 \cdot \Delta u_{\mathrm{dc}}[k] + i_{\mathrm{dc}}[k] - \hat{i}_{\mathrm{dc}}[k]\right) \\ \hat{i}_{\mathrm{dc}}[k] &= \hat{i}_{\mathrm{dc}}[k-1] + h_2 \cdot \Delta u_{\mathrm{dc}}[k] \\ e[k] &= u_{\mathrm{dc}}^{\mathrm{ref}}[k] - u_{\mathrm{dc}}[k] \\ i_q^{\mathrm{ref}}[k] &= k_{\mathrm{p}} \cdot e[k] + k_{\mathrm{i}} \cdot ie[k] + k_{\mathrm{ff}} \cdot \hat{i}_{\mathrm{dc}}[k] \\ \bar{i}_q^{\mathrm{ref}}[k] &= \mathrm{sgn}(i_q^{\mathrm{ref}}[k]) \cdot \min(\mathrm{abs}(i_q^{\mathrm{ref}}[k]), i_q^{\max}) \\ ie[k] &= ie[k-1] + T_{\mathrm{s}} \cdot \left(e[k] + \frac{1}{k_{\mathrm{p}}}(\bar{i}_q^{\mathrm{ref}}[k] - i_q^{\mathrm{ref}}[k]\right). \end{aligned} \tag{4.25}$$

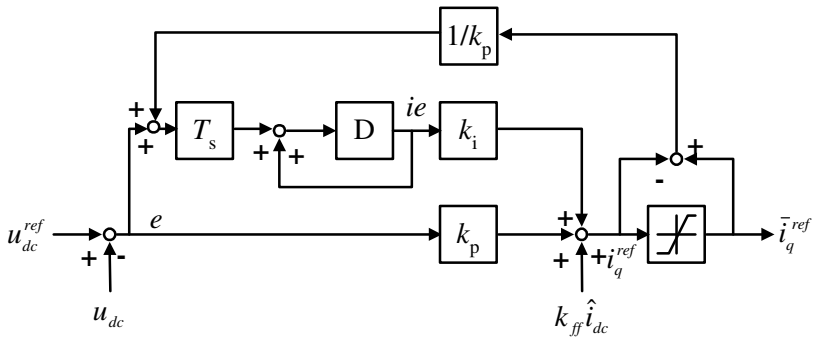

Fig. 4.39. Scheme of dc-link-voltage controller with load current observer. D denotes one sample delay.

The difference between LC and OLC is that the OLC does not measure the dc load current. For the tests, λ equal to 0.8 has been used when nothing else is stated. In Figs. 4.40 and 4.41 the system response when connecting a 0.92 p.u. resistive load is shown. The response of the system is faster compared with EB and slower but without any overshoot compared with LC. The minimum simulated dc-link voltage is 0.96 p.u. which is less than LC but higher than EB.

Figs. 4.42 and 4.43 show the system response when disconnecting the same load. The simulated maximum dc-link voltage is 1.04 p.u. which is equal compared with LC but lower compared with EB. The observer slows down the system since the dc load current must be calculated. This can be seen by comparing i_q^{ref} in Figs. 4.33 and 4.42.

Connection and disconnection of different load types were simulated, and the result is shown in Fig. 4.44. The load type has no influence on the system response like for the LC.

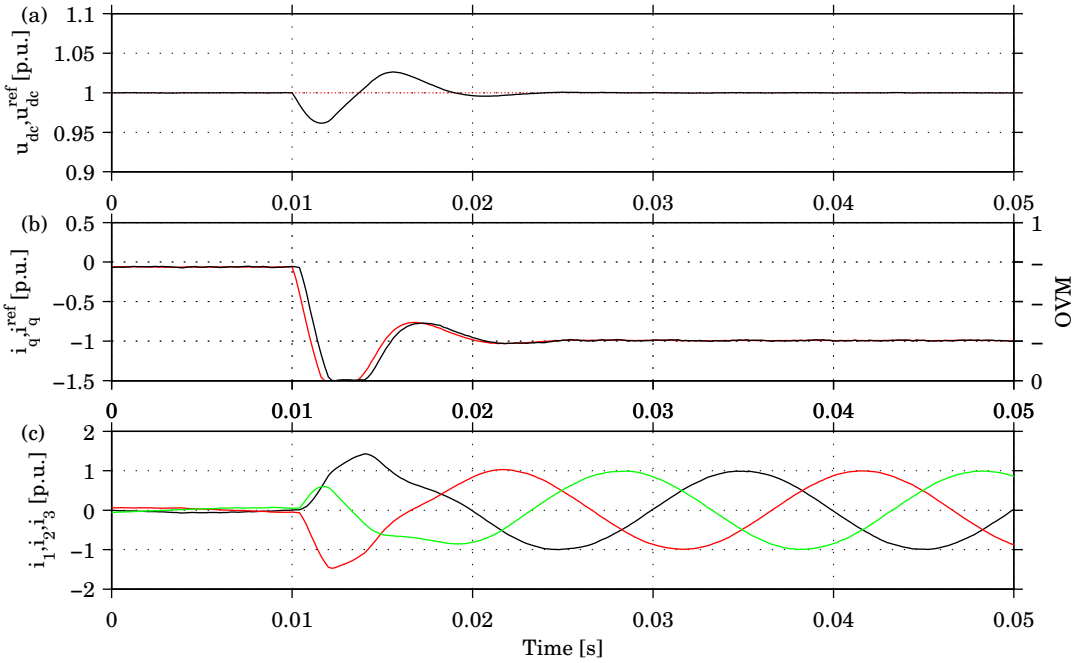

Fig. 4.40. Simulation results for result OLC with a 250 Hz bandwidth and a 2.9 p.u. dc-link capacitance. Disconnection of a 0.92 p.u. resistive load: (a) dc-link voltage, (b) active grid current and OVM signal and (c) three-phase currents.

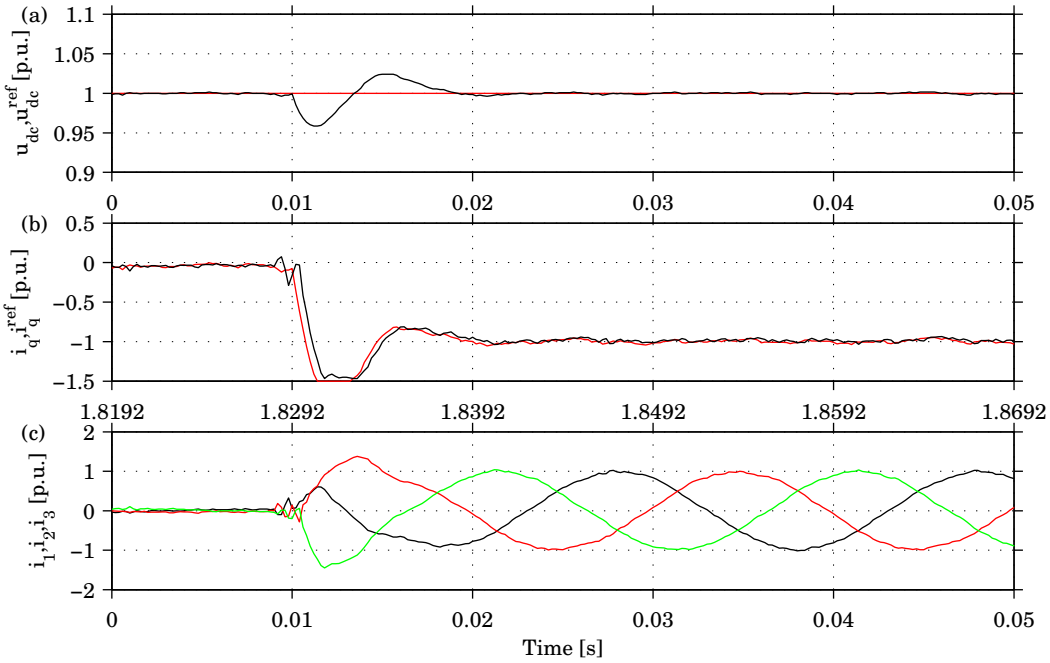

Fig. 4.41. Measurement results for result OLC with a 250 Hz bandwidth and a 2.9 p.u. dc-link capacitance. Disconnection of a 0.92 p.u. resistive load: (a) dc-link voltage, (b) active grid current and (c) three-phase currents.

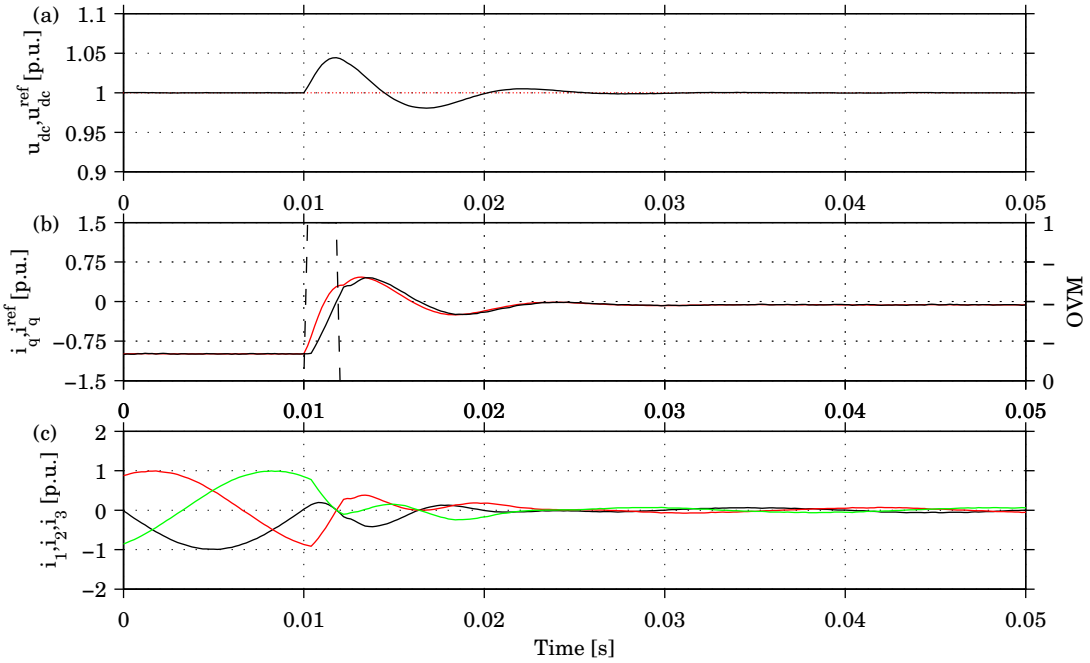

Fig. 4.42. Simulation results for OLC with a 250 Hz bandwidth and a 2.9 p.u. dc-link capacitance. Disconnection of a 0.92 p.u. resistive load: (a) dc-link voltage, (b) active grid current and OVM signal and (c) three-phase currents.

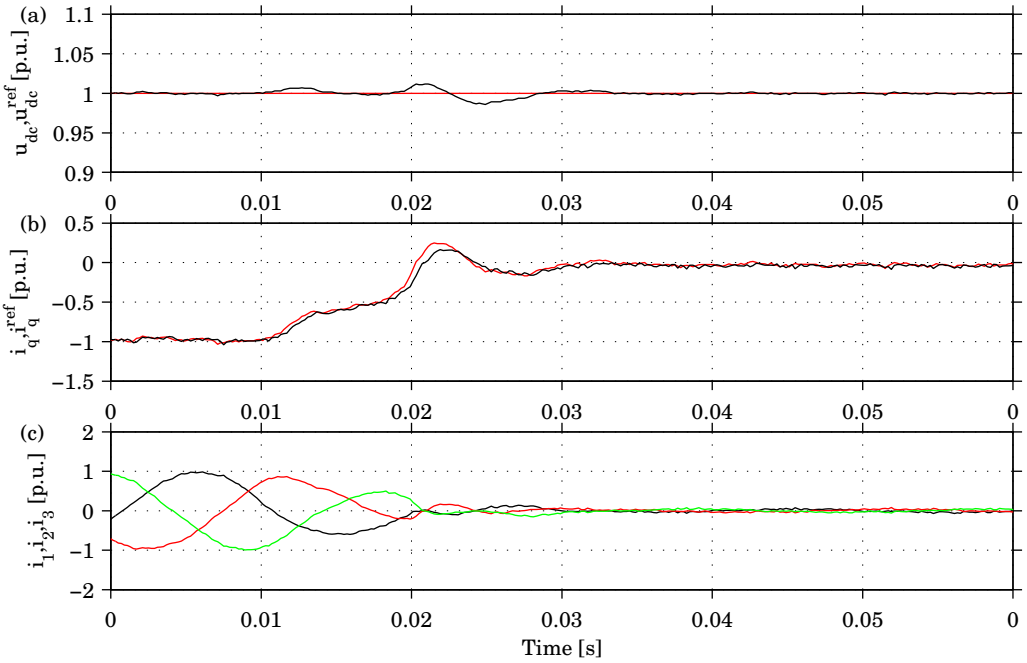

Fig. 4.43. Measurement results for OLC with a 250 Hz bandwidth and a 2.9 p.u. dc-link capacitance. Disconnection of a 0.92 p.u. resistive load: (a) dc-link voltage, (b) active grid current and (c) three-phase currents.

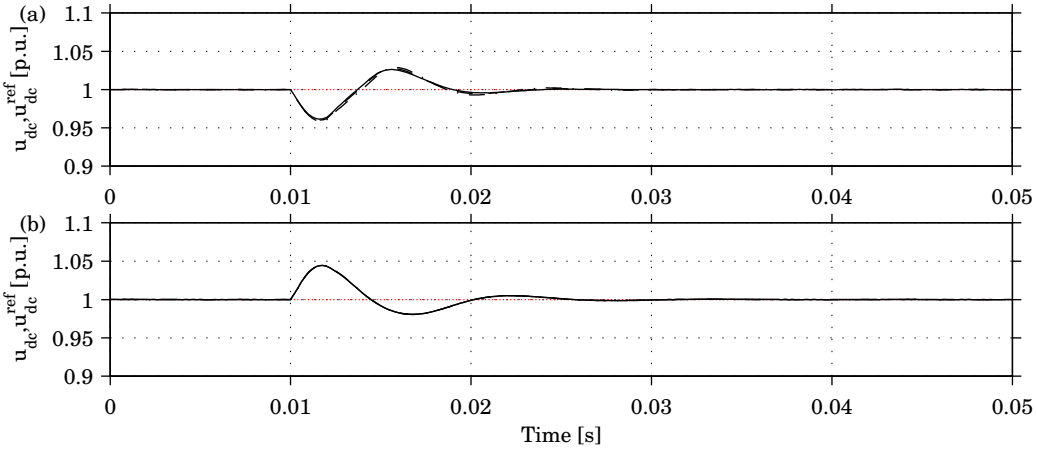

Fig. 4.44. Simulation result OLC with a 250 Hz bandwidth and a 2.9 p.u. dc-link capacitance. Connection (a) and disconnection (b) of different types of loads: CR (solid), CC (dashed) and CP (dashed dotted).

Different sizes of the dc-link capacitance were used when simulating load connection and disconnection to see how it affects the performance of the system. The result is shown in Fig. 4.45. The minimum voltage when connecting a 0.92 p.u. resistive load was 0.93, 0.96 and 0.98 p.u. using 1.45, 2.9 and 5.8 p.u. dc-link capacitors. When disconnecting the load the voltage was maximum 1.08, 1.04 and 1.02 p.u. using the same sizes of capacitors. Also for the OLC a bigger capacitor improves the performance.

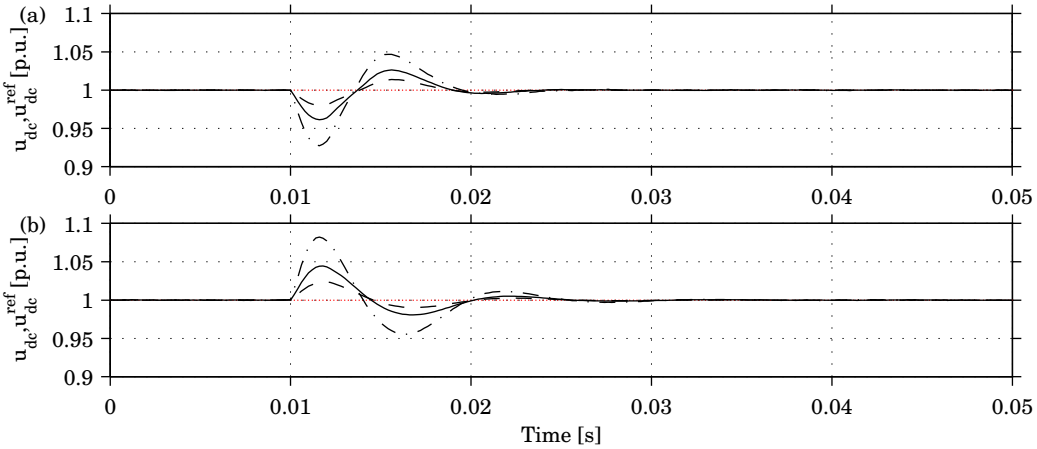

Fig. 4.45. Simulation result OLC with a 250 Hz bandwidth. Connection (a) and disconnection (b) of a 0.92 p.u. resistive load, with 1.45 (dashed dotted), 2.9 (solid) and 5.8 p.u. (dashed) dc-link capacitance.

Different values of λ were used when simulating load connection and disconnection to see how it affects the performance of the system. The result is shown in Fig. 4.46. Values of λ equal to 0.5, 0.8 and 0.95 were tested. A lower value of λ improves the performance of the system.

The last parameter to test is the bandwidth of the OLC controller. Both 250 and 389 Hz have been simulated. The result is shown in Fig. 4.47. Using 250 Hz resulted in 0.96 as minimum and 1.05 p.u as maximum dc-link voltage when connecting and disconnecting the load. Using 389 Hz resulted in a decrease of the minimum dc-link voltage with 0.005 p.u.

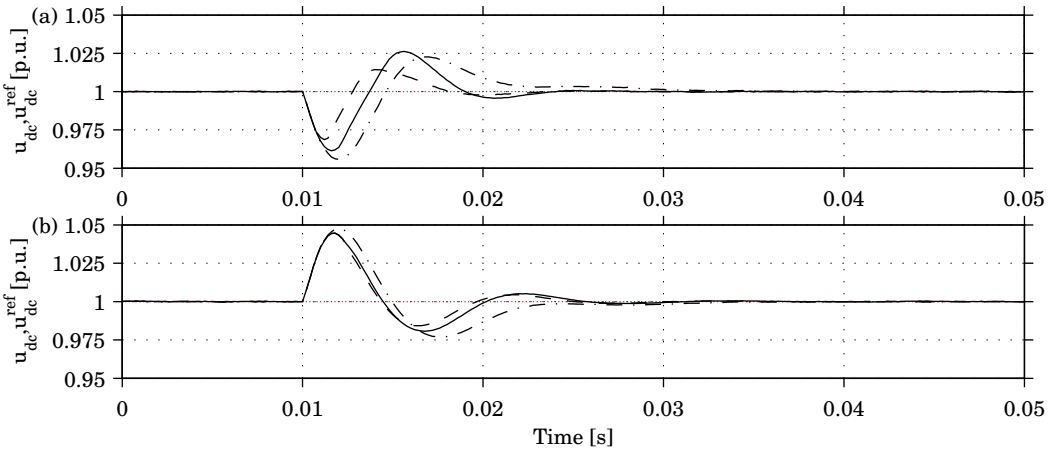

Fig. 4.46. Simulation result OLC with a 250 Hz bandwidth. Connection (a) and disconnection (b) of a 0.92 p.u. resistive load, with λ equal to 0.5 (dashed), 0.8 (solid) and 0.95 p.u. (dashed dotted).

when connecting the load, and the maximum dc-link voltage was unchanged when disconnecting the load, but the minimum was less. However, a faster controller generates more dc-link voltage oscillations.

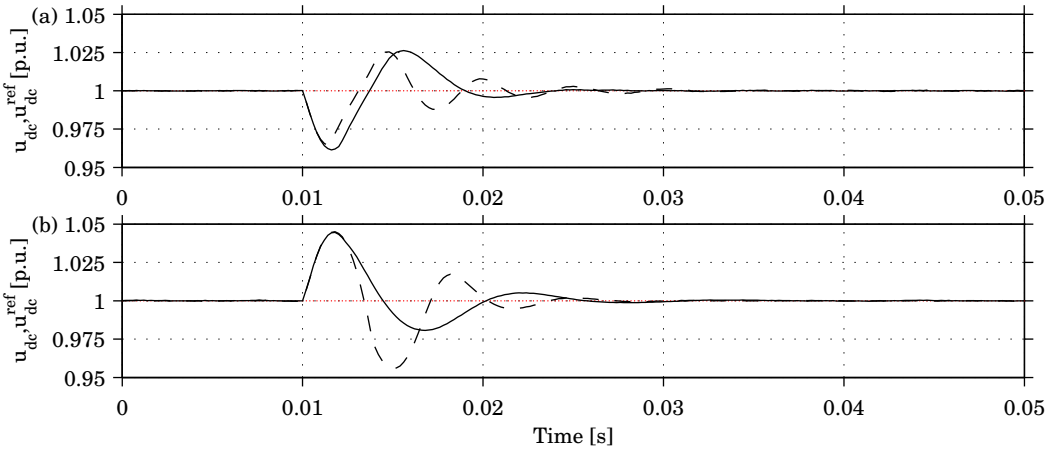

Fig. 4.47. Simulation result OLC with a 2.9 p.u. dc-link capacitance. Connection (a) and disconnection (b) of a 0.92 p.u. resistive load with 250 (solid) and 500 Hz (dashed) bandwidth of the dc-link voltage controller.

Finally, the three dc-link controllers are compared in Fig. 4.48; EB has 250 and 500 Hz bandwidth, and LC and OLC have 250 Hz bandwidth. This to be able to compare their performance. The simulation shows that the LC has the fastest response, OLC has a slower response compared with LC but faster than EB, even if the bandwidth of EBs is increased by a factor two. The minimum level when connecting a load varies between the three controllers. LC decreases least and EB most. When disconnecting a load, all three controllers result in the same maximum overshoot. However, the voltage-time area is different.

4.4.4 Transient Performance of DC-Link-Voltage Controllers

One of the requirements on the VSC was to have a stable dc-link voltage. The performance so far has been measured when connecting and disconnecting a load. Another case which

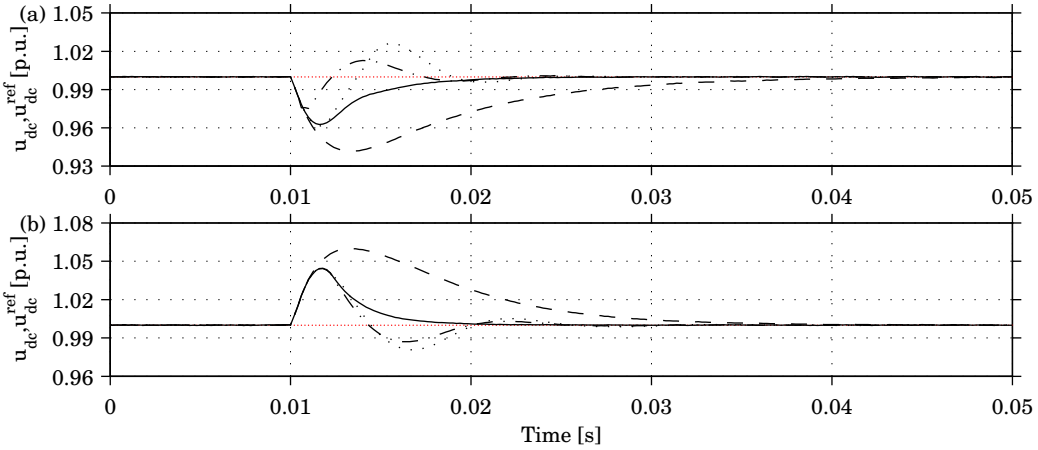

Fig. 4.48. Simulation result EB with 250 Hz (dashed) and 500 Hz bandwidth (solid), LC (dashed dotted) and OLC (dotted) with 250 Hz bandwidth. Connection (a) and disconnection (b) of a 0.92 p.u. load.

is of interest to study is the system performance during disturbances on the ac grid. A symmetrical fault on the ac grid is not a problem for the VSC, since it can boost the dc-link voltage. However, the limit of the retained ac voltage is determined by the maximum reference current $i_q^{\max}$ and the load connected to the dc link. This can be seen from the power balance equation

$$e_q i_q = u_{\mathrm{dc}} i_{\mathrm{dc}} \tag{4.26}$$

which gives the minimum retained ac voltage at a certain load condition as

$$e_q^{\min} = \frac{u_{\mathrm{dc}}^{\mathrm{ref}} i_{\mathrm{dc}}}{i_q^{\max}} \tag{4.27}$$

If a 1.0 p.u. load is connected to the dc link and the maximum reference current is 1.5 p.u., the minimum retained ac voltage is 0.67 p.u. The system performance under a symmetrical fault with basic case parameters for the EB to illustrate (4.27) is shown in Fig. 4.49. The retained grid voltage during the fault is 0.7 p.u., the load is 0.92 p.u. and the maximum reference current 1.5 p.u.. A comparison among the three controllers is shown in Fig. 4.50. All three controllers are able to maintain the dc voltage at the reference level besides a transient due to the change in e_q. EB has a slower response compared with LC and OLC.

The performance of the VSC during an unsymmetrical fault on the ac grid was both simulated and measured in the laboratory. A phase-to-phase fault with 0.75 p.u. retained voltage during 0.07 s, and with 12 % unbalance and a 12° phase-angle jump was used in the simulations, and in the laboratory it was a phase-to-phase fault with 0.79 p.u. retained voltage during 0.07 s, and with 27% unbalance and a 11° phase-angle jump. The unbalance here is defined as the ratio of the negative and the positive sequence, and the phase-angle jump as $\arctan(e_d/e_q)$ [68]. The smaller phase-angle jump will be seen as a smaller transient in the dc-link voltage and the higher unbalance as a higher oscillation in the dc-link voltage and the currents. To be able to make the fault in the laboratory, as explained later in Chapter 6, a weak ac grid was used, and then the grid voltages will be affected by the converter currents. Therefore the gain of the VCC was reduced to 70 % of dead-beat gain and the gain of the DCC to 125 Hz. Physical limitations in the laboratory made it impossible to make faults which are close to the operation limit of converter. During voltage unbalance

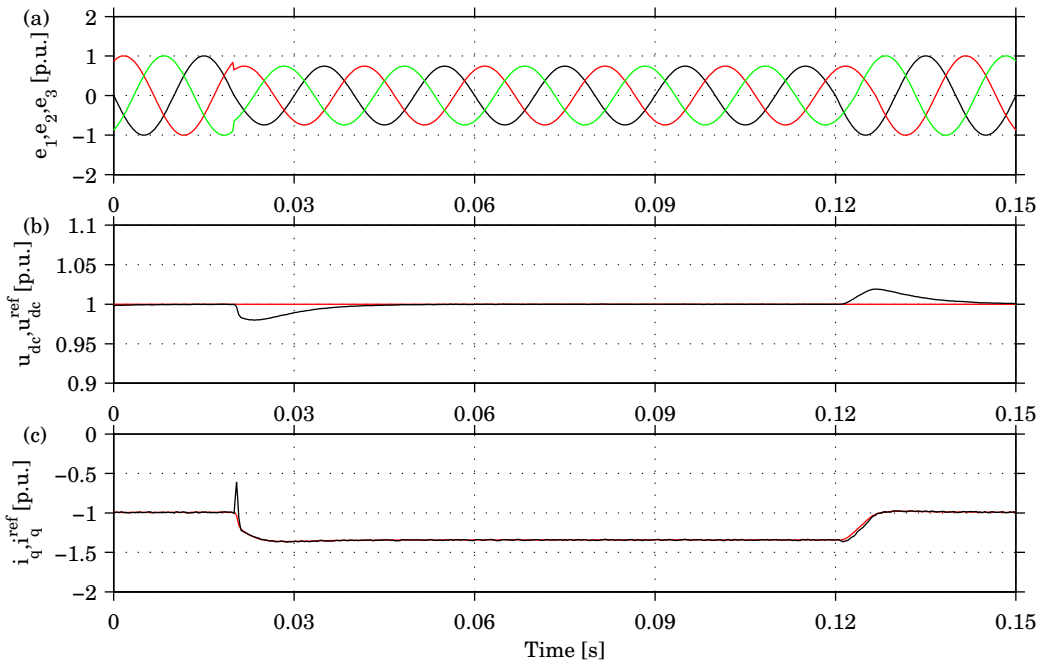

Fig. 4.49. Simulation result for EB with basic case parameters during a symmetric fault. (a) grid voltages, (b) dc-link voltage and (c) active grid current.

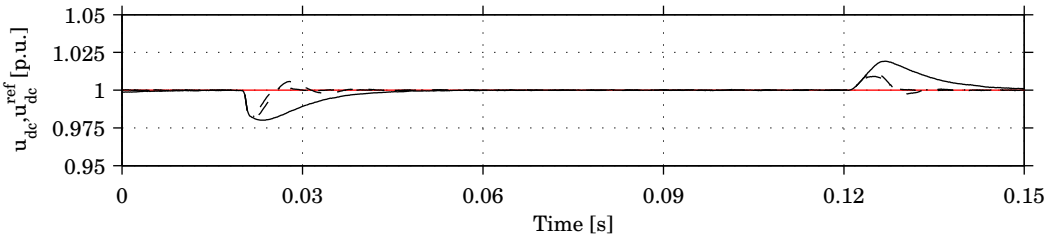

Fig. 4.50. Simulated dc-link voltage for EB (solid), LC (dashed) and OLC (dashed dotted) during a balanced fault.

there will be both a positive and a negative sequence component [64]. The current controller cannot handle a negative sequence voltage, and this will result in a 100 Hz component in the transformed dq-components. This will result in an oscillation on the dc-link voltage with the same frequency. The results using EB are shown in Figs. 4.51 and 4.52. In both cases, the dc-link voltage decreases when the fault is applied and then increases to the reference level but with a 100 Hz oscillation. The measured dc-link voltage increases slower than the simulated one. Using LC results in faster transient in the dc-link voltage compared with EB. The simulation result is shown in Fig. 4.53 and the corresponding measurement in Fig. 4.54. The OLC shows a similar behavior as the LC. The simulation result is shown in Fig. 4.55 and the corresponding measurement in Fig. 4.56. A comparison of the three dc-link voltages is shown in Fig. 4.57. The simulation shows that EB has a larger transient compared with LC and OLC during a symmetric fault, but a smaller steady-state oscillation during an unsymmetric fault. LC has the shortest transient during a balanced fault but the largest steady-state oscillation during an unsymmetrical fault.

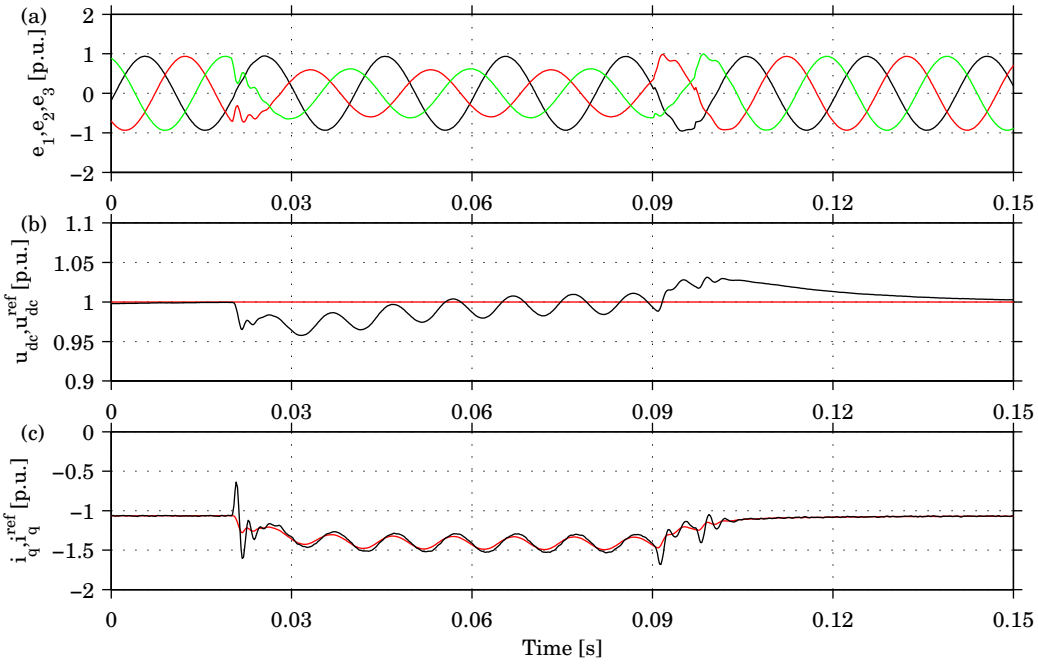

Fig. 4.51. Simulation results for EB with basic case parameters during a un-symmetric fault. (a) grid voltages, (b) dc-link voltage and (c) active grid current.

4.5 Conclusions

In this chapter, the control system of a VSC used as a rectifier has been studied. In the first part, the current controller of a VSC was analyzed and tested. Simulations and measurements show that it is possible to improve the performance of the current controller by extending the PI controller with voltage limitation and integrator anti wind-up.

The dc-link-voltage controller determines how well the system is able to maintain stable dc-link voltage during load transients and grid disturbances. Three different controllers have been analyzed, simulated and tested in a laboratory setup.

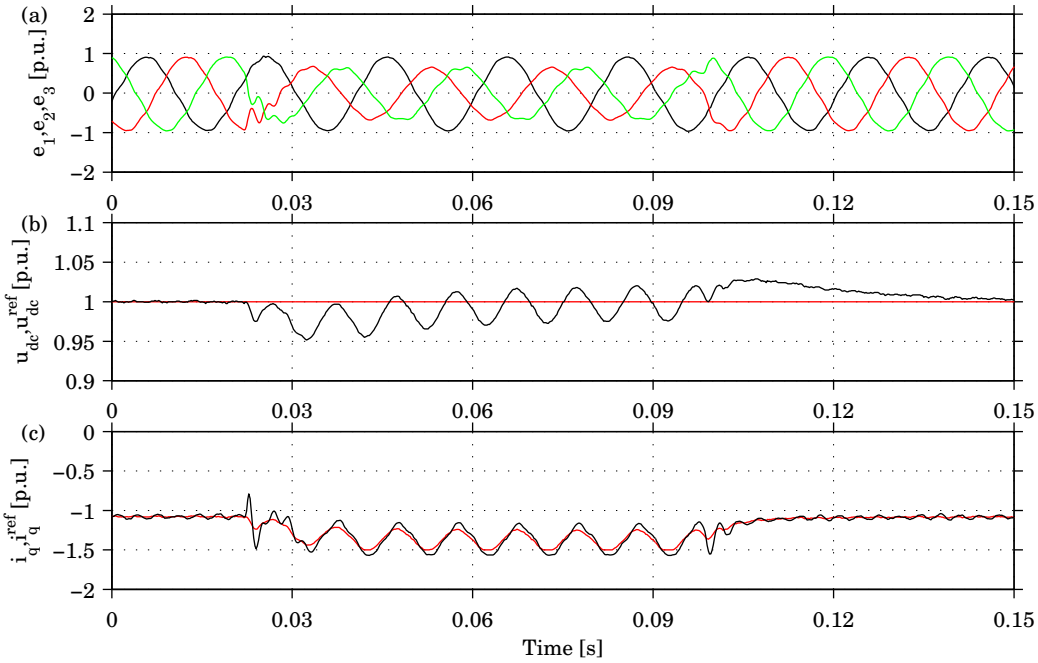

Fig. 4.52. Measurement results for EB with basic case parameters during a un-symmetric fault. (a) grid voltages, (b) dc-link voltage and (c) active grid current.

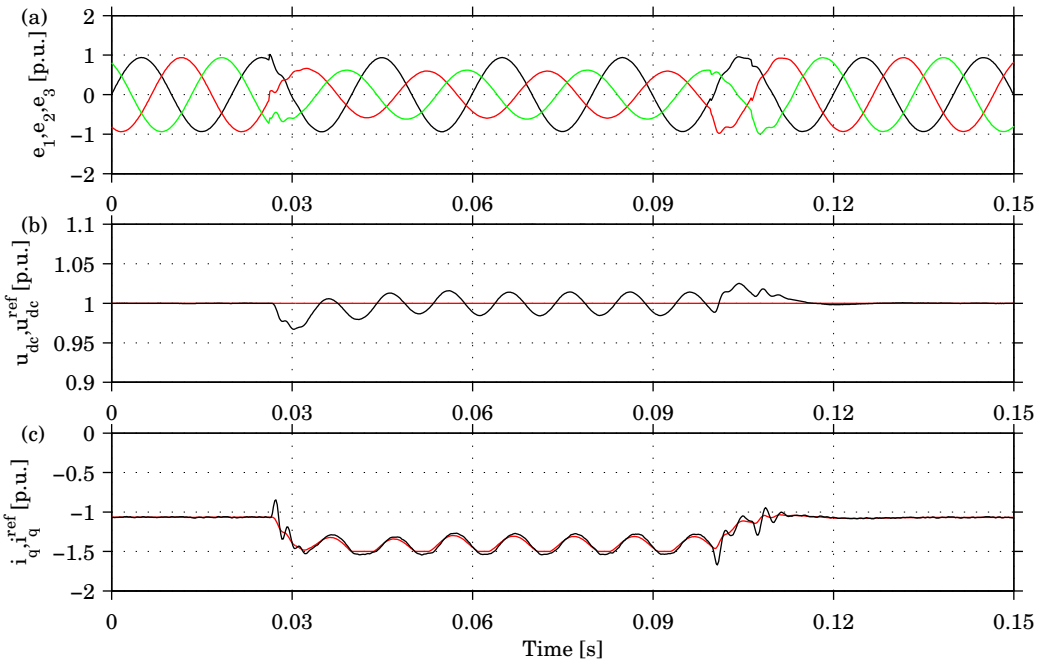

Fig. 4.53. Simulation results for LC with basic case parameters during a un-symmetric fault. (a) grid voltages, (b) dc-link voltage and (c) active grid current.

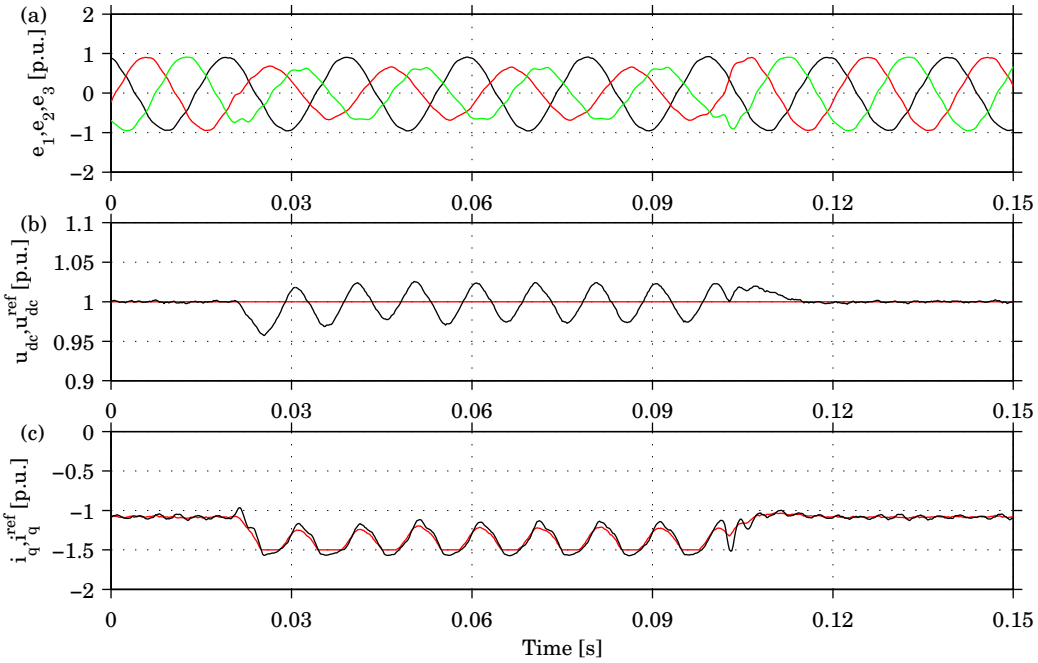

Fig. 4.54. Measurement results for LC with basic case parameters during a un-symmetric fault. (a) grid voltages, (b) dc-link voltage and (c) active grid current.

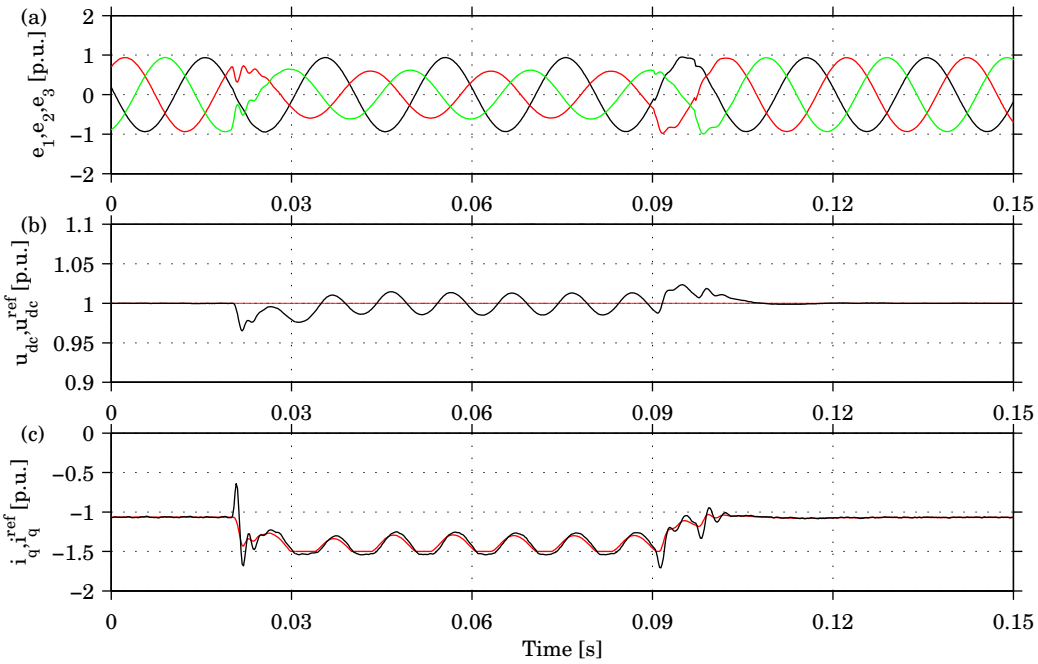

Fig. 4.55. Simulation results for OLC with basic case parameters during a un-symmetric fault. (a) grid voltages, (b) dc-link voltage and (c) active grid current.

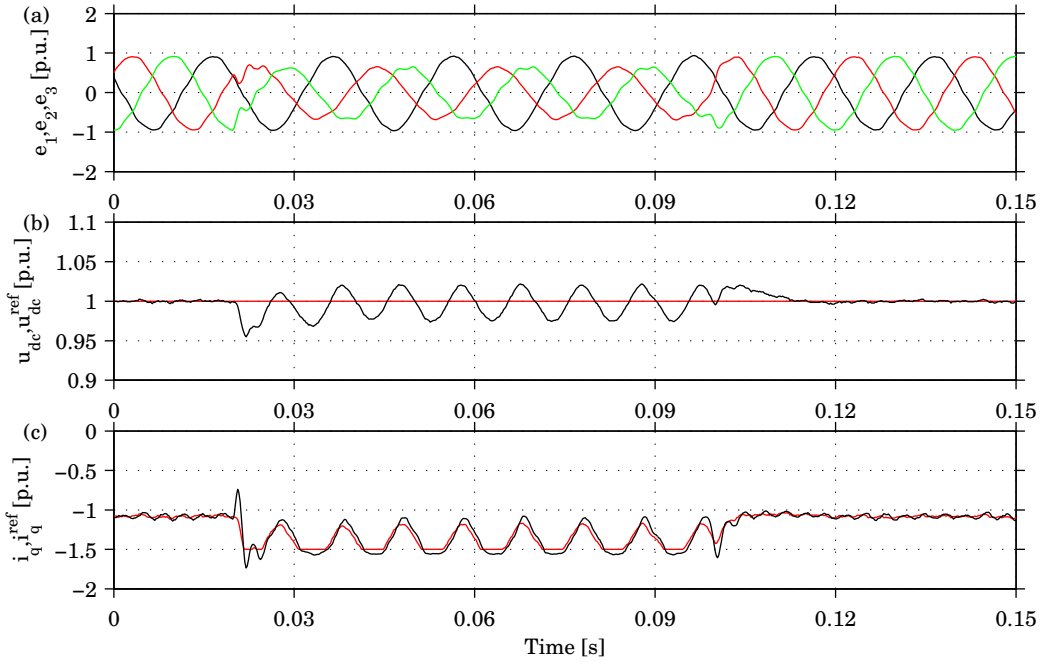

Fig. 4.56. Measurement results for OLC with basic case parameters during unsymmetric fault. (a) grid voltages, (b) dc-link voltage and (c) active grid current.

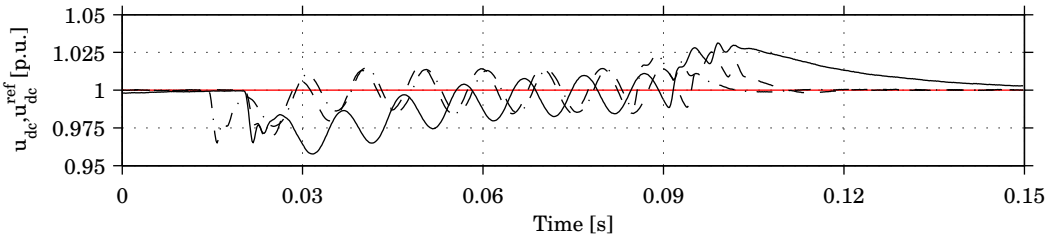

Fig. 4.57. Simulated dc-link voltage for EB (solid), LC (dashed) and OLC (dashed dotted) during a balanced fault.

The performance of the controllers has been measured by the maximum dc-link voltage variation from the reference when connecting and disconnecting a load. Different cases have been studied to see which parameters affect the performance of the dc-link-voltage controller. Different load types, bandwidths of the controller, sizes of the dc-link capacitance have been tested. The results are summarized in Table 4.3. Simulations have shown that different load types do not affect the performance of the dc-link-voltage controller.

TABLE 4.3
OVERVIEW OF DIFFERENT DC-LINK-VOLTAGE-CONTROLLER CONFIGURATION.

DCC	Bandwidth [Hz]	C_{dc} [p.u.]	$u_{\text{dc,min}}$ [p.u.]	$u_{\text{dc,max}}$ [p.u.]
EB	250	1.45	0.89	1.12
EB	250	2.9	0.94	1.06
EB	250	5.8	0.97	1.03
EB	500	2.9	0.96	1.04
LC	250	1.45	0.95	1.08
LC	250	2.9	0.98	1.04
LC	250	5.8	0.99	1.02
LC	389	2.9	0.98	1.04
OLC	250	1.45	0.92	1.08
OLC	250	2.9	0.96	1.04
OLC	250	5.8	0.98	1.02
OLC	389	2.9	0.96	1.05

The results show that it is important to consider within which application the controller will be used to be able to choose the controller which will give the best performance. For load transients, the LC is the best choice if a fast system is desired. If the dc load current is not measured, EB or OLC can be selected. If no voltage oscillation is allowed, EB is the choice due to its first order characteristic, but on the other hand it has a slower response compared with OLC. Considering ac grid faults, LC and OLC give a smaller voltage transient compared with EB.

Chapter 5

Voltage Source Converter with Buck Converter

In this project, an ac/dc-interface consisting of a VSC connected in series with a Buck converter (VSCBC) is proposed. The three-phase VSC, earlier described in Chapter 4, is used to convert ac to a controllable dc voltage, and also provide high power quality and bi-directional power flow. The Buck converter, which is used to step down the VSC dc-link voltage to an appropriate voltage level, also has bi-directional power flow. The proposed interface is designed to maintain a stable dc output voltage during load transients and disturbances on the ac grid.

5.1 Buck Converter

A Buck converter is a step down dc/dc converter, and an electric scheme of which is shown in Fig. 5.1 [45]. This converter has two switches with associated free-wheeling diodes instead of one switch and one diode as in Fig. 2.10(a). The reason is that the converter must be able to handle bi-directional power flow. The output voltage can be varied by utilizing PWM, described earlier in Section 4.2. The input voltage u_{dc}, the output voltage $u_{\text{dc,out}}$, the inductor current i_{ind} and the load current i_{load} of a Buck converter operating with fixed duty ratio are shown in Fig. 5.2. The average output voltage $u_{\text{dc,out}}$ can be calculated from Fig. 5.1 and 5.2 as

$$u_{\text{dc,out}} = \frac{1}{T_{\text{s}}}\int_0^{T_{\text{s}}} u(t)\mathrm{d}t = \frac{1}{T_{\text{s}}}\left(\int_0^{t_{\text{on}}} u_{\text{dc}}(t)\mathrm{d}t + \int_{t_{\text{on}}}^{T_{\text{s}}} 0\ \mathrm{d}t\right) = \frac{t_{\text{on}}}{T_{\text{s}}}u_{\text{dc}} \tag{5.1}$$

where T_{s} is the switching time period, t_{on} is the on time for sw_1 and $u_{\text{dc,in}}$ is the input voltage. Equation (5.1) shows that the output voltage is proportional to the duty ratio D equal to

$$D = \frac{t_{\text{on}}}{T_{\text{s}}}. \tag{5.2}$$

The output filter of the Buck converter consists of an inductor L_{b} and a capacitor C_{b}. When designing the filter, the current ripple in the inductor and the voltage ripple in the capacitor must be taken into consideration. The voltage u_{ind} over the inductor L_{b}, if its resistance is neglected, is related to the current i_{ind} flowing through it as

$$u_{\text{ind}}(t) = L_{\text{b}}\frac{\mathrm{d}i_{\text{ind}}(t)}{\mathrm{d}t}. \tag{5.3}$$

Using (5.3) the ripple Δi_{ind} of the inductor current i_{ind} can be calculated as

$$\Delta i_{\text{ind}} = \frac{u_{\text{dc}}(1-D)DT_{\text{s}}}{L_{\text{b}}}. \tag{5.4}$$

The capacitor current $i_{C_{\text{b}}}$ flowing in a capacitor C_{b} is related to the voltage $u_{\text{dc,out}}$ as

$$i_{C_{\text{b}}}(t) = C_{\text{b}}\frac{\mathrm{d}u_{\text{dc,out}}(t)}{\mathrm{d}t}. \tag{5.5}$$

The voltage ripple $\Delta u_{\text{dc,out}}$ of the capacitor C_{b} is affected by the current ripple Δi_{ind}. Assuming that the ripple current is constant over one switching period, the voltage ripple can be calculated as

$$\Delta u_{\text{dc,out}} = \frac{\Delta i_{\text{ind}} DT_{\text{s}}}{2C_{\text{b}}}. \tag{5.6}$$

From given requirements on current and voltage ripple, the sizes of the inductor and the capacitor can be calculated.

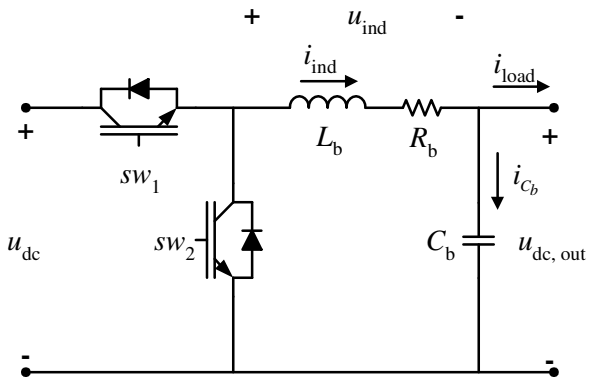

Fig. 5.1. Electric scheme of a Buck converter.

5.2 Controller Design

The output voltage of the Buck converter can during continuous-conduction operation be calculated from (5.1). However, if the output voltage of the converter shall be stable in spite of load variations, a voltage controller must be designed. The idea of the controller is to have one inner controller to control the current through the inductor, which will charge the output capacitor and supply the load, and one outer controller that controls the needed inductor current to charge the capacitor to the reference level.

5.2.1 Current Controller

The current through the inductor L_{b} due to the voltage over it is given by

$$L_{\text{b}}\frac{\mathrm{d}i_{\text{ind}}(t)}{\mathrm{d}t} = u_{\text{ind}}(t) - R_{\text{b}}i_{\text{ind}}(t). \tag{5.7}$$

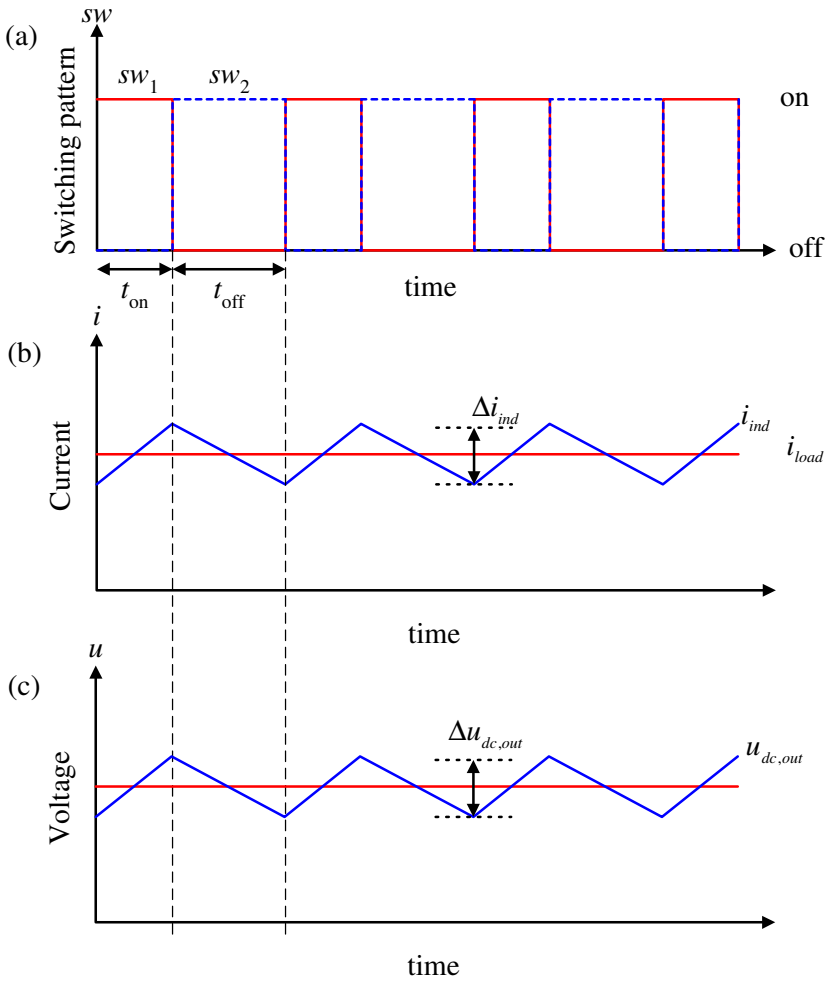

Fig. 5.2. Voltages and current of the Buck converter operating with fixed duty ratio: (a) switching pattern, (b) inductor, capacitor and load currents and (c) capacitor voltage.

With Laplace transformation, the transfer function becomes

$$G(s) = \frac{I_{\text{ind}}(s)}{U_{\text{ind}}(s)} = \frac{1}{sL_{\text{b}} + R_{\text{b}}}. \tag{5.8}$$

If the closed loop system is chosen to have a first order characteristic with bandwidth α_{i}, the controller can be calculated as

$$F(s) = G^{-1}(s)\frac{\alpha_{\text{i}}}{s} = \alpha_{\text{i}}L_{\text{b}} + \frac{\alpha_{\text{i}}R_{\text{b}}}{s}. \tag{5.9}$$

The calculation results in a PI-controller with controller parameters

$$\begin{aligned} k_{\text{p}} &= \alpha_{\text{i}}L_{\text{b}} \\ k_{\text{i}} &= \alpha_{\text{i}}R_{\text{b}}. \end{aligned} \tag{5.10}$$

The controller calculates a voltage reference value $u_{\text{ind}}^{\text{ref}}$, which is used to calculate the duty cycle of the two switches. The mean value of the inductor voltage during one switching period is equal to

$$u_{\text{ind}} = D(u_{\text{dc,in}} - u_{\text{dc,out}}) + (1 - D)(-u_{\text{dc,out}}). \tag{5.11}$$

The duty cycle can be calculated as

$$D = \frac{u_{\text{ind}}^{\text{ref}} + u_{\text{dc,out}}}{u_{\text{dc,in}}}. \tag{5.12}$$

The maximum duty cycle D is 1, and will give a maximum inductor voltage $u_{\text{ind}}^{\text{max}}$ equal to $u_{\text{dc,in}} - u_{\text{dc,out}}$. If the reference voltage $u_{\text{ind}}^{\text{ref}}$ becomes larger than $u_{\text{ind}}^{\text{max}}$ it is limited to $u_{\text{ind}}^{\text{max}}$ and denoted $\overline{u}_{\text{ind}}^{\text{ref}}$. The integral error is then back calculated to avoid wind up of the integral error. The discrete current controller is shown in Fig. 5.3 and can be summarized as

$$\begin{aligned} e[k] &= i_{\text{ind}}^{\text{ref}}[k] - i_{\text{ind}}[k] \\ u_{\text{ind}}^{\text{ref}}[k] &= k_{\text{p}} \cdot e[k] + k_{\text{i}} \cdot ie[k] \\ \overline{u}_{\text{ind}}^{\text{ref}}[k] &= \text{sgn}(u_{\text{ind}}^{\text{ref}}[k]) \cdot \min(\text{abs}(u_{\text{ind}}^{\text{ref}}[k]), u_{\text{ind}}^{\text{max}}) \\ ie[k] &= ie[k-1] + T_{\text{s}} \cdot \left(e[k] + \frac{1}{k_{\text{p}}}(\overline{u}_{\text{ind}}^{\text{ref}}[k] - u_{\text{ind}}[k] \right) \\ D[k] &= \frac{\overline{u}_{\text{ind}}^{\text{ref}}[k] + u_{\text{dc,out}}[k]}{u_{\text{dc,in}}[k]}. \end{aligned} \tag{5.13}$$

5.2.2 Voltage Controller

The voltage over the capacitor C_{b} due to the inductor current i_{ind} and the load current i_{load} is given by

$$C\frac{\text{d}u_{\text{dc,out}}(t)}{\text{d}t} = i_{\text{ind}}(t) - i_{\text{load}}(t) = i_{C_{\text{b}}}(t) \tag{5.14}$$

where $i_{C_{\text{b}}}$ is the current flowing into the capacitor. By Laplace transformation the transfer function becomes

$$G(s) = \frac{U_{\text{dc,out}}(s)}{I_{C_{\text{b}}}(s)} = \frac{1}{sC_{\text{b}}}. \tag{5.15}$$

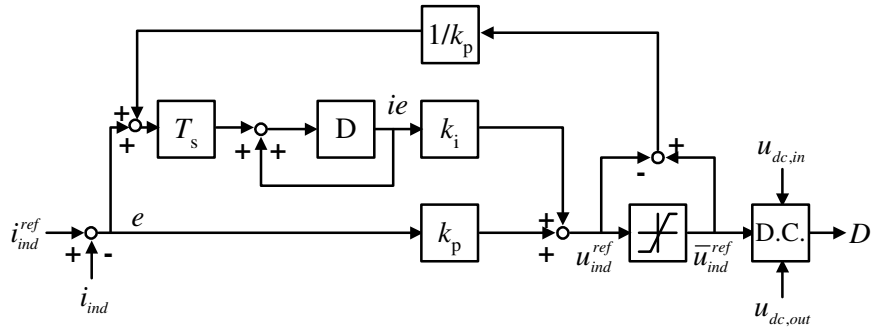

Fig. 5.3. Current controller of the Buck converter. D denotes one sample delay and D.C. calculation of the duty cycle.

The voltage controller is chosen to have a first order characteristic with bandwidth α_{u}. The controller can be designed as for the current controller, resulting in a proportional with gain

$$k_{\mathrm{p}} = \alpha_{\mathrm{u}} C_{\mathrm{b}}. \tag{5.16}$$

The reference inductor current is limited to the maximum inductor current $i_{\mathrm{ref}}^{\mathrm{max}}$. Since only a proportional controller is used, there is no need of anti wind up. The measured load current is fed forward, which can be seen from Fig. 5.4. The discrete voltage controller can be summarized as

$$\begin{aligned} i_{\mathrm{ind}}^{\mathrm{ref}}[k] &= k_{\mathrm{p}} \cdot (u_{\mathrm{dc,out}}^{\mathrm{ref}}[k] - u_{\mathrm{dc,out}}[k]) + i_{\mathrm{load}}[k] \\ \bar{i}_{\mathrm{ind}}^{\mathrm{ref}}[k] &= \mathrm{sgn}(i_{\mathrm{ind}}^{\mathrm{ref}}[k]) \cdot \min(\mathrm{abs}(i_{\mathrm{ind}}^{\mathrm{ref}}[k]), i_{\mathrm{ref}}^{\mathrm{max}}). \end{aligned} \tag{5.17}$$

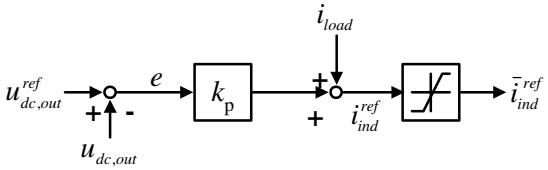

Fig. 5.4. Voltage controller of the Buck converter.

5.3 Simulations and Measurements

The proposed interface is shown in Fig. 5.5, and its performance to maintain a stable dc voltage when connecting and disconnecting loads, and during ac faults is simulated in PSCAD/ EMTDC and measured in the laboratory. Details on the laboratory setup will be given later in Chapter 6. As for the VSC, three different dc-link-voltage controllers of the VSC, and three load types are tested: CR, CC and CP (only a CR load was used in the laboratory). The result from the analysis of the VSC showed that an increased bandwidth of the controller and an increased size of the capacitor improves the performance of the system. For this study a moderate size of the capacitor is chosen for the output of the Buck converter. The result from the VSC analysis also showed that the oscillation on the VSC dc-link during an unsymmetric fault is twice the grid frequency. In a 50 Hz system this results in a 100 Hz

oscillation. The bandwidth of the voltage controller of the Buck converter must be selected higher than 100 Hz to be able to handle the voltage oscillation. The bandwidth shall also be one decade slower than the current controller, which has a selected bandwidth equal to 3 kHz. The bandwidth of the voltage controller is set to 300 Hz. The connection between the VSC and the Buck converter with two capacitors with a inductor in between forces the controller gains of the DCC to be reduced to 125 Hz for EB and 25 Hz for LC and OLC. The reason is that a higher gain tends to generate oscillations between the two capacitors, which affects the dc current of the VSC, which in turn affects the ac grid currents. EB does not take advantage of the dc load current which makes it possible to use a higher gain. The parameters used for the simulations are reported in Table 5.1.

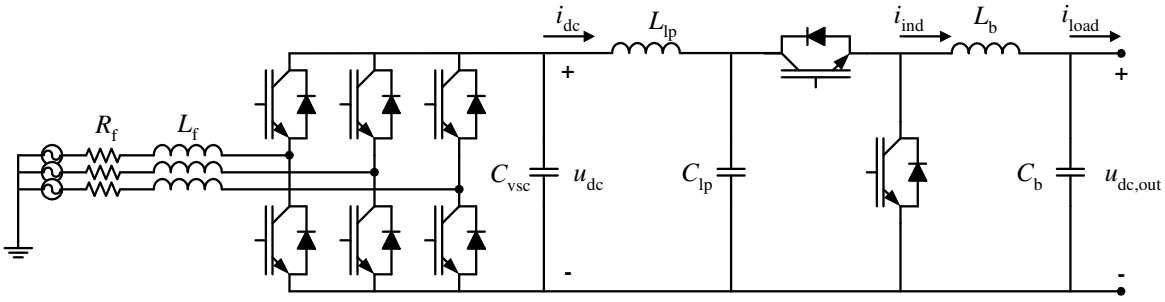

Fig. 5.5. Laboratory setup of VSC with Buck converter.

TABLE 5.1
PARAMETERS OF VSCBC SYSTEM.

Grid voltage	E	325 V	1.0 p.u.
Grid current	I	5.8 A	1.0 p.u.
Maximum reference current	$\overline{i}_q^{\text{ref}}$	10.65 A	1.5 p.u.
Filter resistance	R_f	0.213 Ω	0.0038 p.u.
Filter inductance	L_f	15 mH	0.0841 p.u.
VSC DC-link capacitance	C_vsc	165 µF	2.9 p.u.
DC-link voltage	u_dc	650 V	1.0 p.u.
Low-pass filter capacitance	C_lp	340 µF	5.98 p.u.
Low-pass filter inductance	L_lp	1 mH	0.0421 p.u.
Buck dc output voltage	$u_\text{dc,out}$	325 V	1.0 p.u.
Maximum reference current	$\overline{i}_\text{ind}^{\text{ref}}$	18.45 A	1.5 p.u.
Buck output capacitance	C_bc	1100 µF	19.3 p.u.
Grid frequency	f_g	50 Hz	
Sampling frequency	f_s	5 kHz	

5.3.1 Load Transients

The aim is to investigate the three dc-link-voltage controllers that can be used together with the Buck converter. It is of interest to study the output dc voltage when connecting and disconnecting a load. The performance of the system can be determined by seeing how the dc output voltage is affected. Also the dc-link voltage and the grid current are of interest

to study, to see how well the dc-link-voltage controller of the VSC works together with the Buck converter.

The system response when connecting a 0.67 p.u. resistive load using EB is shown in Figs. 5.6 and 5.7. The measured output dc voltage is 0.994 p.u. before the load is connected, then decreases to 0.977 p.u. and reaches a new steady state at 0.988 p.u. The simulation has a faster transient and smaller steady-state deviation than the measurement. However, simulation result shows that a measurement error of the inductor current and the load current results in a transient in the output dc voltage and a bigger steady state deviation. Comparing simulation and measurement shows that the larger transient in the measured output dc voltage results in a smaller transient in the measured dc-link voltage compared with the simulated dc-link voltage. The measured dc-link voltage decreases to 0.97 p.u., and the response time of the voltage controller of the Buck converter can be seen since it takes some time before the dc-link voltage starts to decrease, both in simulation and in measurement. Disconnection of the same load is shown in Figs. 5.8 and 5.9. The output dc voltage increases by 0.01 p.u. and the dc-link voltage by 0.03 p.u.. A comparison of connecting and disconnecting different load types is shown in Fig. 5.10, and the simulation result shows that there is no difference between the three load types.

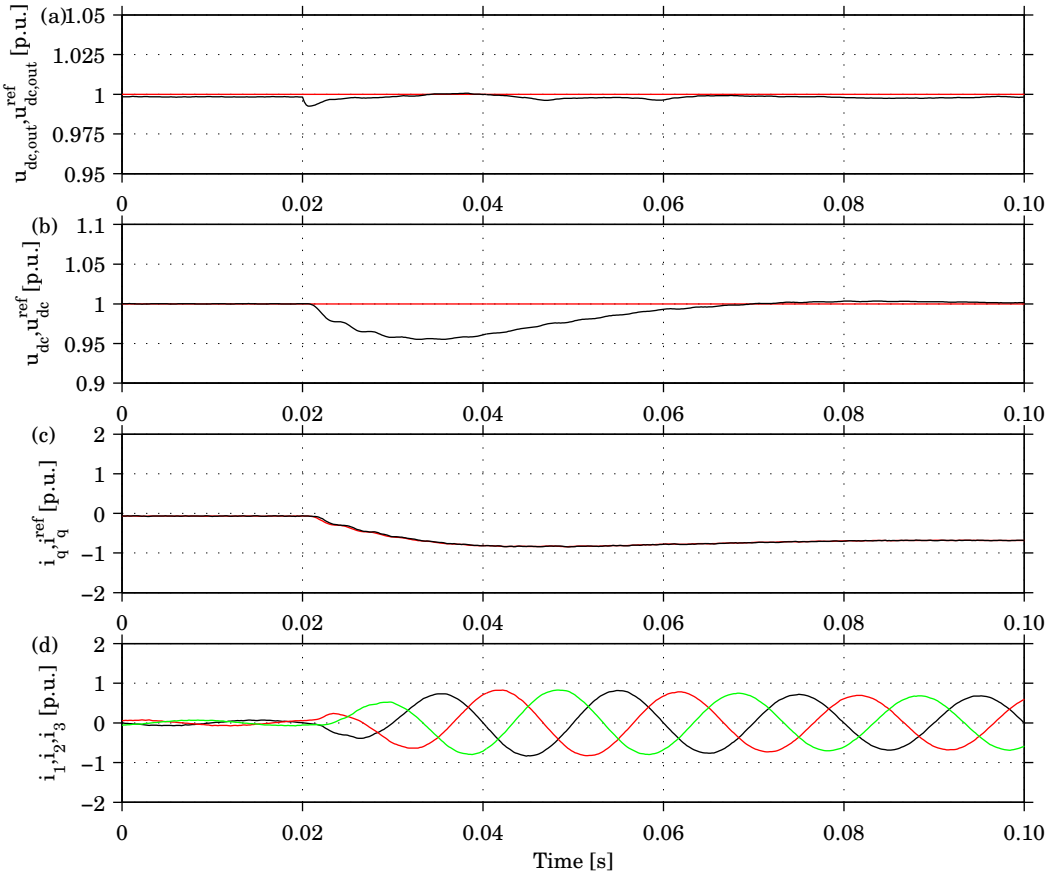

Fig. 5.6. Simulation results for Buck converter and EB dc-link-voltage controller. Connection of a 0.67 p.u. resistive load: (a) dc-output voltage, (b) dc-link voltage, (c) active grid current, and (d) three-phase currents.

The result of connecting a resistive load using LC is shown in Figs. 5.11 and 5.12. The output dc voltage and the dc-link voltage decrease by 0.02 p.u. and 0.01 p.u., respectively.

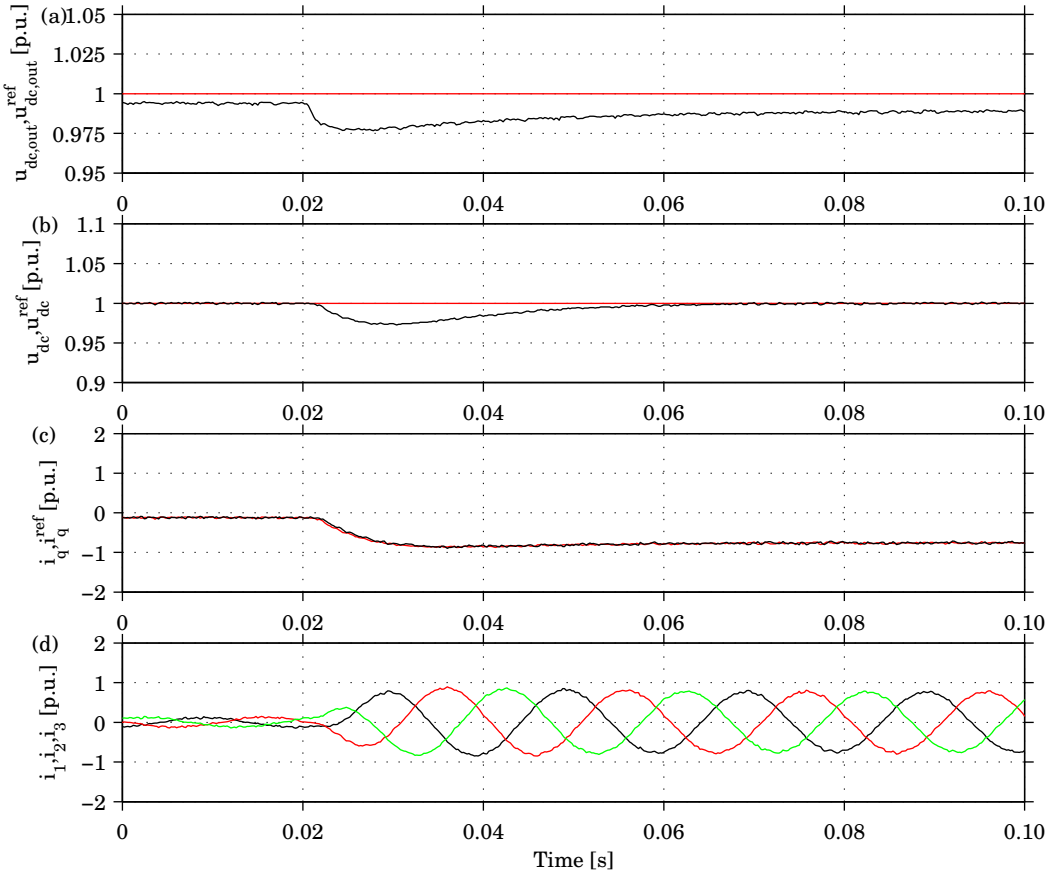

Fig. 5.7. Measurement results for Buck converter and EB dc-link-voltage controller. Connection of a 0.67 p.u. resistive load: (a) dc-output voltage, (b) dc-link voltage, (c) active grid current, and (d) three-phase currents.

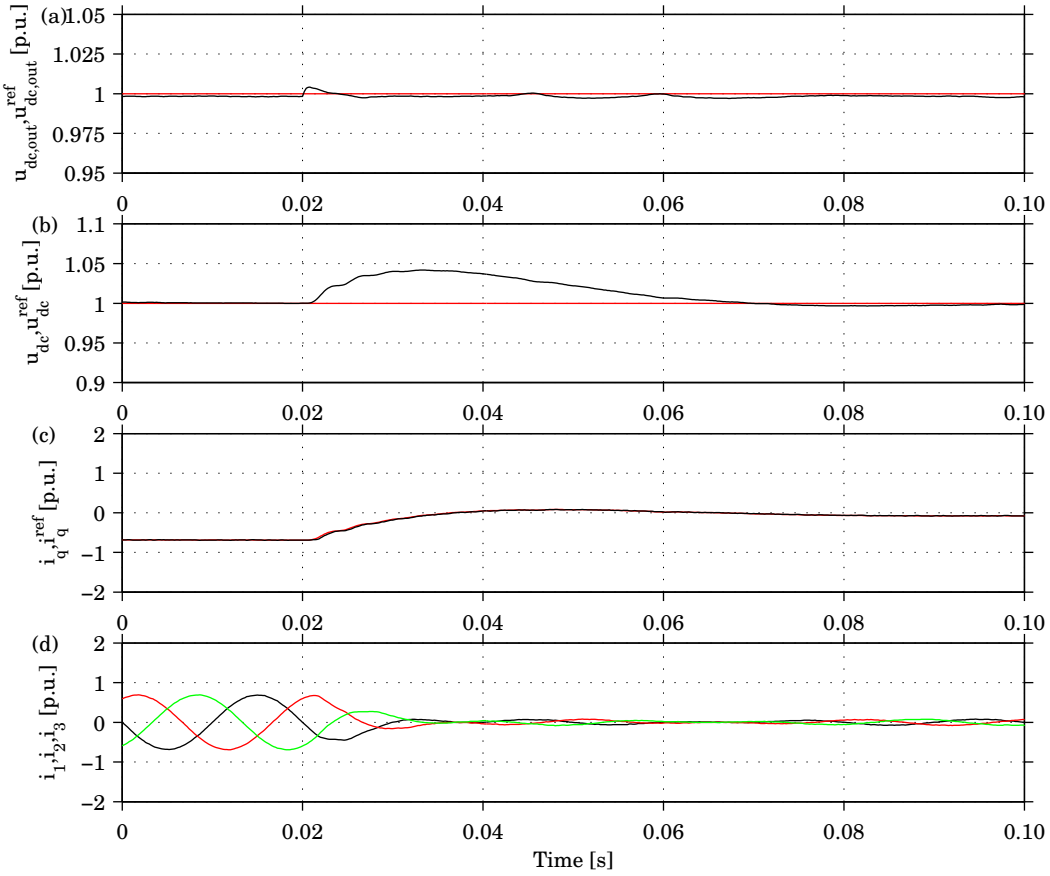

Fig. 5.8. Simulation results for Buck converter and EB dc-link-voltage controller. Disconnection of a 0.67 p.u. resistive load: (a) dc-output voltage, (b) dc-link voltage, (c) active grid current, and (d) three-phase currents.

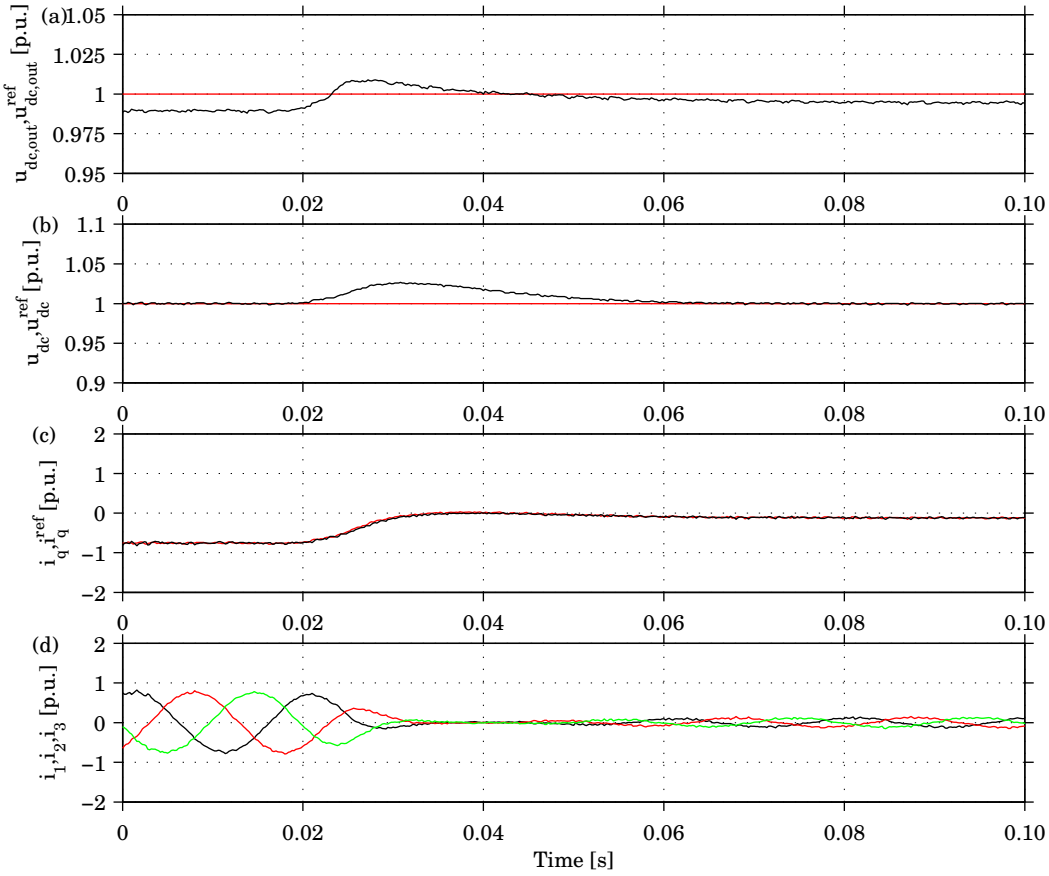

Fig. 5.9. Measurement results for Buck converter and EB dc-link-voltage controller. Disconnection of a 0.67 p.u. resistive load: (a) dc-output voltage, (b) dc-link voltage, (c) active grid current, and (d) three-phase currents.

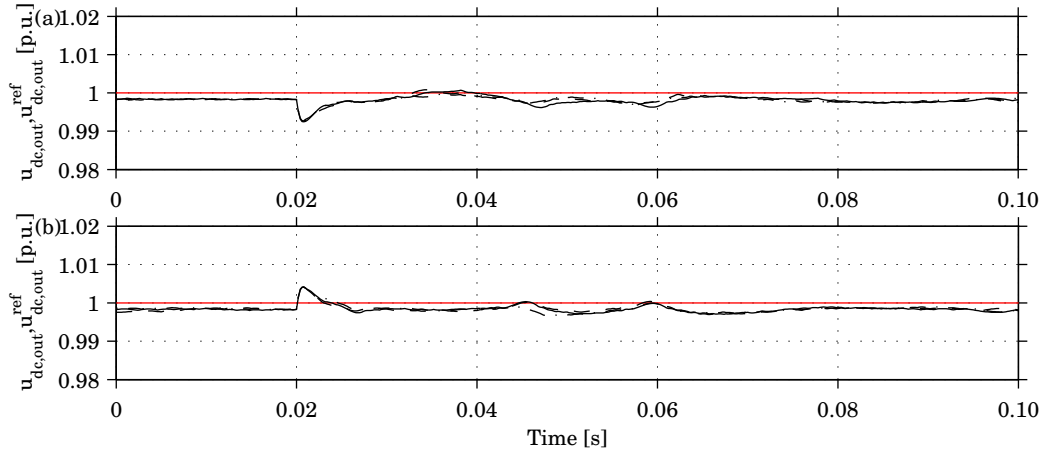

Fig. 5.10. Simulation results for Buck converter and EB dc-link-voltage controller. Connection (a) and disconnection (b) of different types of loads: CR (solid), CC (dashed) and CP (dashed-dotted).

The output dc voltage has the same steady-state value as the case using EB. Comparing the results of LC and EB shows that a transient on the dc link is faster with LC than EB, in spite of a lower controller gain. This shows the influence of feeding forward the dc current of the VSC. Figs. 5.13 and 5.14 show the result of disconnecting the load. The output dc voltage and the dc-link voltage increase by 0.02 p.u.. Also LC was tested with different load types, and Fig. 5.15 shows that the load type does not affect the dc output voltage.

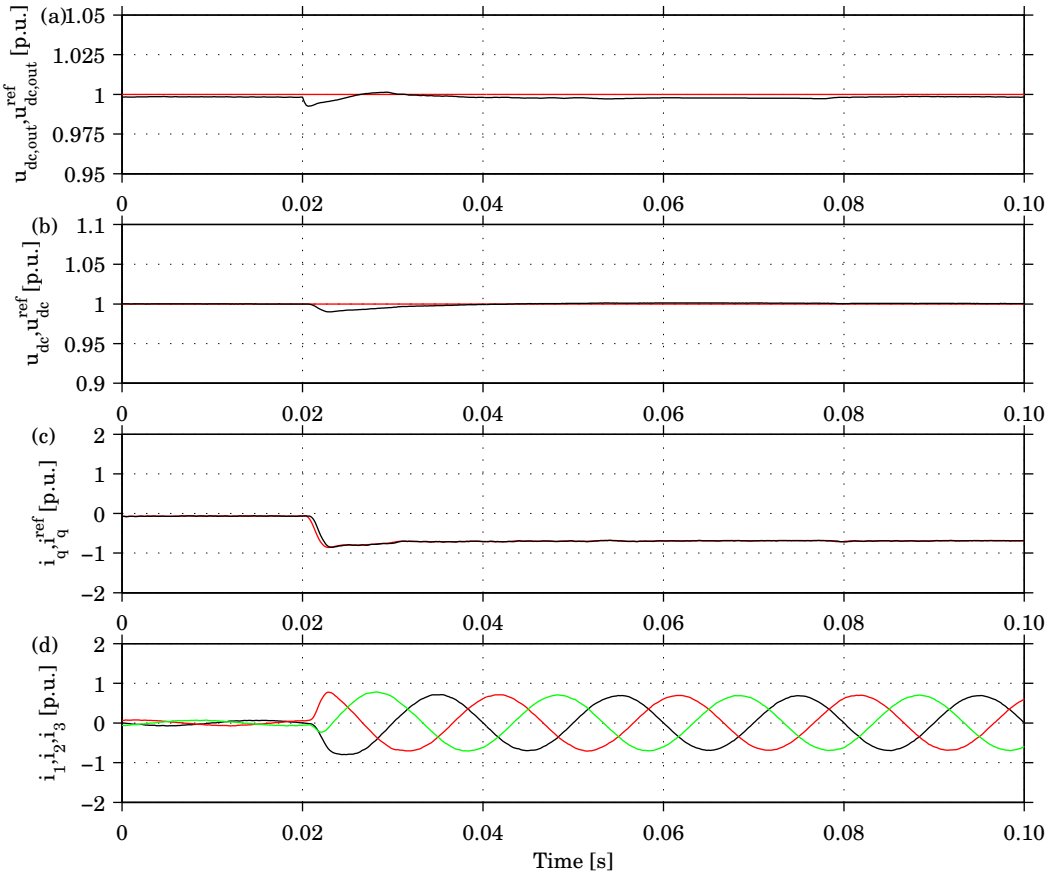

Fig. 5.11. Simulation results for Buck converter and LC dc-link-voltage controller. Connection of a 0.67 p.u. resistive load: (a) dc-output voltage, (b) dc-link voltage, (c) active grid current, and (d) three-phase currents.

The result when connecting a load using OLC is shown in Figs. 5.16 and 5.17, which shows that using a current observer will result in a smaller transient on the dc link compared with EB since OLC feeds forward the observed dc current. Compared with LC it has a longer transient, since it takes some time for the observer to calculate the dc current. The voltage decrease when connecting the load is 0.02 p.u. for both the output dc voltage and the dc-link voltage. The output dc voltage has the same steady-state value as EB and LC both before and after the load is connected. Figs. 5.18 and 5.19 show the result when disconnecting the load. The voltage increases by 0.01 p.u. for the output dc voltage and by 0.02 p.u. for the dc-link. The output dc voltage is not affected by the load type when using OLC, which can be seen from Fig. 5.20.

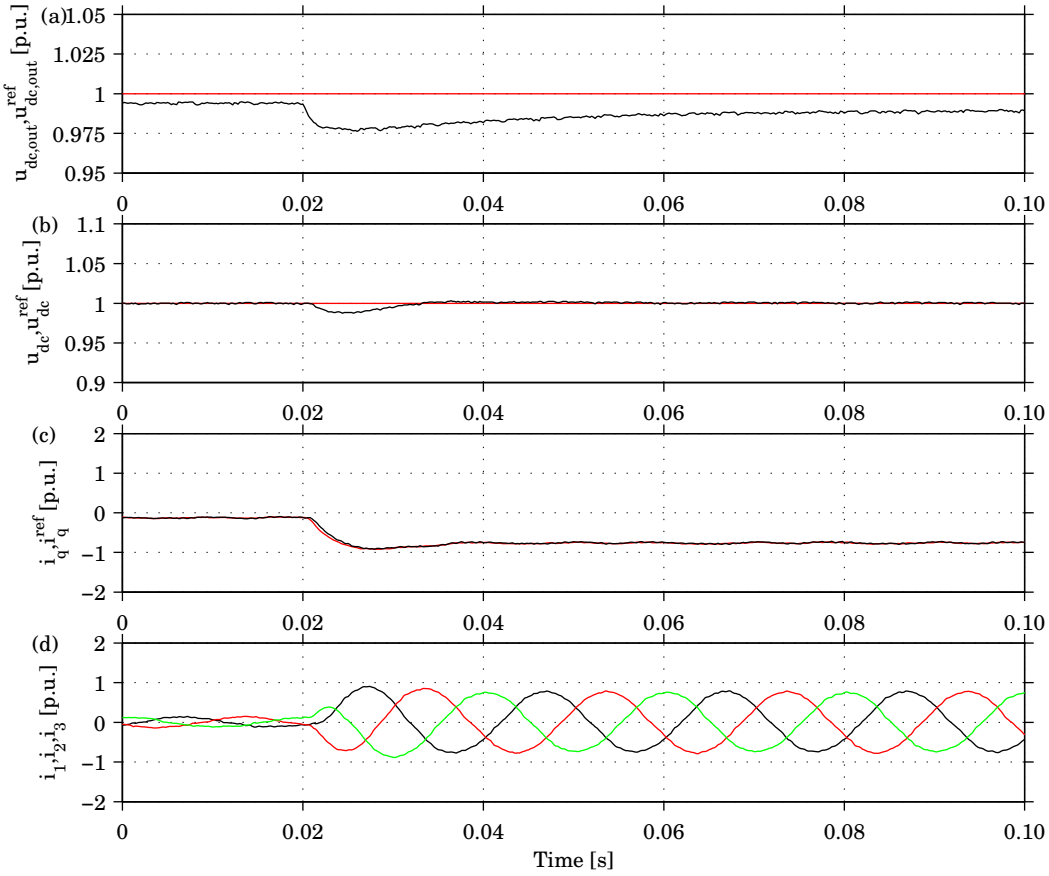

Fig. 5.12. Measurement results for Buck converter and LC dc-link-voltage controller. Connection of a 0.67 p.u. resistive load: (a) dc-output voltage, (b) dc-link voltage, (c) active grid current, and (d) three-phase currents.

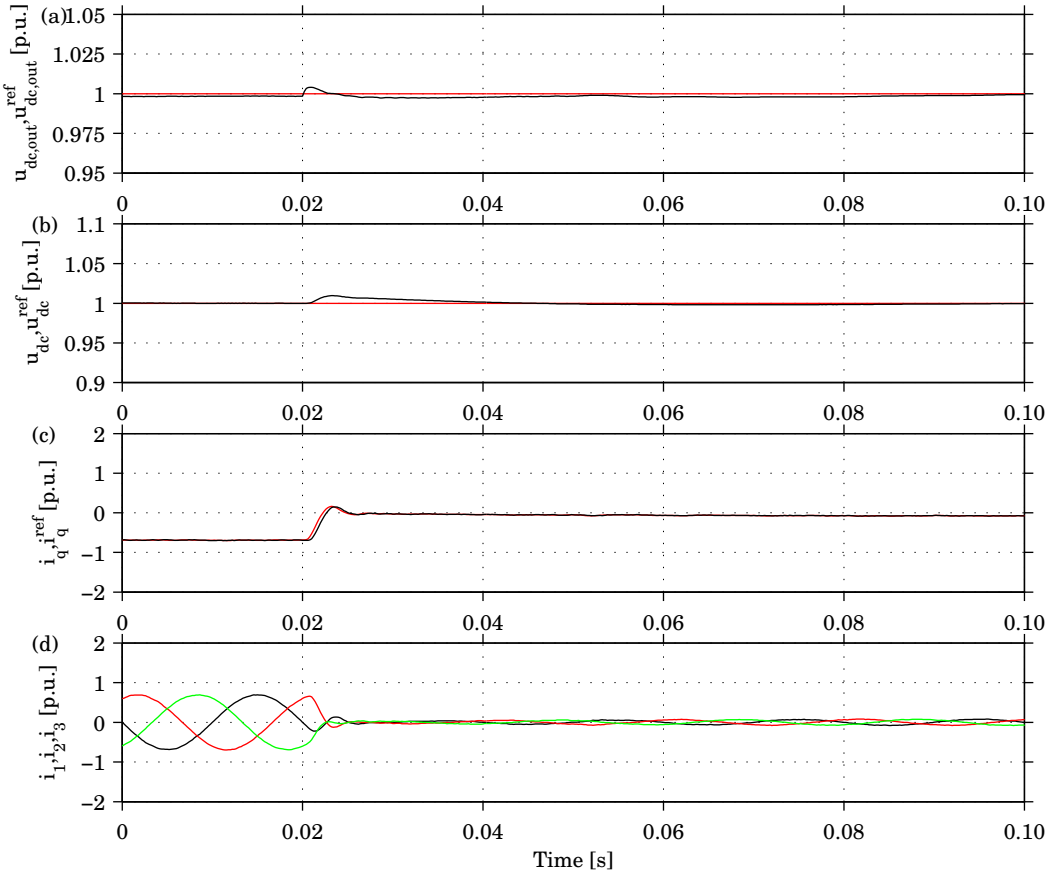

Fig. 5.13. Simulation results for Buck converter and LC dc-link-voltage controller. Disconnection of a 0.67 p.u. resistive load: (a) dc-output voltage, (b) dc-link voltage, (c) active grid current, and (d) three-phase currents.

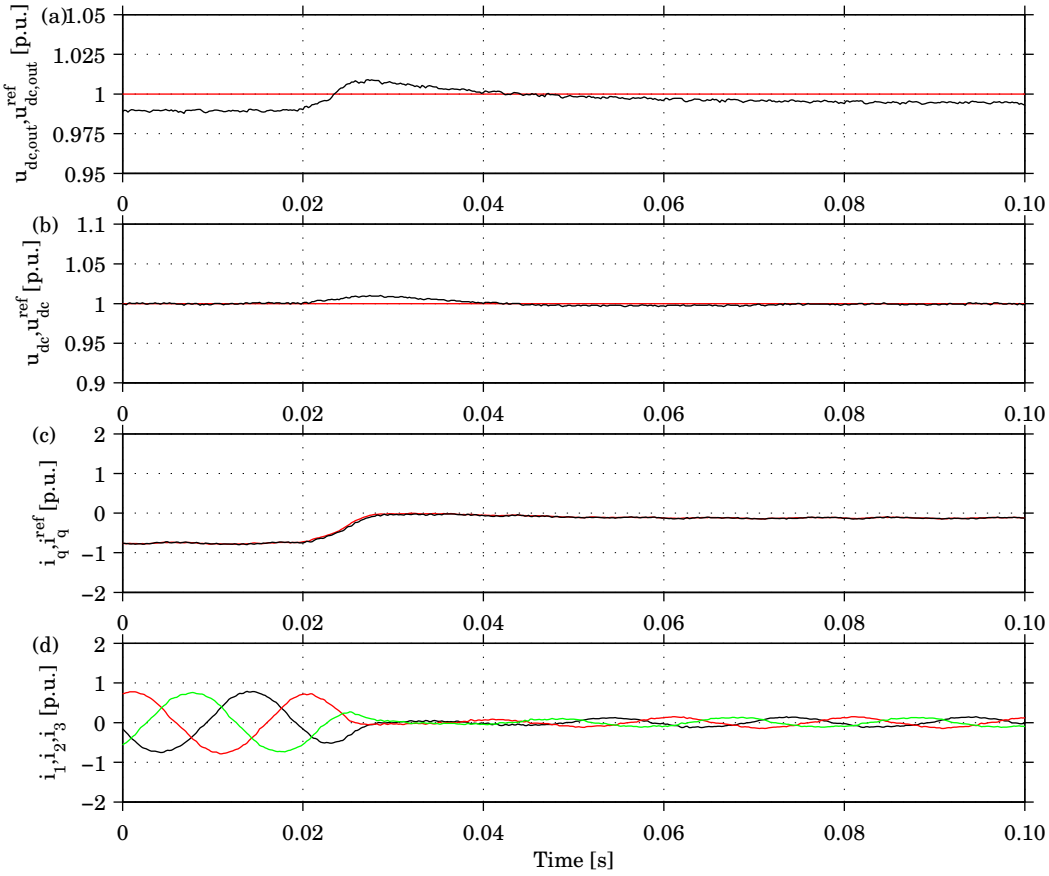

Fig. 5.14. Measurement results for Buck converter and LC dc-link-voltage controller. Disconnection of a 0.67 p.u. resistive load: (a) dc-output voltage, (b) dc-link voltage, (c) active grid current, and (d) three-phase currents.

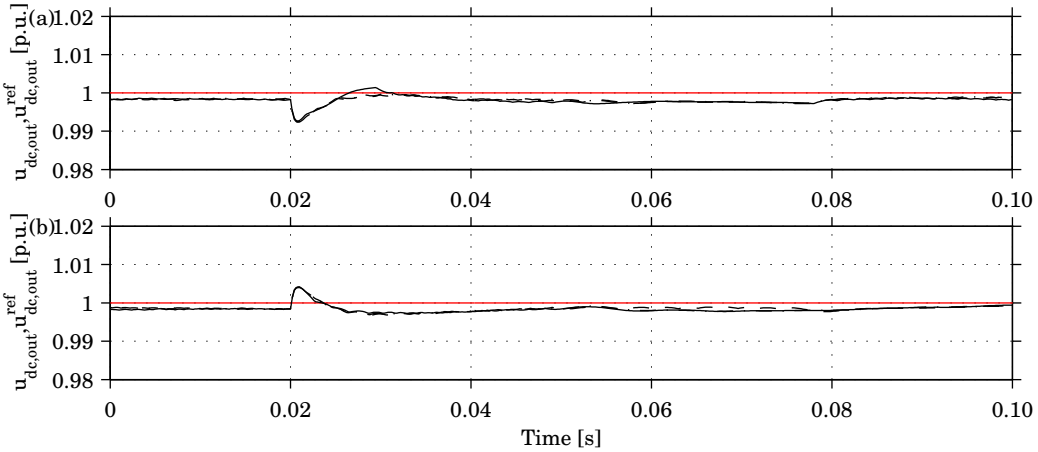

Fig. 5.15. Simulation results for Buck converter and LC dc-link-voltage controller. Connection (a) and disconnection (b) of different types of loads: CR (solid), CC (dashed) and CP (dashed-dotted).

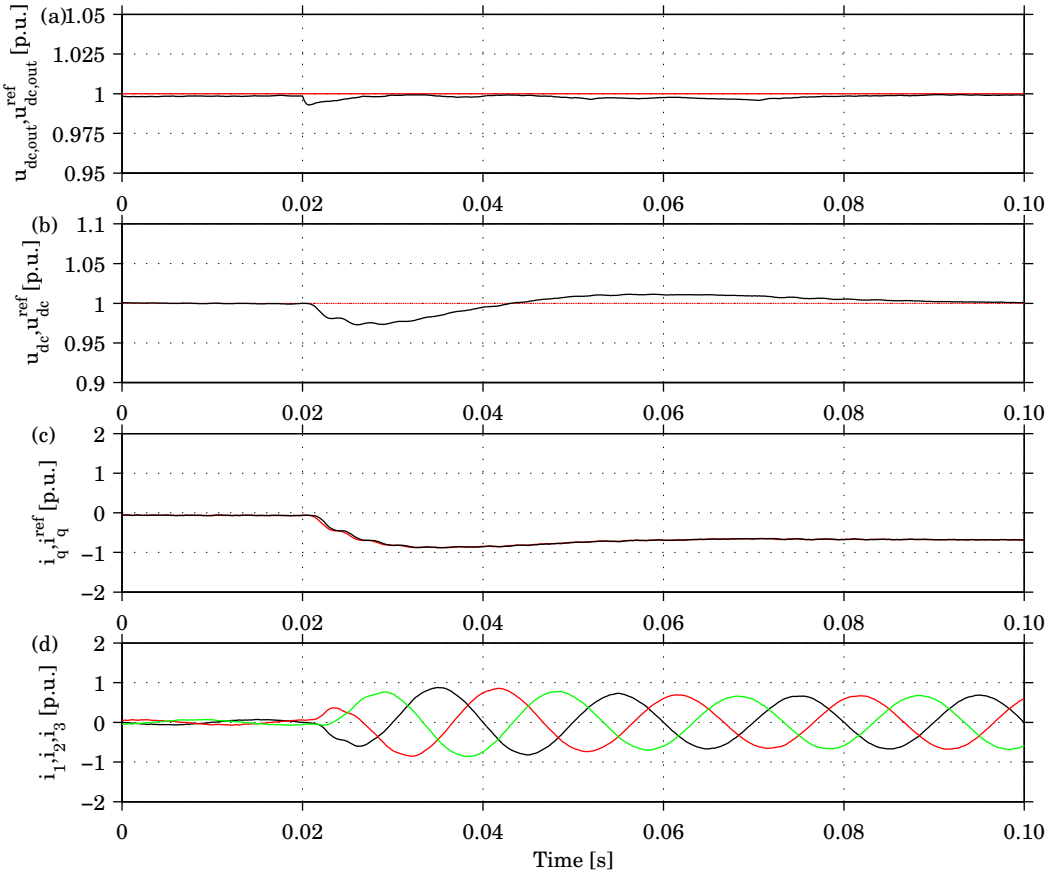

Fig. 5.16. Simulation results for Buck converter and OLC dc-link-voltage controller. Connection of a 0.67 p.u. resistive load: (a) dc-output voltage, (b) dc-link voltage, (c) active grid current, and (d) three-phase currents.

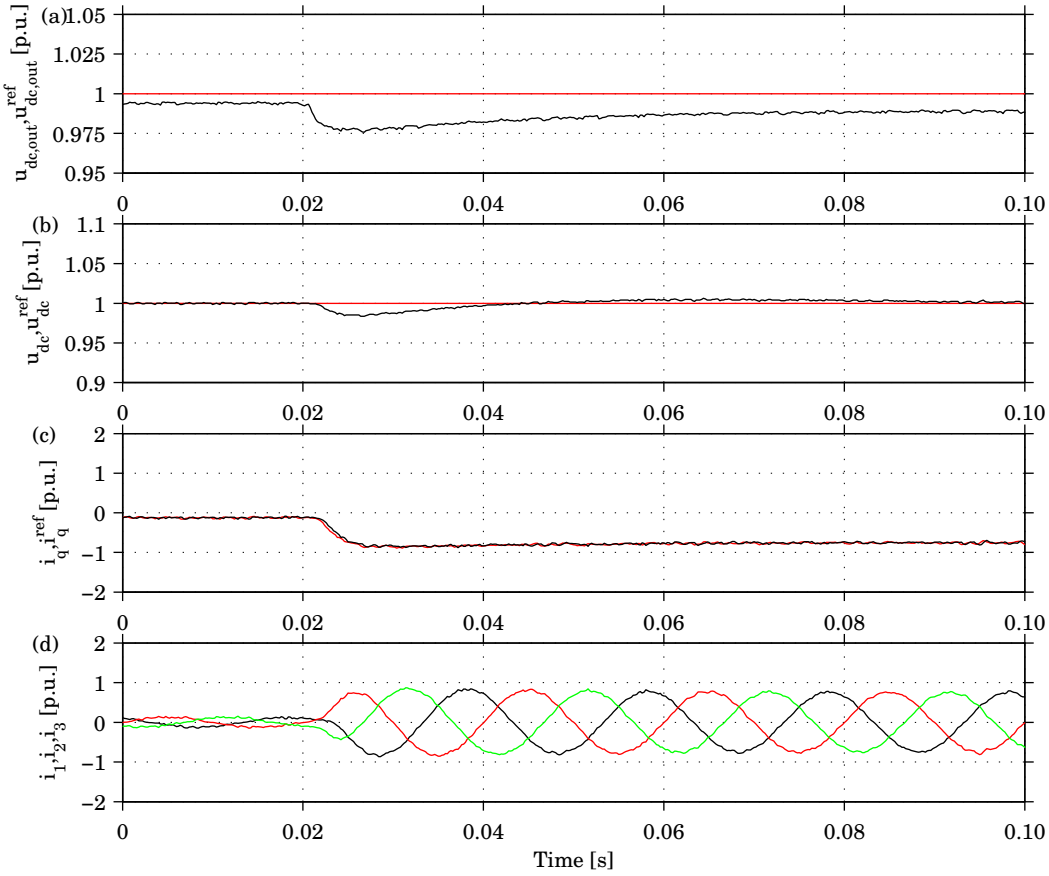

Fig. 5.17. Measurement results for Buck converter and OLC dc-link-voltage controller. Connection of a 0.67 p.u. resistive load: (a) dc-output voltage, (b) dc-link voltage, (c) active grid current, and (d) three-phase currents.

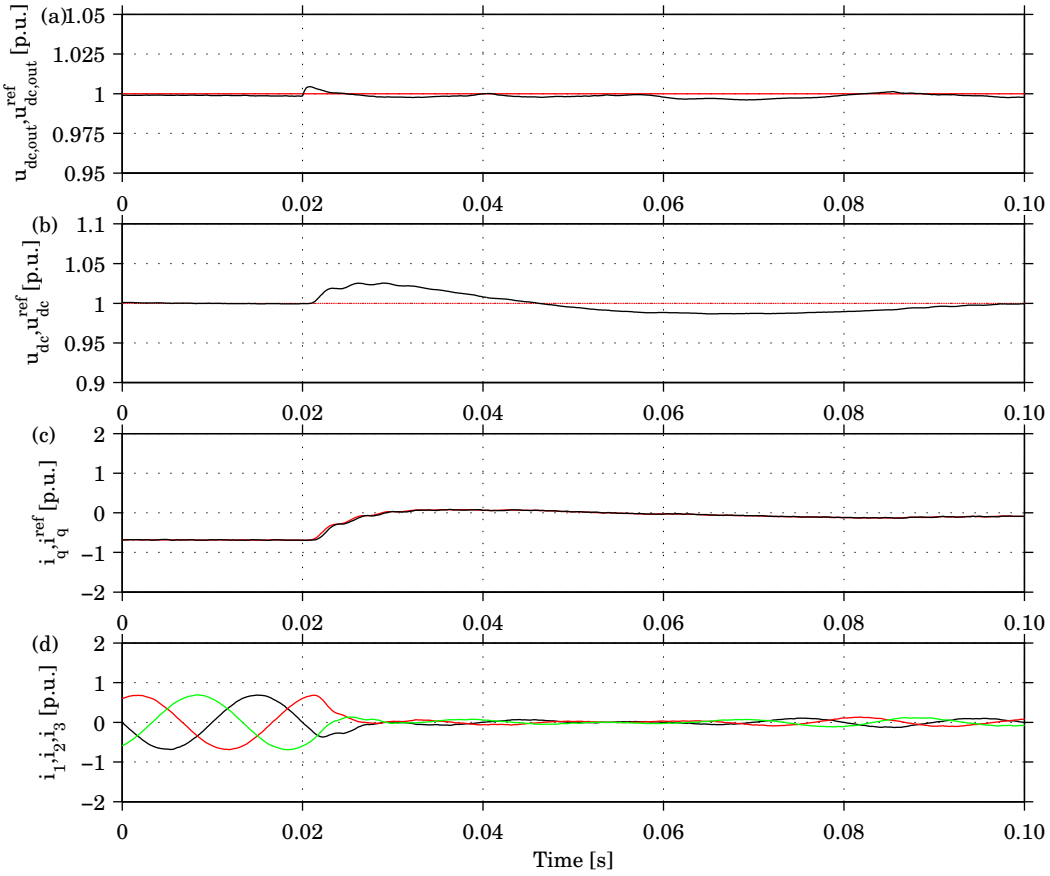

Fig. 5.18. Simulation results for Buck converter and OLC dc-link-voltage controller. Disconnection of a 0.67 p.u. resistive load: (a) dc-output voltage, (b) dc-link voltage, (c) active grid current, and (d) three-phase currents.

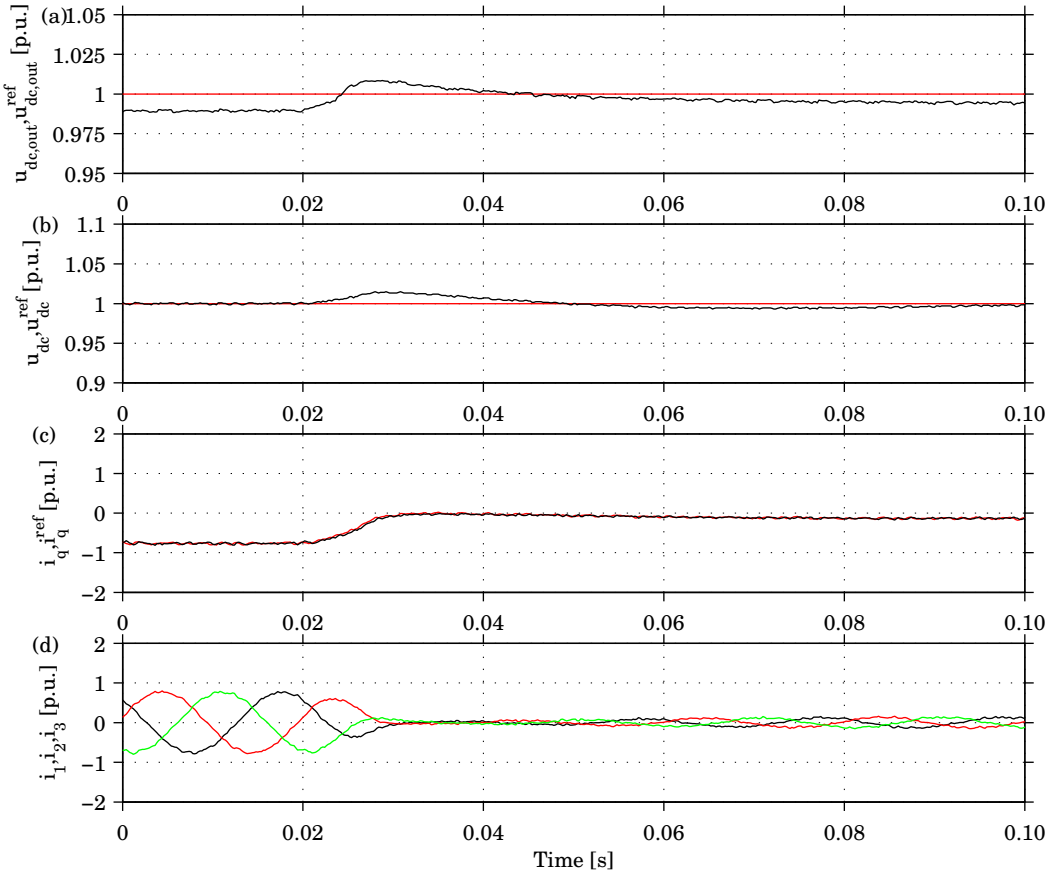

Fig. 5.19. Measurement results for Buck converter and OLC dc-link-voltage controller. Disconnection of a 0.67 p.u. resistive load: (a) dc-output voltage, (b) dc-link voltage, (c) active grid current, and (d) three-phase currents.

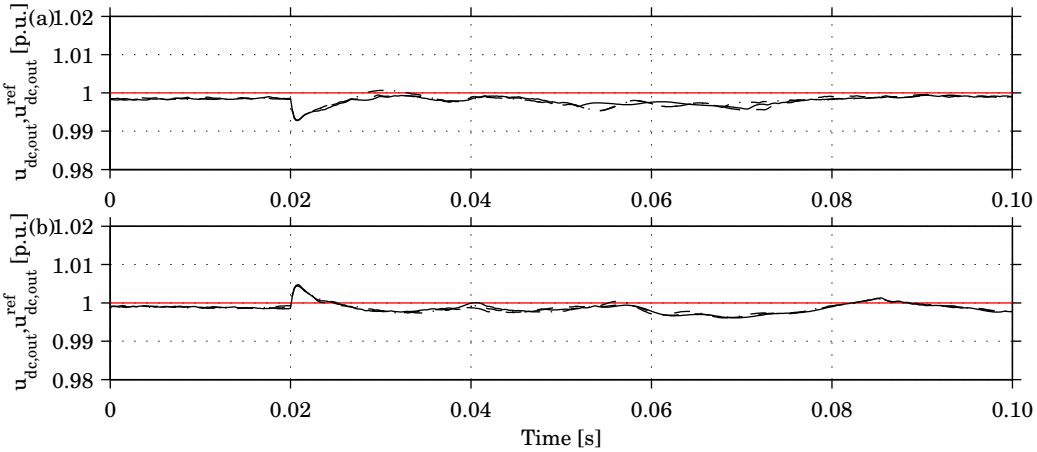

Fig. 5.20. Simulation results for Buck converter and OLC dc-link-voltage controller. Connection (a) and disconnection (b) of different types of loads: CR (solid), CC (dashed) and CP (dashed-dotted).

5.3.2 Disturbances

The system performance during disturbances on the ac grid is simulated and verified in the laboratory setup. As long as the output voltage of the VSC is higher than the desired output voltage of the Buck converter, and the output voltage of the VSC does not vary faster than the voltage controller of the Buck converter can follow, the output voltage can be maintained at the reference level. According to (4.27), the minimum retained grid voltage is determined by the maximum current that the VSC can handle. The system has been tested with a phase-to-phase fault with 0.75 p.u. retained voltage, 12 % unbalance, and 12° phase-angle jump in the simulation. In the laboratory it was a phase-to-phase fault with 0.79 p.u. retained voltage during 0.07 s, and with 27% unbalance and 11° phase-angle jump [68]. The smaller phase-angle jump will be seen as a smaller transient in the dc-link voltage and the higher unbalance as a higher oscillation in the dc-link voltage and the currents. To be able to make the fault in the laboratory, a weak ac grid was used, which is explained later in Chapter 6, and the gain of the VCC was therefore reduced to 70 % times dead-beat gain. The gain for EB was reduced to 125 Hz and for LC and OLC to 25 Hz. Due to the reduced gain only a 0.47 p.u. resistive load could be used.

The simulation results using EB, LC and OLC are shown in Figs. 5.21, 5.23 and 5.25, and the corresponding measurements are shown in Figs. 5.22, 5.24 and 5.26. All three controllers result in an oscillating dc-link voltage. The voltage controller of the Buck converter can follow the oscillation and the output voltage is unaffected. Practical limitations in the laboratory made it impossible to make faults which are close to the operation limit of converter. A simulation with a single-phase fault with 0.1 p.u. retained voltage is shown in Fig. 5.27, which clearly shows that the steady-state oscillation on the dc link does not affect the output dc voltage.

5.4 Conclusions

In this chapter, a proposed ac/dc interface consisting of a VSC and a Buck converter in series has been analyzed, simulated and tested in the laboratory. The results show that this interface is suitable to convert ac to an appropriate dc voltage. The performance of the system has been studied during connection/disconnection of loads and during disturbances on the ac grid, and the influence of the dc-link-voltage controller has been studied. Simulation results show that using LC will result in an oscillation of the dc-link voltage when the load is connected. The load step generates a current flowing between the dc-link capacitor and the low-pass-filter capacitor, and this current affects the LC and results in distorted grid currents. EB and OLC, which both do not measure the dc current, have a better transient response.

The system was also studied during an unsymmetrical disturbance on the ac grid, and simulations show that the output voltage of the Buck converter is not affected by the disturbance.

The conclusion is that the EB or OLC are preferable to use in a setup consisting of one VSC and one Buck converter. The fact that the EB is slower than the OLC does not affect the output voltage, as long as the dc-link voltage is higher than the output voltage.

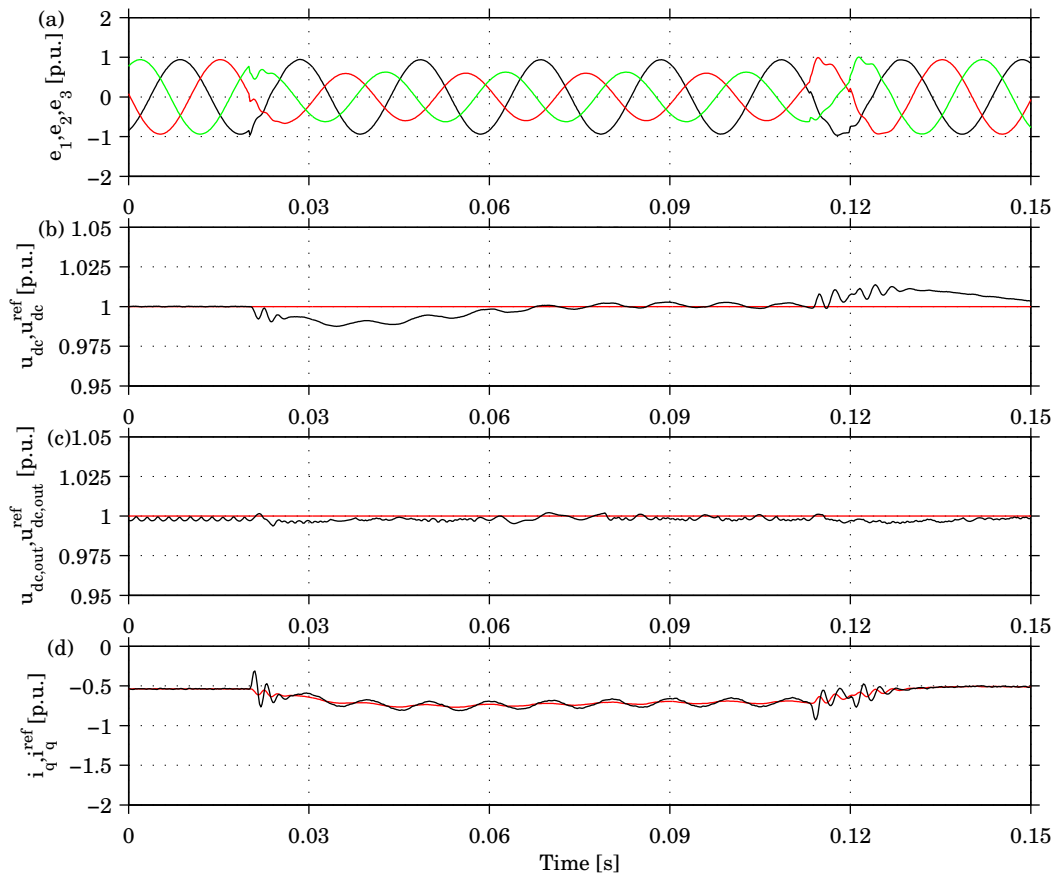

Fig. 5.21. Simulation results for Buck converter and EB during phase-to-phase fault: (a) grid voltages, (b) dc-link voltage, (c) dc output voltage, and (d) active grid current.

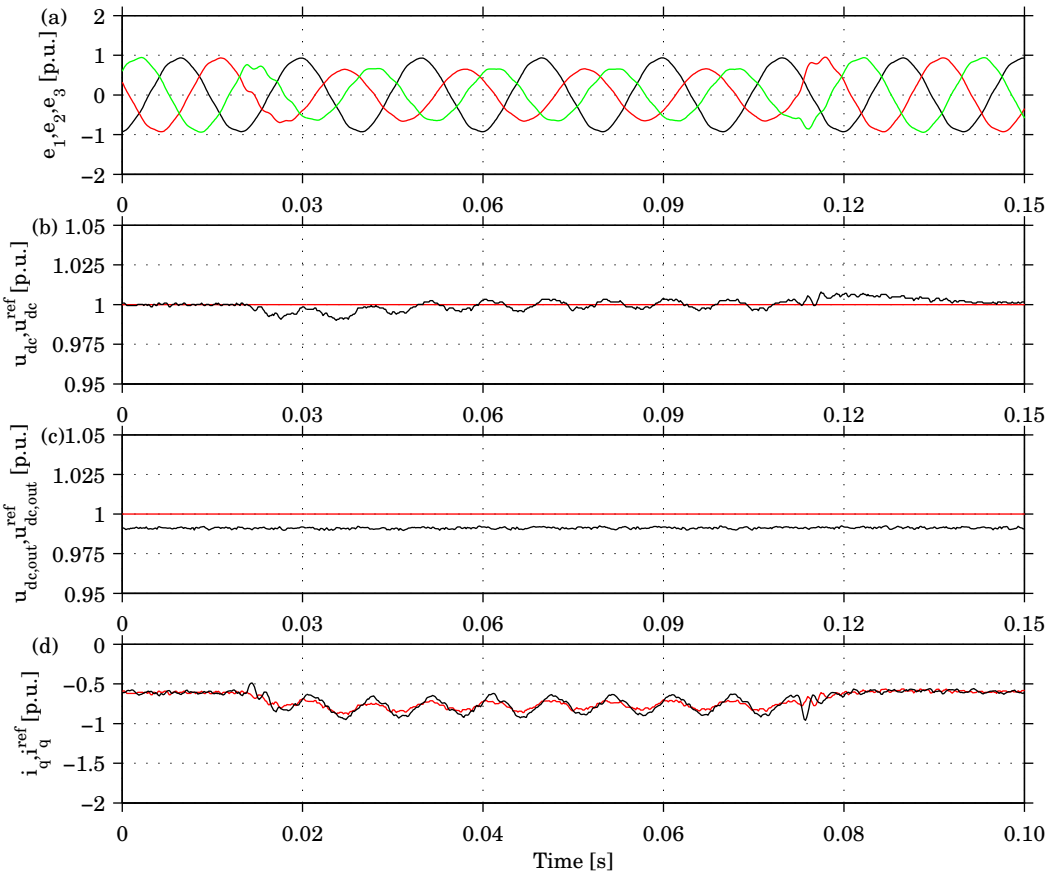

Fig. 5.22. Measurement results for Buck converter and EB during phase-to-phase fault: (a) grid voltages, (b) dc-link voltage, (c) dc output voltage, and (d) active grid current.

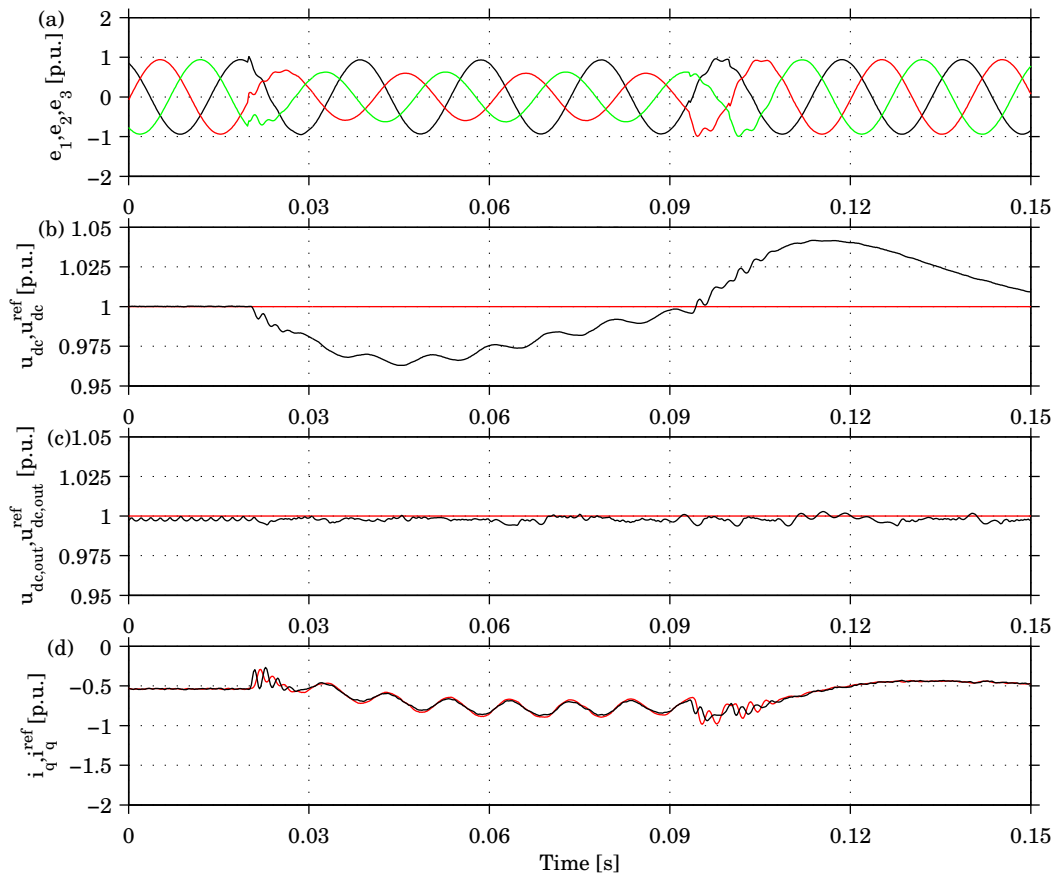

Fig. 5.23. Simulation results for Buck converter and LC during phase-to-phase fault: (a) grid voltages, (b) dc-link voltage, (c) dc output voltage, and (d) active grid current.

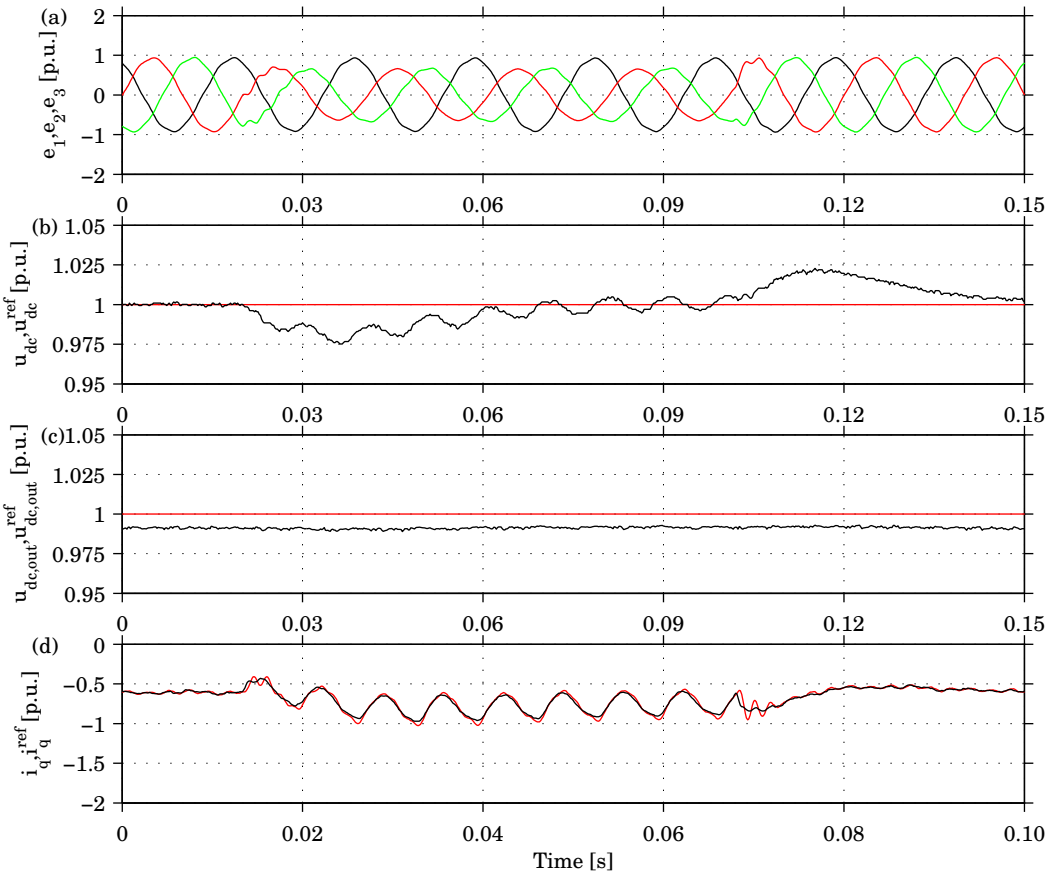

Fig. 5.24. Measurement results for Buck converter and LC during phase-to-phase fault: (a) grid voltages, (b) dc-link voltage, (c) dc output voltage, and (d) active grid current.

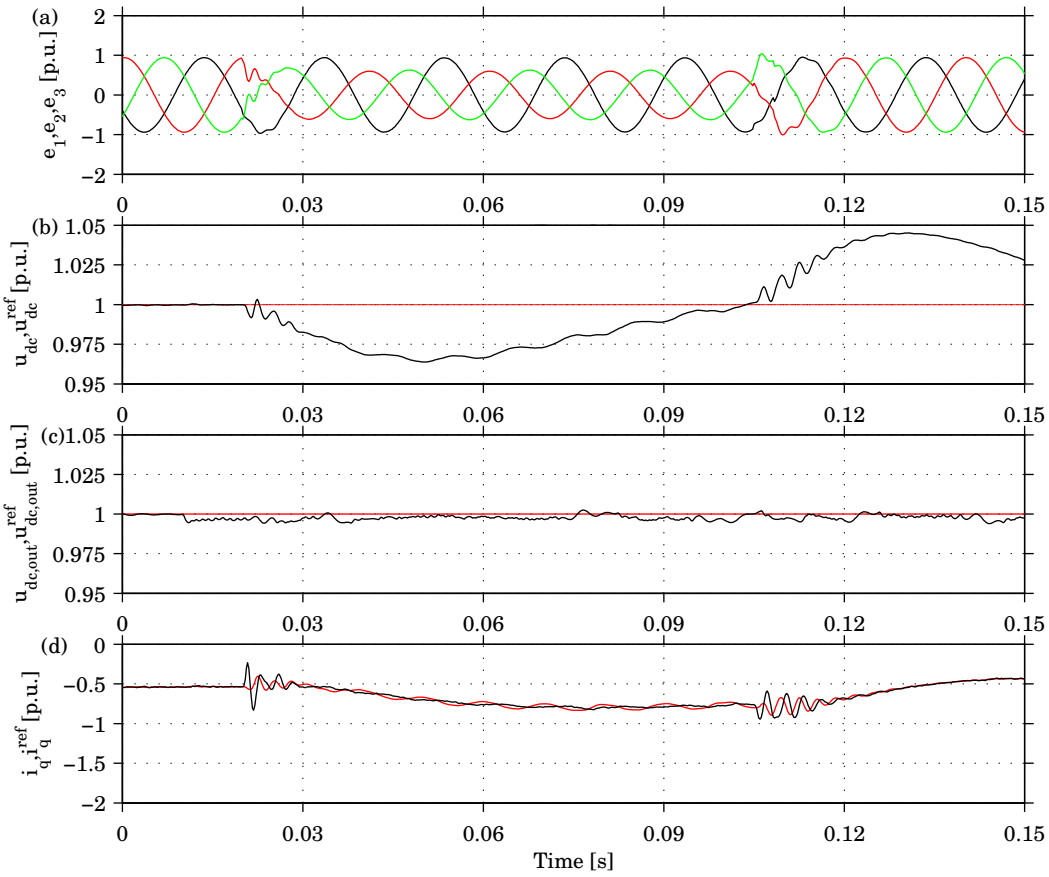

Fig. 5.25. Simulation results for Buck converter and OLC during phase-to-phase fault: (a) grid voltages, (b) dc-link voltage, (c) dc output voltage, and (d) active grid current.

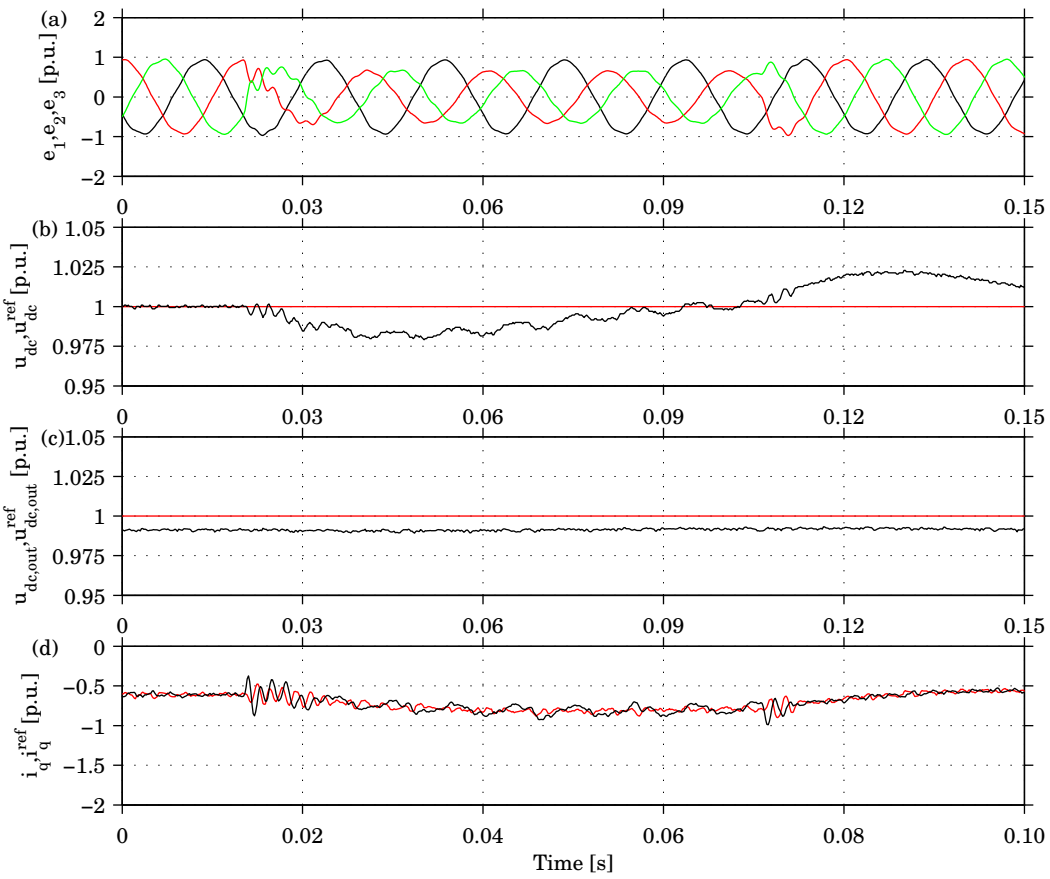

Fig. 5.26. Measurement results for Buck converter and OLC during phase-to-phase fault: (a) grid voltages, (b) dc-link voltage, (c) dc output voltage, and (d) active grid current.

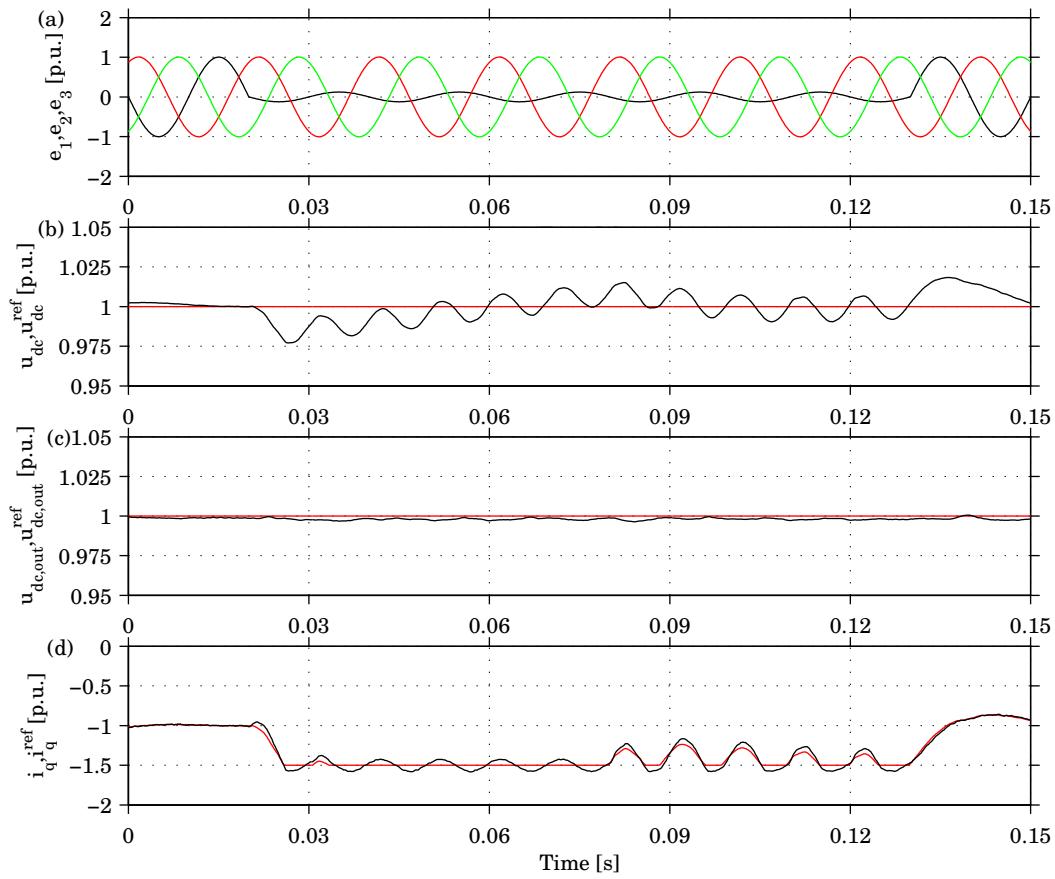

Fig. 5.27. Simulation results for Buck converter and EB during single-phase fault: (a) grid voltages, (b) dc-link voltage, (c) dc output voltage, and (d) active grid current.

Chapter 6

Experimental Setup of a Small DC Network

In this chapter, the experimental setup used for all measurement results presented in Chapter 4 and 5 is presented. The VSC converter and the Buck converter used during the work are described. A small dc network is built consisting of four loads and a VSCBC interface. The system was tested during steady-state operation, load transients and disturbances on the ac grid. The loads were also supplied with ac and the results were compared.

6.1 Experimental Setup

The experimental setup used to test and verify the simulation results is described in this section. An overview of the system is shown in Fig. 6.1 where the different parts are shown. The system consists of the two converters which are a three-phase two-level VSC and a step-down dc/dc converter, protection unit, voltage and current measurement equipment and a control system. A detailed scheme of the converters is shown in Fig. 6.2. A photo of the laboratory setup is shown in Fig. 6.3. The voltage and current measurement sensors are built inside a box to reduce the interference with the surrounding converters, which generates RFI.

6.1.1 Control System

The control system is a dSPACE DSP system DS 1103 [69]. The measured voltages and currents are connected to the analogue inputs of the DSP. The control algorithms which are implemented in C code and MatLab/Simulink building blocks generate the control signals to the system. The analogue firing signals to the converters are converted into lighting pulses using an optical transmitter, which are transferred through optical fibres to the control cards of the converters. Analogue control signals are used to control the protection unit of the system.

6.1.2 VSC

The three-phase VSC is a Danfoss VLT 5003 [70], and it has a rated power of 2.8 kW (4.1 A). The VSC is connected to the ac grid through a protection unit and three 15 mH L-filters, one for each phase. The VSC and the grid filter mounted in a rack are shown in Fig. 6.4.

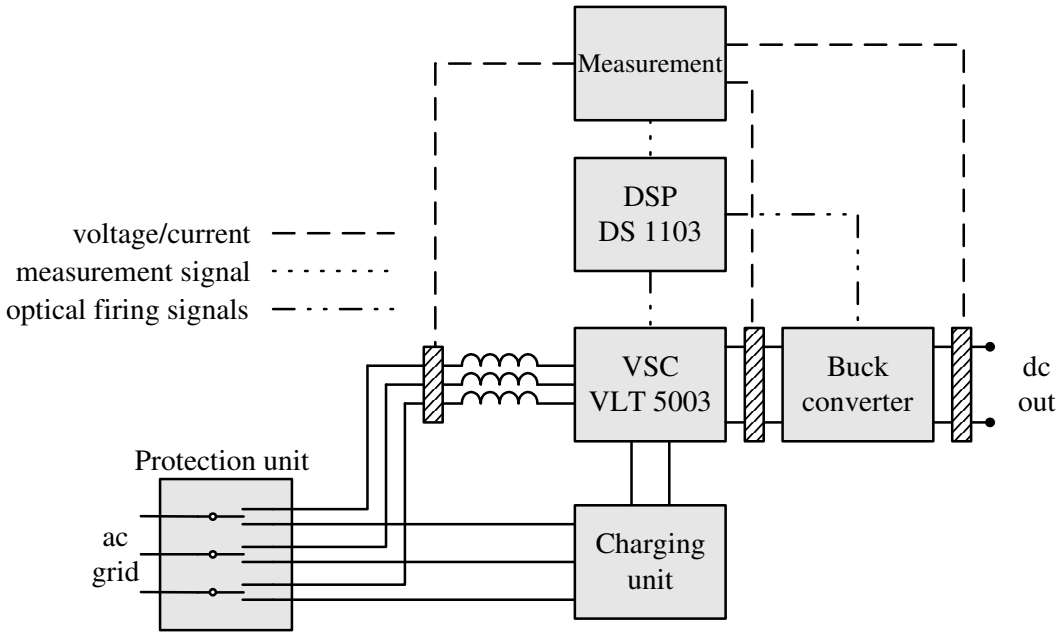

Fig. 6.1. Laboratory setup consisting of a VSC, a Buck converter, a protection unit, a charging unit, voltage and current measurement, and a control system.

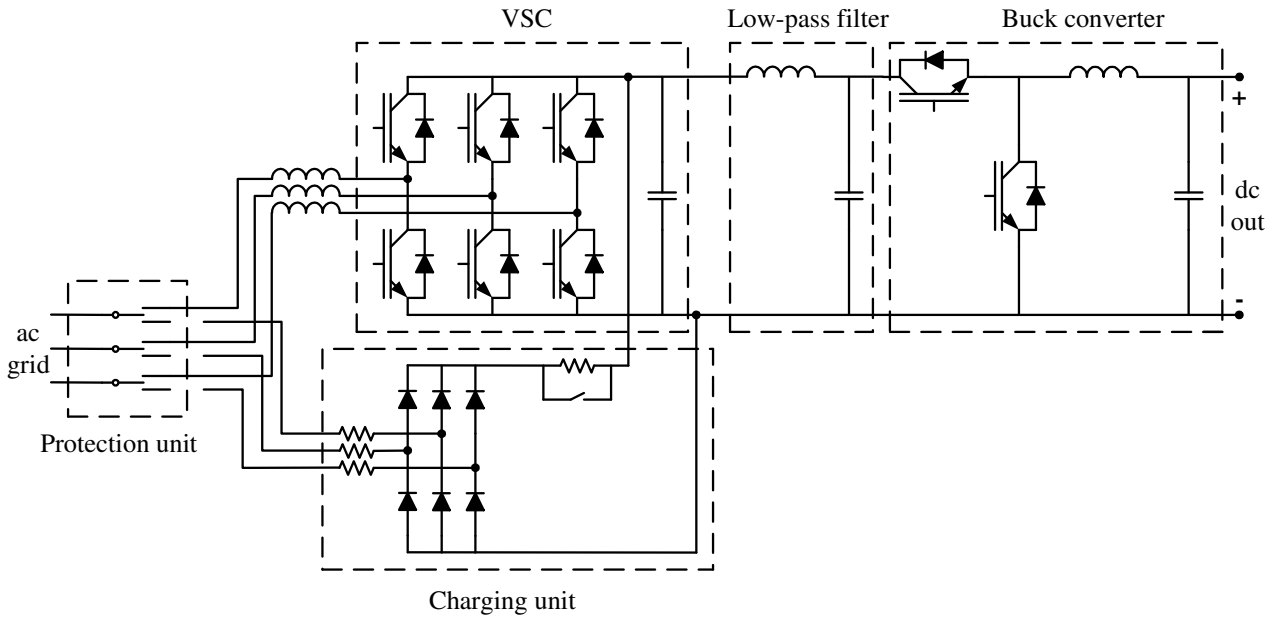

Fig. 6.2. Scheme of the the VSC connected in series with the Buck converter.

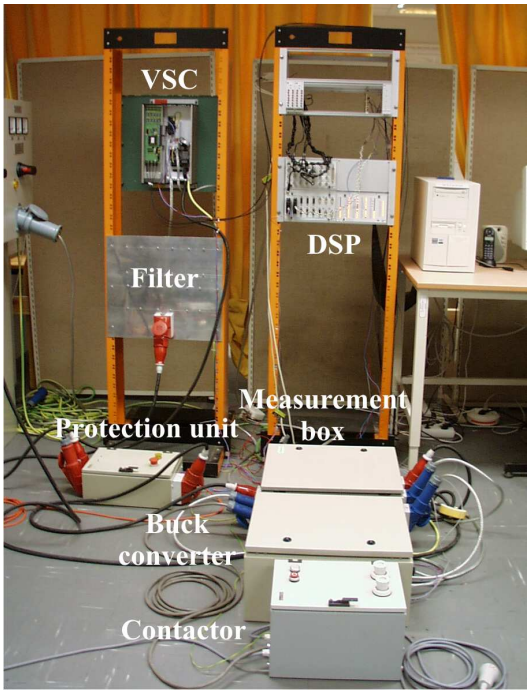

Fig. 6.3. Photo of the laboratory setup with DSP, VSC, grid filters, Buck converter, measurement box, protection unit and a contactor.

The optical firing pulses are converted to control signals to the six IGBT valves using a control/protection card built by Aalborg University, Denmark. The card has overcurrent protection, and dc-link-over- and under-voltage protection, with the same settings as the protection unit. However, it uses analogue signals which makes it faster than the protection unit, which is used as back up. The converter is used with 5 kHz switching frequency, and the dead-time of the IGBTs is 1 µs. The VSC is also protected by a protection unit. If the ac currents become higher than 2.0 p.u., or the dc-link voltage becomes lower than 0.75 p.u. or higher than 1.15 p.u. the protection unit disconnects the VSC from the ac grid. The protection unit shown in Fig. 6.5 is controlled via the DSP using sampled values; this makes the protection slow.

6.1.3 Buck Converter

The Buck converter is designed for input voltage up to 800 V, output voltage up to 800 V, and a 15 A rms maximum inductor current. The inductance is 2 mH and the output capacitor is 1100 µF. A low-pass filter consisting of a 1 mH inductance and a 340 µF capacitor is connected between the VSC and the Buck converter which will help to damp the oscillations between the two dc-link capacitors. The switching frequency of the converter is 5 kHz, and the dead-time of the IGBTs is 3 µs. A photo of the converter is shown in Fig. 6.6.

6.1.4 Network Model and Supply

The laboratory setup is supplied with a stiff 400 V ac grid and was used for the steady state measurements. A scaled transmission line model in the department laboratory was used to generate the unsymmetrical fault which was used both with the VSC and the VSCBC. The scaled model consists of six π-section connected in series, were each section represents a

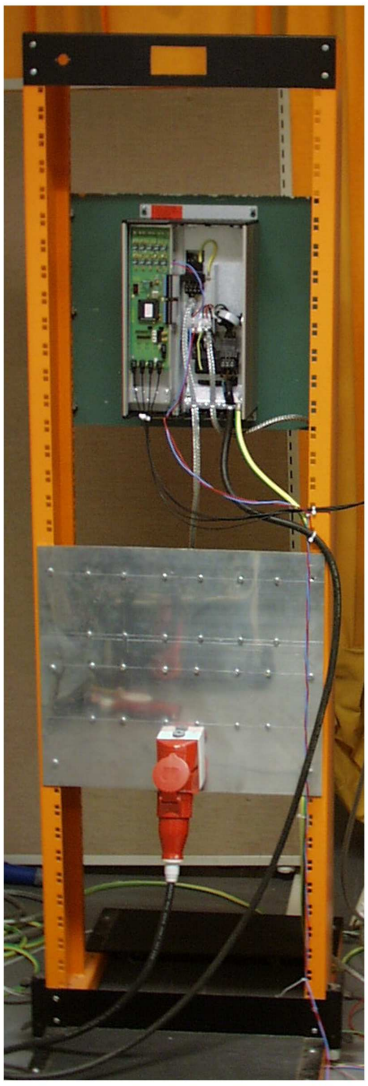

Fig. 6.4. The Danfoss VLT 5003 connected to the ac grid via grid filters.

Fig. 6.5. Photo of the protection unit.

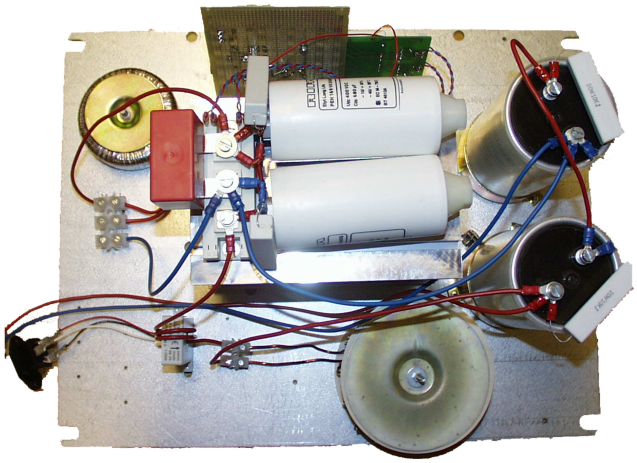

Fig. 6.6. Buck converter.

TABLE 6.1
PARAMETERS OF THE SCALED TRANSMISSION LINE MODEL.

Parameter	Value
e	400 V
R_π	0.05 Ω
L_π	2 mH
C_π	46 µF
R_{fault}	1.4 Ω
R_{load}	6 Ω

150 km long transmission line. The model is supplied from a strong 400 V ac grid. To avoid Ferranti effect on the transmission line, a resistive load is connected at the end of it. The parameters of the model is reported in Table 6.1, a scheme of the setup is shown in Fig. 6.7, and a photo of the transmission line model is shown in Fig. 6.8.

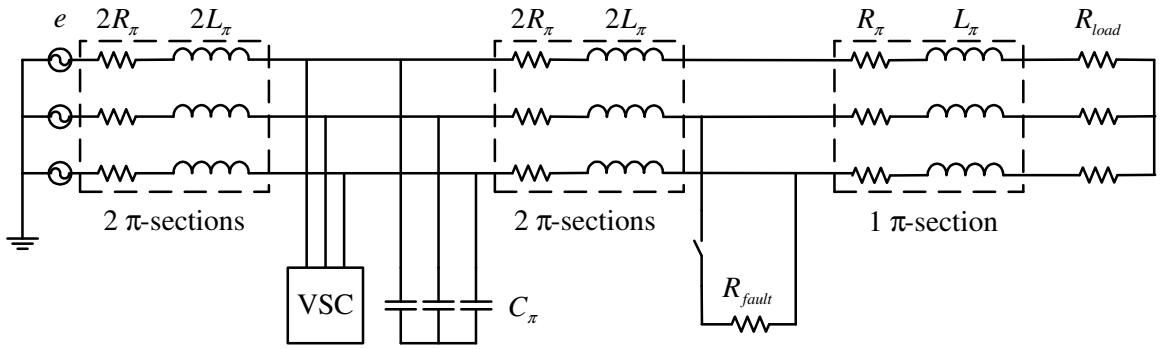

Fig. 6.7. Scheme of the transmission line model.

6.2 System Start-Up

When the system is started, the voltages of the dc-link and the output capacitors are zero. The protection unit and the built-in diode rectifier of the VSC (charging unit) are used to first charge the dc link to a steady-state level and then after a preset charge time, connect the VSC

Fig. 6.8. Photo of the transmission line model.

to the grid and disconnect the charging unit. The charging of the dc link is shown in Fig. 6.9. The resistors used to limit the inrush current when charging the capacitor lead to a voltage drop. The drop can be seen in Fig. 6.9 (Diode → IGBT) as a step when the protection unit connects the VSC to the ac grid. When the dc-link is supplied by the IGBTs, it is possible to start switching and control the dc-link voltage. The start of the VSC is shown in Fig. 6.10. The dc-link voltage is boosted up to the reference value. Finally, the Buck converter is started. The output capacitor of the Buck converter is uncharged in the beginning, and the capacitor is charged to the reference output level. This is shown in Fig. 6.11.

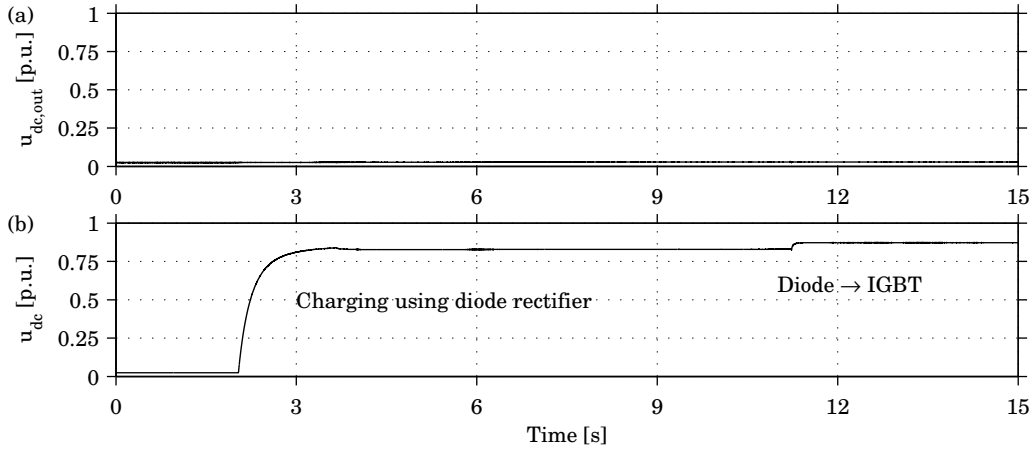

Fig. 6.9. Charging the VSC: (a) output dc voltage and (b) dc-link voltage.

6.3 Steady-State Operation

The proposed ac/dc interface which was built and tested in the laboratory was also used to supply a small dc system. Four loads (see Chapter 3) were used in the test, and they are shown in Figs. 6.12 and 6.13. Each load was connected to the interface by circuit breakers designed for both ac and dc voltage, which makes it possible to switch the load on and off.

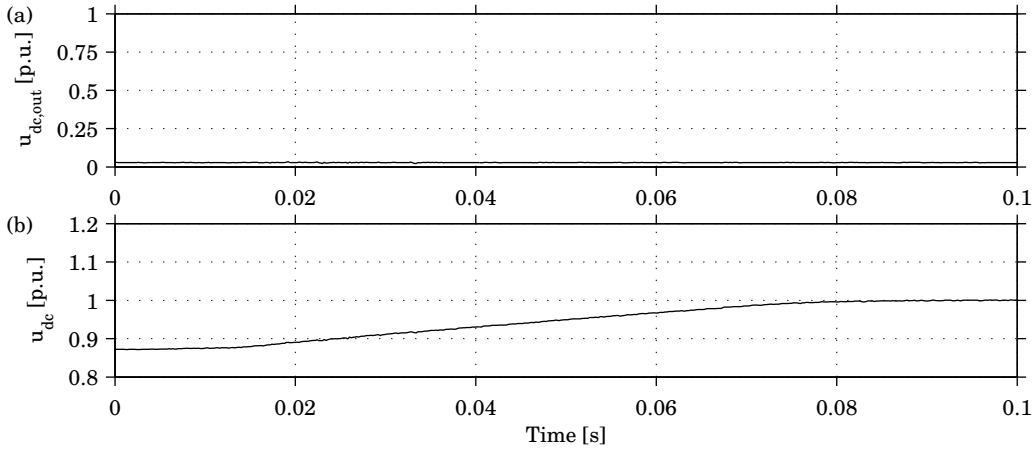

Fig. 6.10. Start of the VSC: (a) output dc voltage and (b) dc-link voltage.

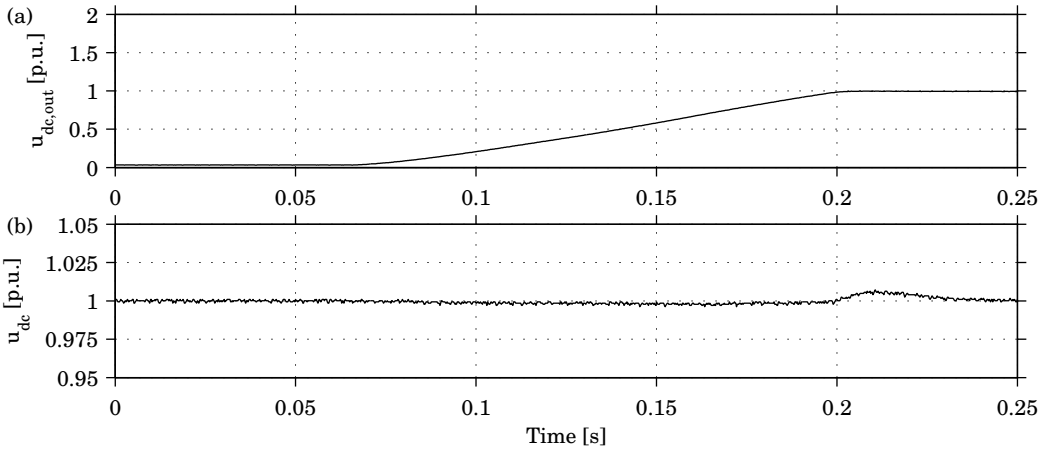

Fig. 6.11. Start of the Buck converter: (a) output dc voltage and (b) dc-link voltage.

TABLE 6.2
COMPONENTS OF THE SMAL DC SYSTEM.

Component	Model	Rating
Circuit breaker	Siemens 3RV 1321-1J10	400 V, 10 A
Fluorescent lamp	Philips	72 W
Compact fluorescent lamp	Philips	11 W
Computer		80 W
Coffee maker	Philips	900 W

The circuit breakers which are shown in Fig. 6.14 are rated 400 V dc and 10 A (10 kA maximum breaking capacity). Data of the components are reported in Table 6.2.

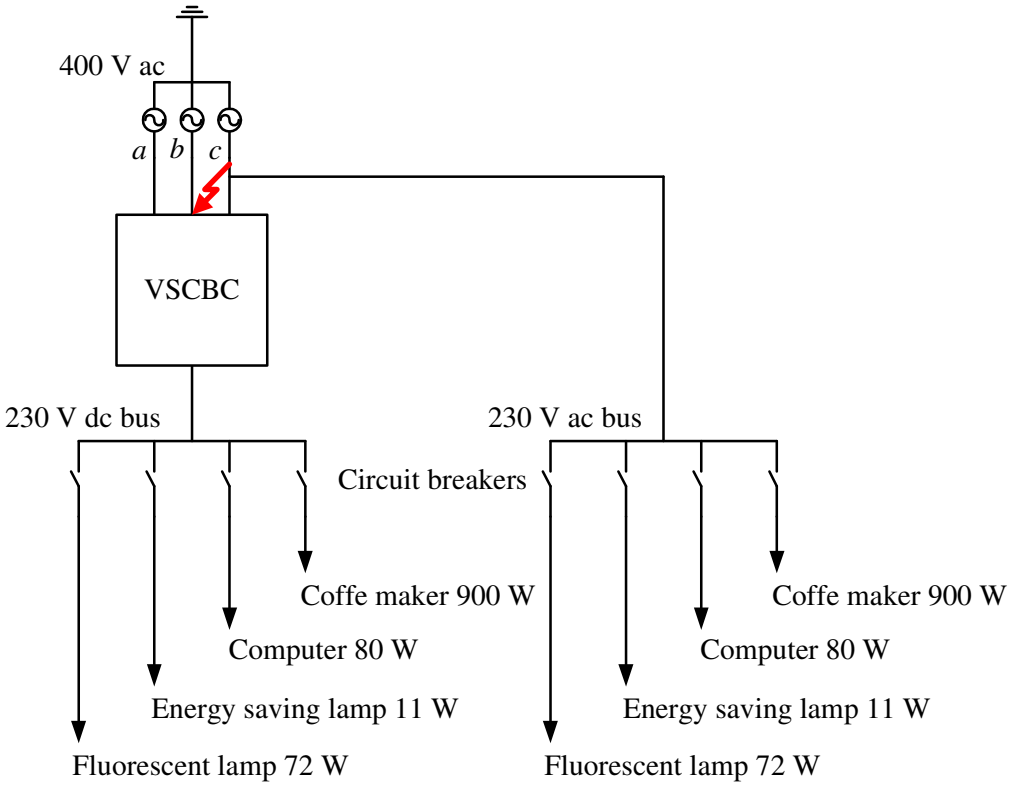

Fig. 6.12. Scheme of the small dc system for unsymmetrical fault tests.

The dc load current, the output dc voltage, the dc-link voltage and the three-phase grid currents when all four loads are connected to the Buck converter is shown in Fig. 6.15. The dc load current is almost constant, which indicates that the loads are suitable to supply with dc. The three-phase ac grid currents are also sinusoidal, and a zoom of phase a is shown in Fig. 6.16 together with its frequency spectrum, which shows that there are no low-frequency harmonics present in the grid current. To be able to compare the steady-state performance, the loads were also supplied with ac. The load current of all four loads were recorded and the FFT of the current calculated. Fig. 6.17 shows the load current of the compact fluorescent lamp. It contains a high amount of low-order harmonics since it is using a diode rectifier. The fluorescent lamp has a PFC which reduces the harmonics which can be seen in Fig. 6.18. The computer also uses a diode rectifier without PFC and the load current contains low-order harmonics which can be seen in Fig. 6.19. Fig. 6.20 shows the load current for the coffee

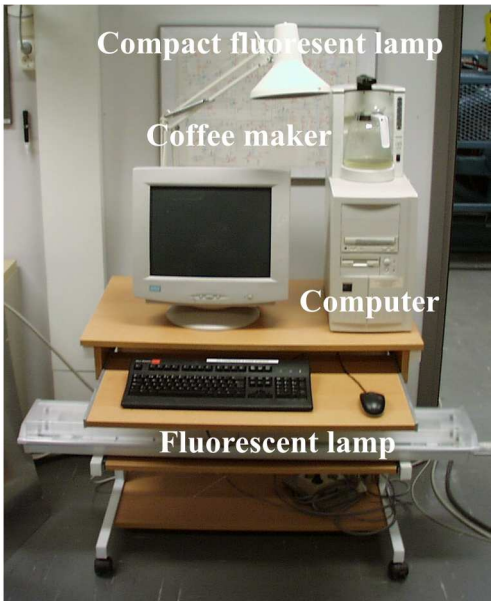

Fig. 6.13. Loads in the small dc system: a fluorescent lamp, a compact fluorescent lamp, a computer and a coffee maker.

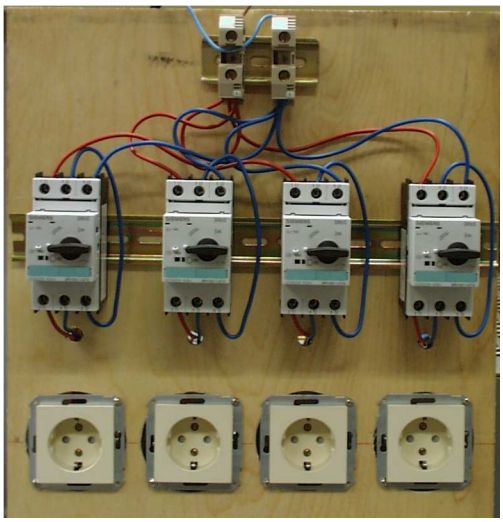

Fig. 6.14. DC circuit breakers used to protect and connect/disconnect the loads (Siemens 3RV 1321-1J10).

maker which is a purely resistive load, and therefore draws a purely sinusoidal grid current. The total load current is shown in Fig. 6.21. The load current is dominated by the coffee maker, which reduces the content of harmonics in the grid current. Using only loads like the computer would generate a high amount of harmonics. For supplying these loads, the dc system has the advantage of gaining balanced and harmonics free three-phase grid currents.

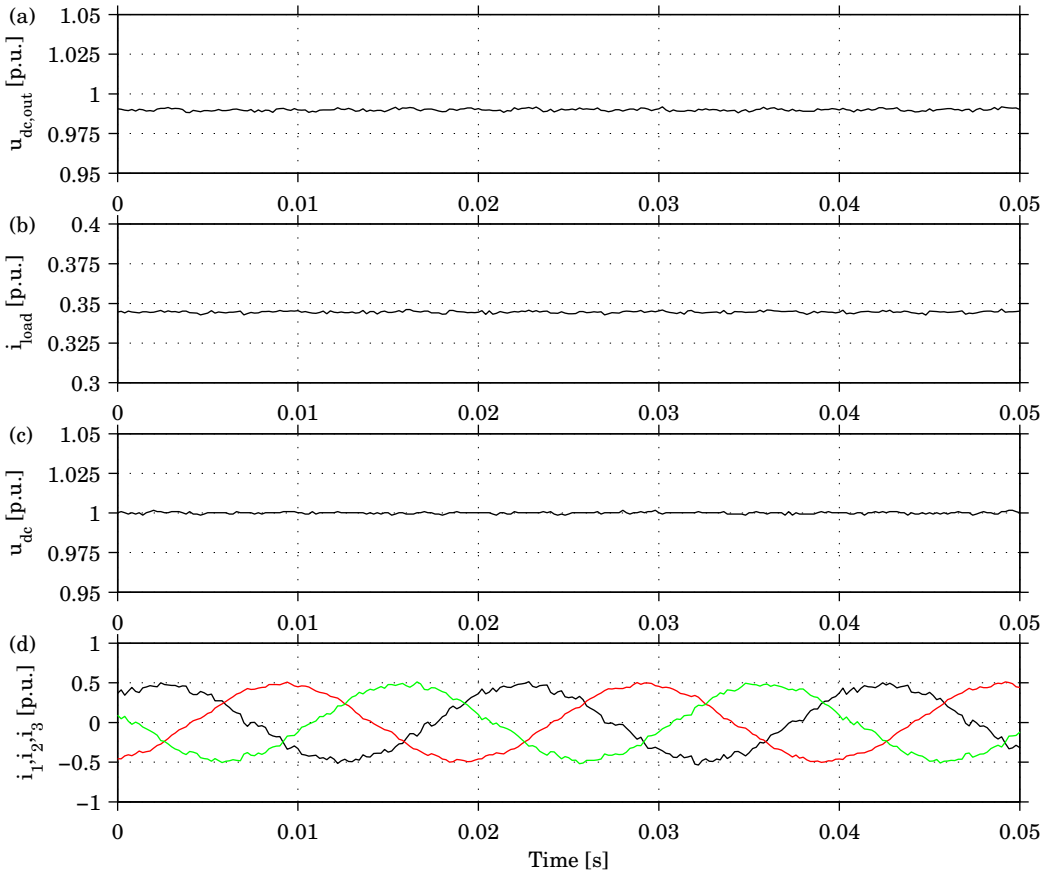

Fig. 6.15. Operation of small dc network: (a) output dc voltage, (b) dc load current, (c) dc-link voltage and (d) three-phase grid currents.

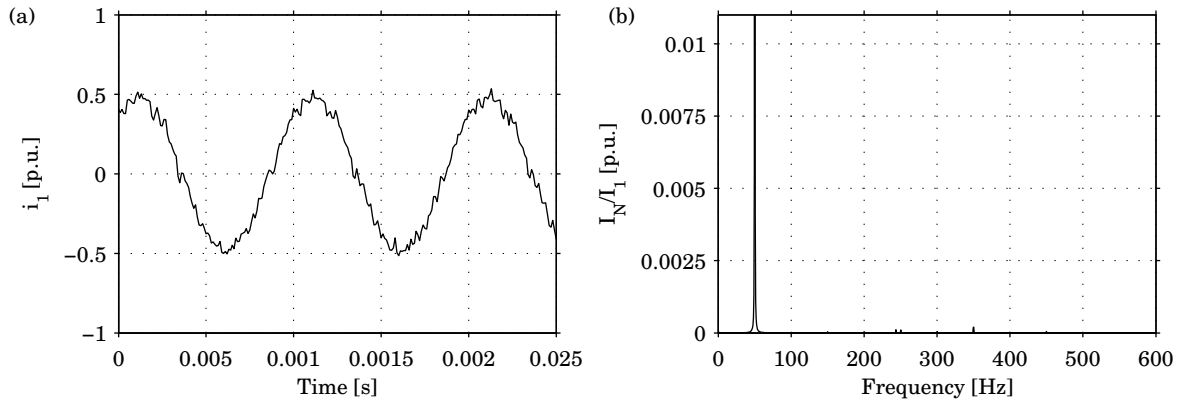

Fig. 6.16. Phase current a of the VSC when all four loads are connected: (a) phase current and (b) FFT of the phase current.

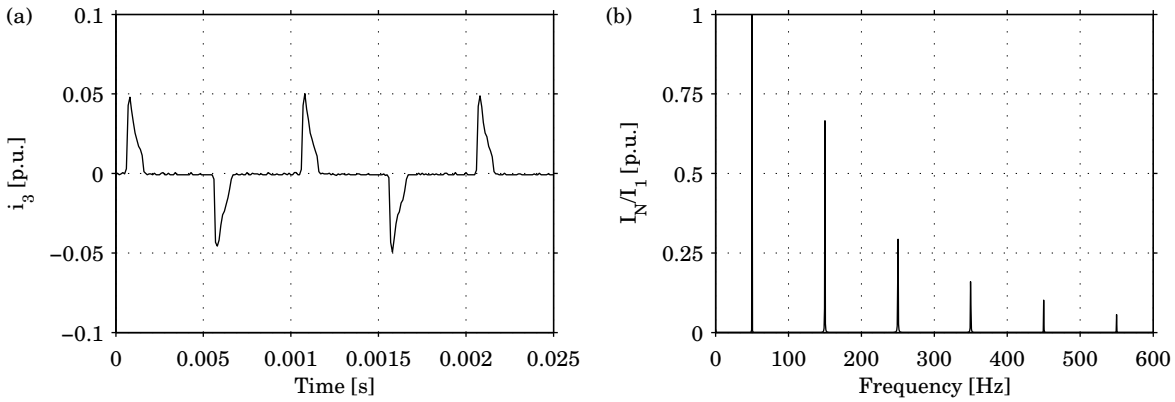

Fig. 6.17. Load current of the compact fluorescent lamp: (a) phase current and (b) FFT of the phase current.

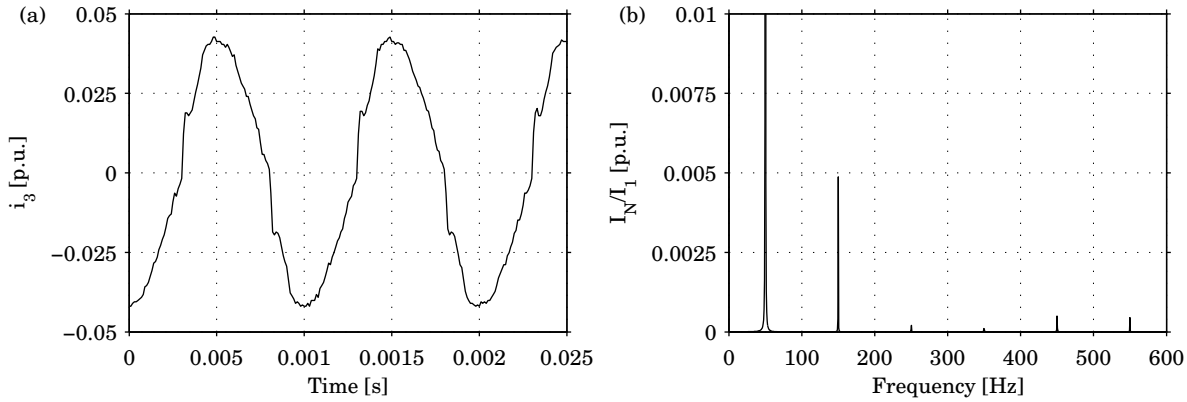

Fig. 6.18. Load current of the fluorescent lamp: (a) phase current and (b) FFT of the phase current.

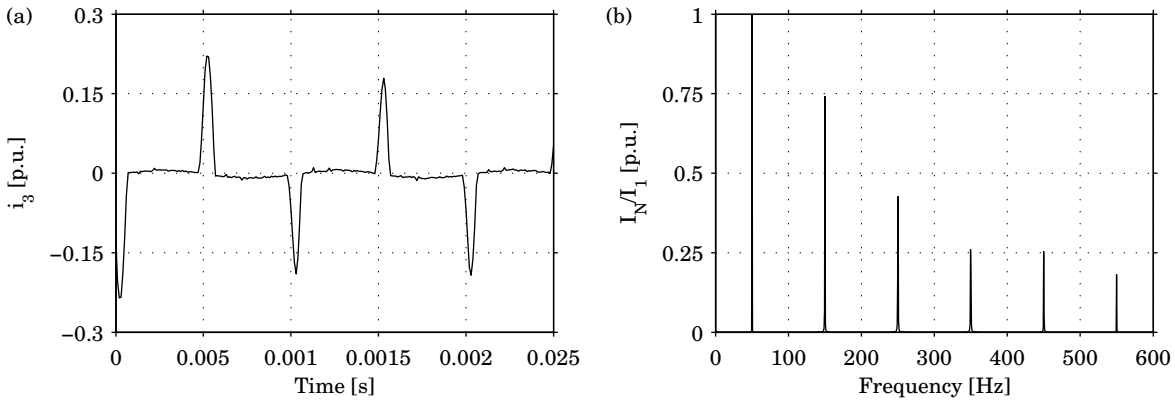

Fig. 6.19. Load current of the computer: (a) phase current and (b) FFT of the phase current.

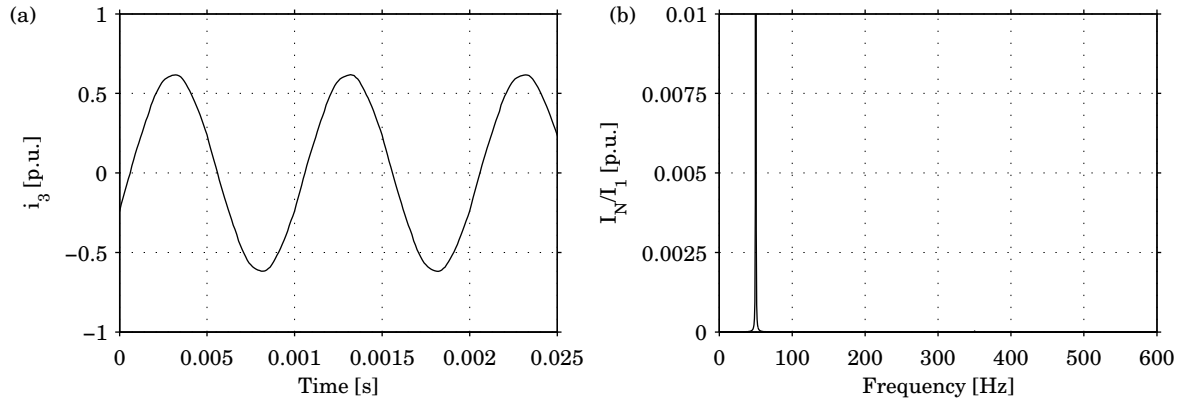

Fig. 6.20. Load current of the coffee maker: (a) phase current and (b) FFT of the phase current.

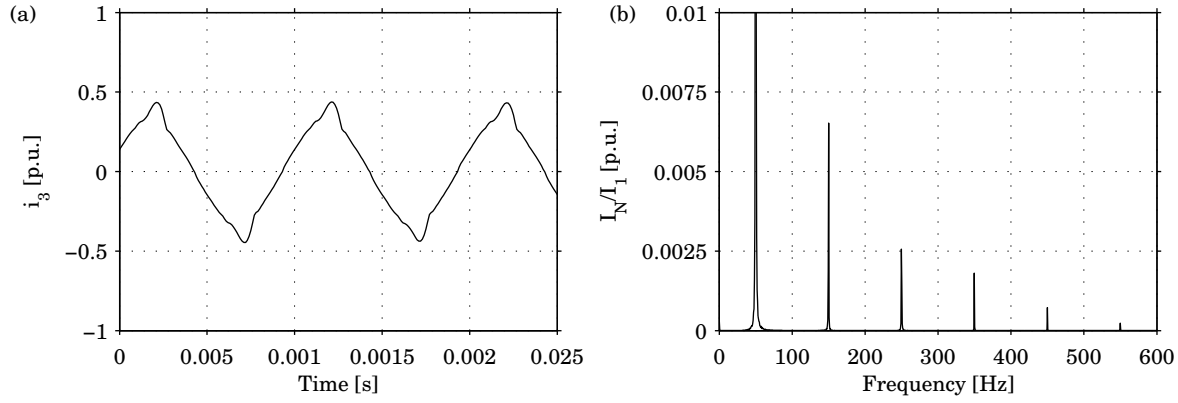

Fig. 6.21. Load current when all four loads are connected: (a) phase current and (b) FFT of the phase current.

6.4 Transient Operation

The system was studied during loads transients (connection and disconnection) and during a disturbance on the supplying ac grid.

6.4.1 Load Changes

The loads were connected in the following sequence: fluorescent lamp, compact fluorescent lamp, computer and finally the coffee maker. The idea was to reproduce a normal working day in the office room. The loads are disconnected in the opposite order. Figs. 6.22, 6.23, 6.24 and 6.25 show connection of the loads. The measurements show that the electronic loads (all loads except the coffee maker) have a large current transient when they are connected. The reason is that the loads have a capacitor which is charged when it is connected. The measurement using ac is shown in Fig. 6.26, which shows that the electronic loads also here have a large current transient when it is connected.

Figs. 6.27, 6.28, 6.29 and 6.30 show disconnection of the loads. The measurement shows that the electronic loads have a small current transient when they are disconnected. The coffee maker which is a large load causes a small voltage overshoot when it is disconnected. The measurement using ac shown in Fig. 6.31 show also that the loads have no current transients when they are disconnected.

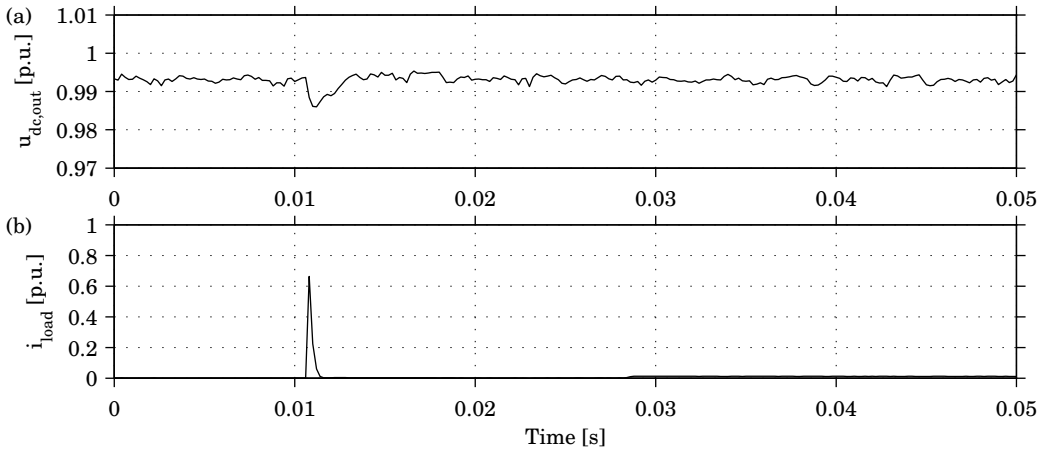

Fig. 6.22. Connection of fluorescent lamp: (a) output dc voltage and (b) dc load current.

6.4.2 Voltage Dips

The performance of the small dc network during a phase-to-phase fault [68] on the supplying ac grid is shown in Fig. 6.32. The measurement shows that during the dip the dc-link starts to oscillate due to the unbalance, but the output dc voltage is not affected, and the loads operate as normal during the fault. If the same load is supplied with single phase ac connected to one of the faulted phases as shown in Fig. 6.12; and making a new fault using the same fault impedance the computer restarts and the fluorescent lamp is shut off. This can be seen from the current waveform, shown in Fig. 6.33(b), which changes 100 ms after the fault is applied. This is due to the computer which restarts. Since a dip occurs randomly the fault was not applied at the same point on wave.

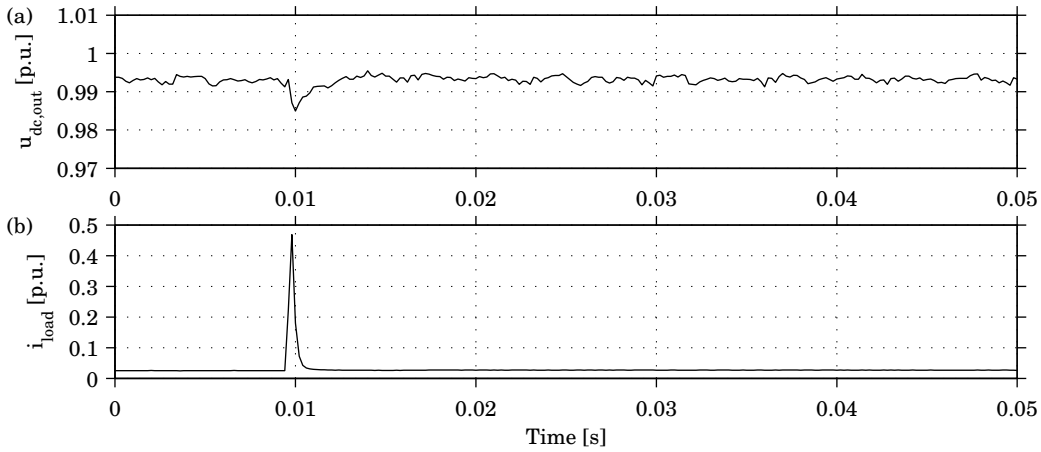

Fig. 6.23. Connection of compact fluorescent lamp: (a) output dc voltage and (b) dc load current.

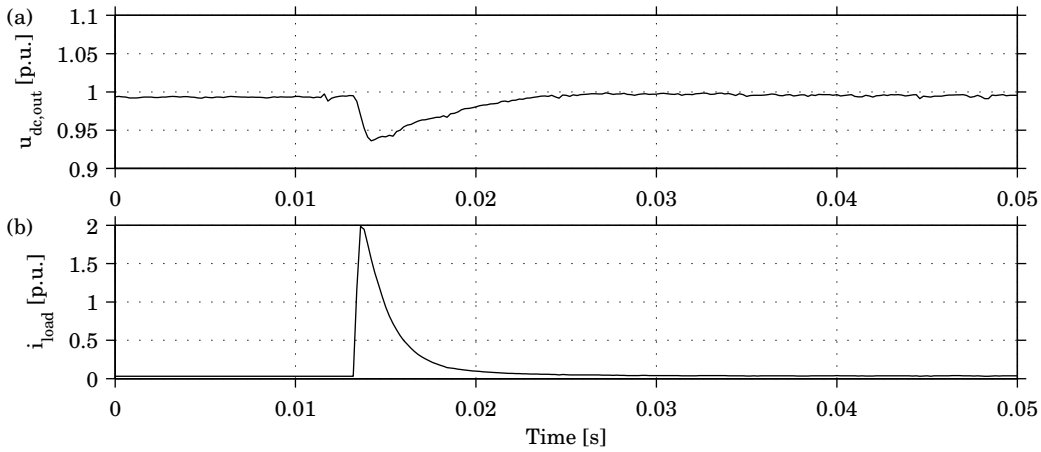

Fig. 6.24. Connection of computer: (a) output dc voltage and (b) dc load current.

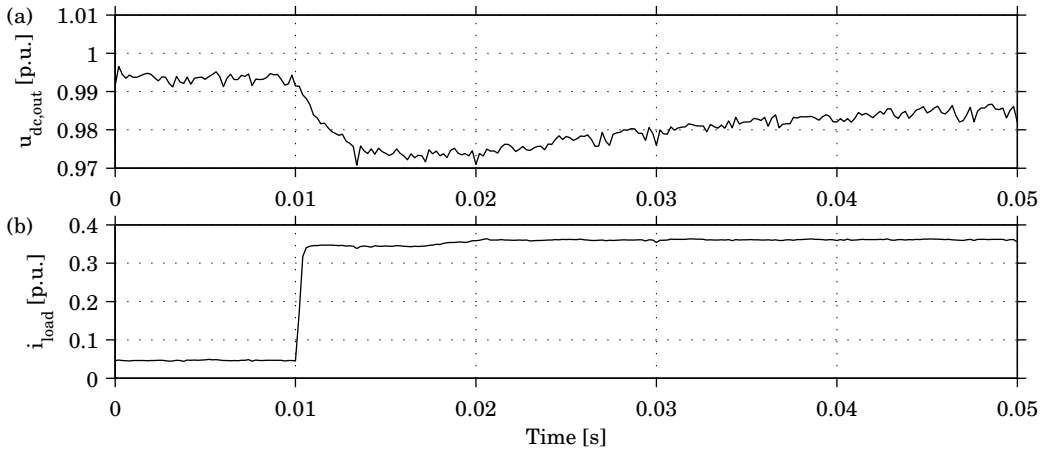

Fig. 6.25. Connection of coffee maker: (a) output dc voltage and (b) dc load current.

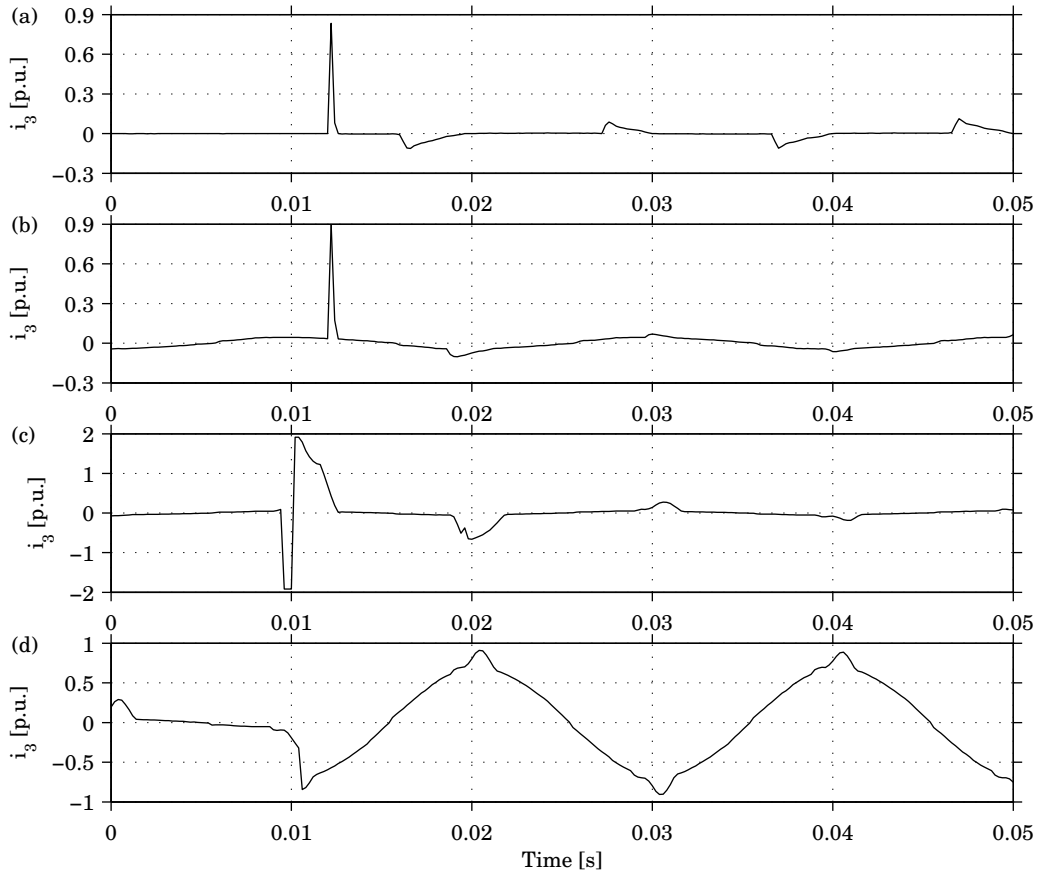

Fig. 6.26. Connection of loads using ac: (a) fluorescent lamp, (b) compact fluorescent lamp, (c) computer and (d) coffee maker.

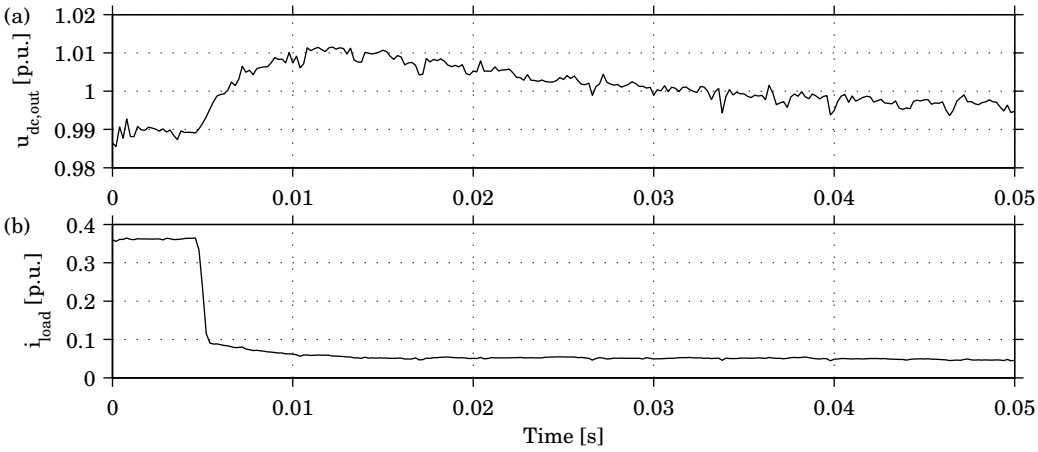

Fig. 6.27. Disconnection of coffee maker: (a) output dc voltage and (b) dc load current.

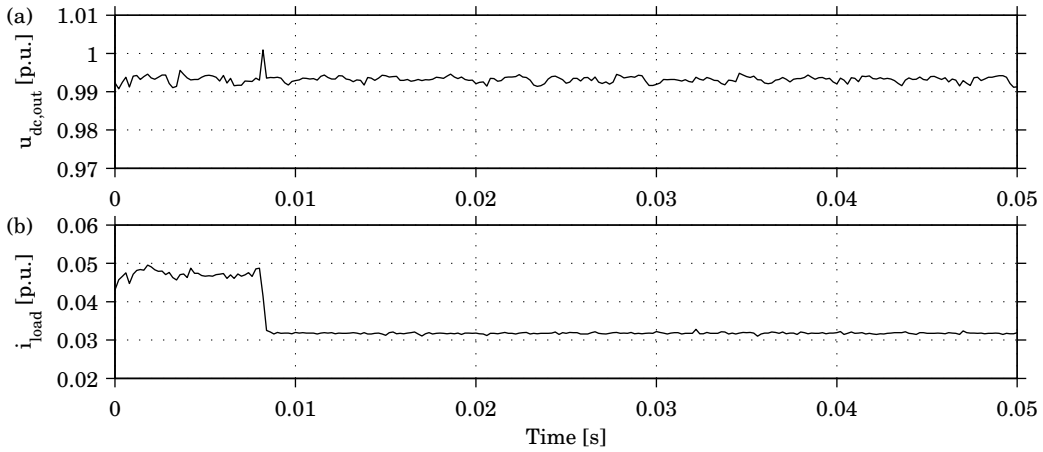

Fig. 6.28. Disconnection of computer: (a) output dc voltage and (b) dc load current.

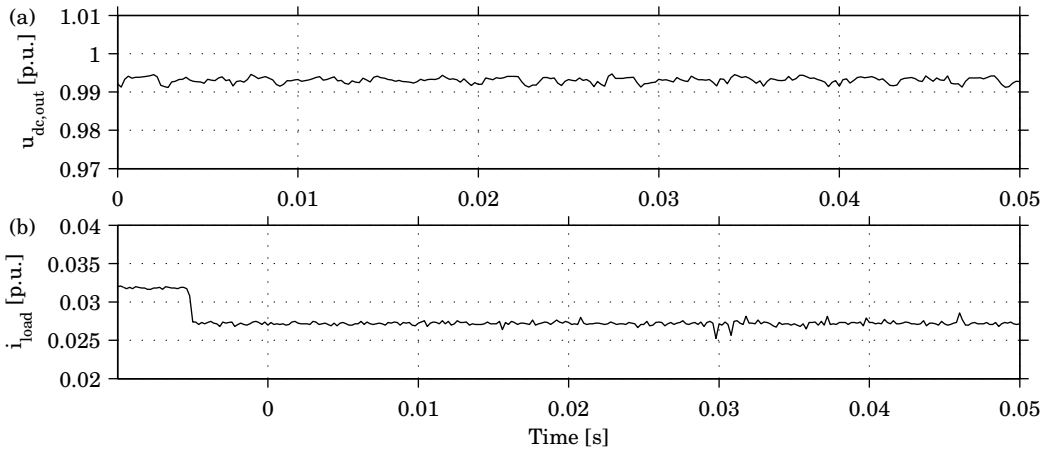

Fig. 6.29. Disconnection of compact fluorescent lamp: (a) output dc voltage and (b) dc load current.

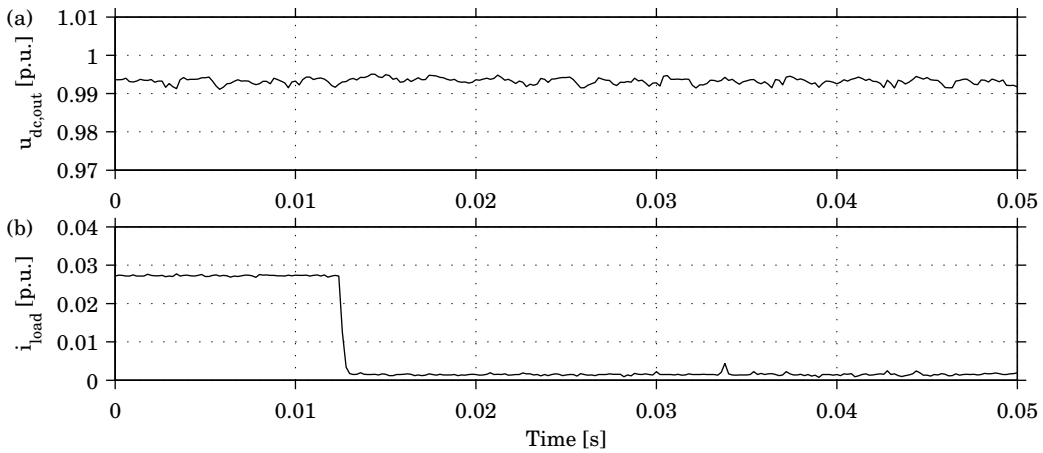

Fig. 6.30. Disconnection of fluorescent lamp: (a) output dc voltage and (b) dc load current.

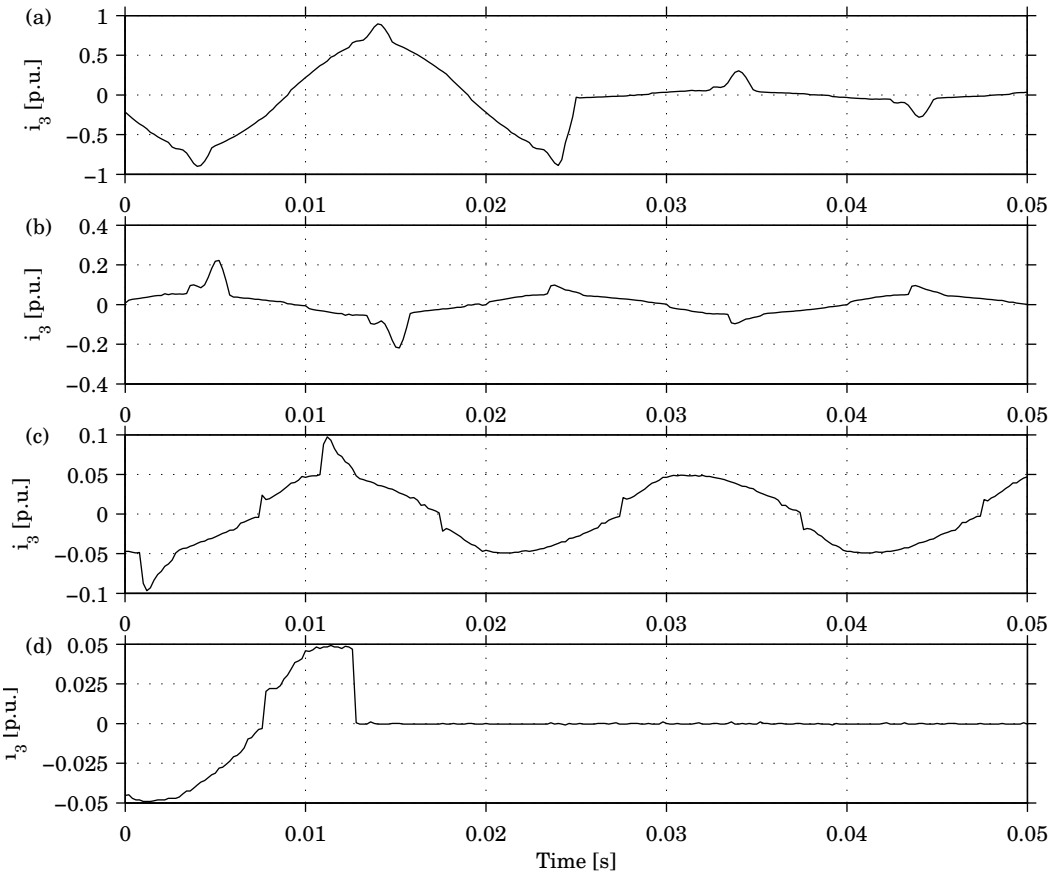

Fig. 6.31. Disconnection of loads using ac: (a) coffee maker, (b) computer, (c) compact fluorescent lamp and (d) fluorescent lamp.

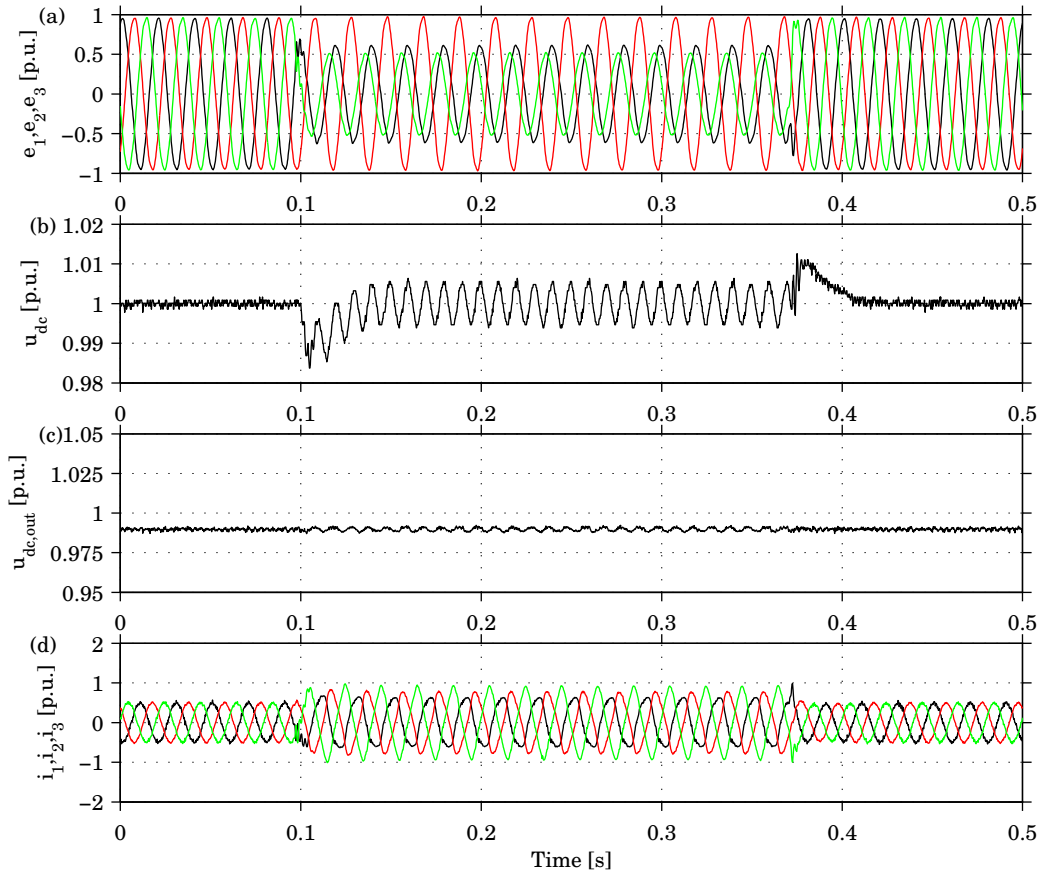

Fig. 6.32. Performance of the small dc network during a two-phase fault on the ac grid: (a) grid voltages, (b) dc-link voltage, (c) output dc voltage and (d) grid currents.

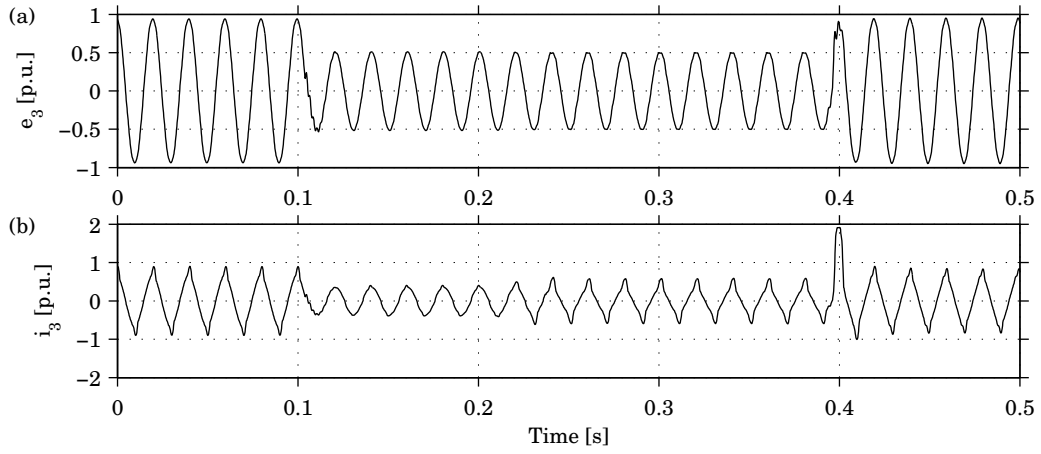

Fig. 6.33. Performance of the same loads supplied with ac during the same fault: (a) grid voltages and (b) grid currents.

6.5 Conclusions

In this chapter, a laboratory system built to test the developed ac/dc interface is described. This system was used to obtain all measurements presented in Chapter 4 and 5, and also to supply a small dc system with four loads. The system was compared with an identical system supplied with ac both during steady state and ac faults. The steady-state measurements show that the interface produces sinusoidal grid currents without low-order harmonics and the loads, when supplied with ac, produce low-order harmonics. Using the interface improves the power quality by removing low-order harmonics and balancing the three phase currents. The comparison during an ac disturbance is not quite fair in the sense that the ac loads are supplied by a single phase and the dc system with three phases. Practical limitations in the laboratory when making faults also made it difficult to show how the design and control improves the sensitivity of the interface more than that "adding capacitors will save the system".

Chapter 7

Conclusions and Future Work

7.1 Conclusions

In this thesis, the use of dc in low-voltage systems has been studied. Chapter 2 presented an overview of existing dc systems and a brief survey of loads, generation and components for use in dc systems clearly indicating that a low-voltage dc distribution system has a potential to be used in future power systems.

Load modeling for transient and steady-state analysis of low-voltage dc systems was the subject of Chapter 3. One important conclusion from the measurement series carried out on common household appliances is that most loads are able to operate with dc supply in a wide voltage range without any modifications. These can be classified into three main categories: resistive loads; electronic loads; and rotating loads. Exceptions are loads with inductive parts and some rotating loads, which cannot operate without an alternating supply. Resistive loads could be further divided into heaters, which are modeled by a constant resistance both in steady state and during transients, and lighting appliances, which are modelled as a current dependent resistor with a time constant that models the transient behavior. For rotating loads, the steady-state model was found to be a voltage dependent current source, whereas the transient behavior could only be reproduced using a mathematical expression. Electronic loads were further divided into power supplies, modeled as a constant power load combined with an RLC-circuit behind a diode rectifier, and lighting appliances, modeled as a constant current load or a constant power load (depending on the control of the ballast), also combined with an RLC-circuit behind a diode rectifier.

To provide a high-quality interface between the ac and dc systems, a Voltage Source Converter (VSC) in series with a Buck converter was chosen for this project. Chapter 4 described the control of the VSC. This is a combination of current control, to keep the ac currents sinusoidal and balanced, and dc-link voltage control, which provides the active current reference to the current control in order to keep the dc voltage constant in case of load changes and ac system disturbances. Three different dc-link voltage controllers were implemented and tested both in simulations and through experiments on a small laboratory system. The effect of different capacitor sizes, bandwidths of the controllers and load types was studied. Among the three, the energy-balance dc-link-voltage controller (EB) showed the slowest response, but is free from oscillations due to its first order characteristic. The load-current-feed-forward dc-link-voltage controller (LC), which measures the dc load current, shows a faster response but with oscillations of the dc-link voltage. In the observer-load-current-feed-forward dc-link-voltage controller (OLC), a variant of the LC where the dc load current

is calculated by an observer, the calculation time taken by the observer makes the response slower with respect to LC, but still faster than EB. The main conclusion is that LC is the best choice if the dc load current can be measured. Otherwise EB should be used if the requirements on maximum allowed dc-voltage ripple are particularly tight.

However, when the VSC is connected in series to a Buck converter, which also is controlled by PWM in order to keep a stable output dc voltage, the differences among the three controllers are of less importance. As shown in Chapter 5, EB shows the best performance in this case, since it is not affected by the distorted dc load current generated by the Buck converter. It is important here to remark that the proposed interface fulfills the requirements specified for this project, ensuring sinusoidal ac grid currents and good performance during load step changes and faults and disturbances on the ac system. However, this topology is expected to be quite costly and to have high losses, at least with the components available today. Nevertheless, it is particularly suited for a laboratory setup, since it gives a controllable dc-link voltage that can be varied in a wide range.

Chapter 6 presented in detail the laboratory system built to test the ac/dc interface developed. The interface, rated 3 kVA, was used to supply a small dc system with four loads, representing a typical office. The system was compared with an identical system supplied with ac both during steady state and ac grid faults. The steady-state measurements show that the dc system with the proposed interface improves the power quality by balancing the three ac phase currents and removing low-order harmonics, otherwise present in the current when the loads are supplied with ac. It can be argued that the comparison during an ac disturbance is quite not fair in the sense that the ac loads are supplied by a single phase and the dc system with three phases, which are not all faulted. Practical limitations when applying faults in the laboratory made it difficult to show how the design and control improves the sensitivity of the interface.

Despite these limitations, the small laboratory test setup built within this project proved that a dc system for low-voltage installations is fully feasible and can be preferred to a conventional, 50-Hz ac system in applications where many electronic loads are used, high reliability and power quality are desired, and/or low magnetic fields are required. Besides common office buildings, these might be for example web hotels, data centers, banks, telecom stations, hospitals, and military applications.

7.2 Future Work

Remaining Issues: System Optimization, Protection and Grounding

An item of interest for future work is the study of a larger dc system including energy storage and generation. A question is how to control the system during different operation modes. During periods of high generation and low consumption, the surplus power can be either stored in the energy storage or injected into the ac system. This problem can be extended to include an economical aspect. When is it better to sell the power than to store it? This will depend also on the speed of response of different generating sources and energy storage technologies to dynamic changes. Other questions are what would be the most suitable energy storage technology for such applications and how should the optimal size of energy storage be chosen? With the proposed interface between ac and dc system, the short circuit power of the dc system is limited to the energy in the dc-link capacitance. This will not

be enough to use fuses for interrupting short circuit currents due to faults in the dc system. Moreover, fault detection becomes difficult. What other types of devices can be used to disconnect a fault, and how is the fault detected? Protection issues, along with personell safety and grounding, are important questions to answer before a dc distribution system can be applied in practice. For practical applications, a more strictly cost-driven design of the ac/dc interface should also be carried out.

DC Microgrid Systems

Recently, in conjunction with several blackouts and supply interruptions due to human error, poor maintenance, and extreme weather events [71], the concept of local small grids equipped with some form of local generation and/or storage, called "microgrids" [72], has been gaining increasing attention. A microgrid should be able to operate both connected to a larger grid and in "island" operation, and be able to switch between the two operating modes without any impact on the operation of the local loads [73]. A dc-based microgrid can be an option to combine high reliability and low magnetic fields with high controllability and a simpler system, due to simpler connection of generators and energy storage. A challenge is how to design such system optimizing supply availability vs. cost, particularly if the generation used is renewable-based, using intermittent sources such as wind or sun. Charge/discharge cycles of the energy storage devices should be considered, possibly in combination with load management systems. Other interesting questions are how to detect the conditions for disconnection/reconnection of the dc island and how to perform the sequence of operations leading from grid-connected to island operation and vice versa.

Multilevel DC Systems and Other Applications

On a longer time scale, a future dc distribution system might include more than one voltage level, where dc could be used for high or medium voltage distribution in a part of a town, down to dc/dc-converter stations, replacing traditional transformer stations. There, the dc voltage is stepped down to low voltage, which is used to transmit the power locally, i.e. to buildings and offices. One could even go one step further and imagine a central, high power dc-dc converter station receiving power through a HVDC link, and stepping it down to a medium voltage dc network.

Another area for possible dc applications is industrial systems [74]. Rolling mills or paper mills today are completely automated and use drive systems. By using dc, all rectifying stages can be removed and the motors with their inverters can be coupled to the dc bus. Normally, much more freedom is allowed in the design of industrial systems, as opposed to utility systems, which results in a higher level of acceptance of new ideas. Moreover, a number of new factories are being built today in emerging economies in East Asia, which makes it possible to adopt a new concept for the design if it can be shown to have major advantages. The power level is much higher than what has been considered in this project, so a feasibility study should be made to determine the most suitable voltage level, and the availability of necessary switching and protection devices for this application. Due to obvious similarities with an industrial system, an offshore wind park is another possible application of low- or medium-voltage dc system [75], particularly if using wind turbines with full-size power-electronic conversion.

References

[1] J. Benner and L. Kazmerski, "Photovoltaics gaining greater visibility," *IEEE Spectr.*, vol. 36, no. 9, pp. 34–42, Sept. 1999.

[2] R. Wolk, "Fuel cells for home and hospitals," *IEEE Spectr.*, vol. 36, no. 5, pp. 45–52, May 1999.

[3] *Short-circuit currents in dc auxiliary installations in power plants and substations*, IEC 61660, 1997.

[4] *IEEE Recommended practice for the design of dc auxiliary power systems for generating stations*, IEEE Std. 946, 1992.

[5] C. Sulzberger, "Triumph of ac - from Pearl Street to Niagara," *IEEE Power Energy Mag.*, vol. 1, no. 3, pp. 64–67, May/June 2003.

[6] ——, "Triumph of ac - the battle of the currents," *IEEE Power Energy Mag.*, vol. 1, no. 4, pp. 70–73, July/Aug. 2003.

[7] G. Woodward, "History of a single-phase high-voltage distribution system," *Proc. IEEE*, vol. 140, no. 3, pp. 207–214, May 1993.

[8] T. Gruzs, "Powering telecom and info technology systems," *Power Quality Assurance*, pp. 22–29, Apr. 2001.

[9] K. Mizuguchi, S. Muroyama, Y. Kuwata, and Y. Ohashi, "A new decentralized dc power system for telecommunications systems," in *Proc. IEEE INTELEC'90*, Orlando, FL, Oct. 21–25 1990, pp. 55–62.

[10] T. Yamashita, S. Muroyama, S. Furubo, and S. Ohtsu, "270 V dc system - a highly efficient and reliable power supply system for both telecom and datacom systems," in *Proc. IEEE INTELEC'99*, Copenhagen, Denmark, June 6–9 1999.

[11] T. Gruzs and J. Hall, "AC, dc or hybrid power solutions for today's telecommunications facilities," in *Proc. IEEE INTELEC'00*, Phoenix, AZ, Sept. 2000, pp. 361–368.

[12] C. Chan, "An overview of electric vehicle technology," *Proc. IEEE*, vol. 81, no. 9, p. 1202, 1993.

[13] A. Emadi, M. Ehsani, and J. Miller, *Vehicular electric power systems*, 1st ed. New York, NY: Marcel Dekker, 2004.

[14] C. Chan, "The state of the art of electric and hybrid vehicles," *Proc. IEEE*, vol. 90, no. 2, pp. 247–275, Feb. 2002.

[15] J. Miller, "Power electronics in hybrid electric vehicle applications," in *Proc. IEEE APEC'03*, vol. 1, Miami Beach, FL, Feb. 9–13 2003, pp. 23–29.

[16] "Technology for Future Naval Forces," [online] Available: http://www.nap.edu/html/tech_21st/ (last accessed on 2005-05-09).

[17] M. Baran and N. Mahajan, "DC distribution for industrial systems: opportunities and challenges," *IEEE Trans. Ind. Applicat.*, vol. 39, no. 6, pp. 1596–1601, Nov./Dec. 2003.

[18] T. Doyle, H. Stevens, and H. Robey, "An historical overview of navy electric drive," [online] Available: www.onr.navy.mil/fncs/aces/docs/history.pdf (last accessed on 2005-03-07).

[19] J. Momoh, S. Kaddah, and W. Salawu, "Security assessment of dc zonal naval-ship power system," in *Large Engineering Systems Conference on Power Engineering (LESCOPE'01)*, Halifax, NS, Canada, July 11–13 2001, pp. 206–212.

[20] T. McCoy, "Trends in ship electric propulsion," in *Proc. IEEE Power Engineering Soc. Summer Meeting*, vol. 1, Chicago, IL, July 21–25 2002, pp. 343–346.

[21] D. Paul, "DC traction power system grounding," *IEEE Trans. Ind. Applicat.*, vol. 38, no. 3, pp. 818–824, May/June 2002.

[22] R. Hill, "Electric railway traction. Part 3. Traction power supplies," *Power Engineering Journal*, vol. 8, pp. 275–286, Dec. 1994.

[23] N. Hingorani, "High-voltage dc transmission: a power electronics workhorse," *IEEE Spectr.*, vol. 33, no. 4, pp. 63–72, Apr. 1996.

[24] D. Andersson and A. Henriksson, "Passive and active dc breakers in the Three Gorges-Changzhou HVDC project," in *Proc. IPCS02*, Wuhan, Hubei, China, Sept. 3–5 2002.

[25] G. Asplund, K. Eriksson, and K. Svensson, "DC transmission based on voltage source converters," in *CIGRE Conf.*, no. 14-302, Paris, France, 1998.

[26] Y. Ito, Z. Yang, and H. Akagi, "DC micro-grid based distribution power generation system," in *Proc. International Power Electronics and Motion Control Conference (IPEMC'04)*, vol. 3, Aug. 14–16 2004, pp. 1740–1745.

[27] *EMC levels in low voltage distribution systems (in Swedish)*, SS 4211811, 1989.

[28] *Voltage characteristics of electricity supplied by public distribution systems*, EN 50160:2000, 2000.

[29] *IEEE Recommended pratice and requirements for harmonics control in electric power systems*, IEEE Std. 519-1992, 1992.

[30] J. Enslin, "Interconnection of distributed power to the distribution system," in *Proc. IEEE PSCE'04*, New York, NY, Oct. 10–13 2004, pp. 1718–1723.

[31] A. Agustoni, E. Borioli, P. Ferrari, A. Mariscotti, E. Picco, P. Pinceti, and G. Simioli, "LV dc networks for distributed energy resources," in *Proc. Cigré Symposium on Power System with Dispersed Generation*, Athens, Greece, Apr. 13–16 2005.

[32] J. Ferreira and H. van der Broeck, "Alternative power distribution in residential and commercial buildings," in *Proc. of Fifth European Conference on Power Electronics and Applications (EPE'93)*, vol. 7, Brighton, UK, Sept. 13–16 1993, pp. 188–193.

[33] L. Po-Wa, L. Yim-Zhu, and L. Bo-Tao, "Power distribution systems for future homes," in *Proc. IEEE PEDS'99*, vol. 2, Hong Kong, July 27–29 1999, pp. 1140–1146.

[34] A. Sannino, G. Postiglione, and M. Bollen, "Feasibility of a dc network for commercial facilities," *IEEE Trans. Ind. Applicat.*, vol. 39, no. 5, pp. 1499–1507, Sept./Oct. 2003.

[35] Elforsk, Ericsson, SEK, Stockholm Energi, Telia, Sydkraft och Vattenfall, "Likström för drift av elektrisk utrustning i fastigheter - Förstudie," ELFORSK, Sweden, Tech. Rep. 99:3 (in Swedish), 1999.

[36] J.-E. Alm, "Alternativt spänningssystem i bostäder, Tech. Rep. (in Swedish), 1998.

[37] J. Pellis, "The dc low-voltage house," Master's thesis, Eindhoven University of Technology, The Netherlands, Sept. 1997.

[38] *Power cables of rated voltage 0,6/1 kV - Specifications for design and testing (in Swedish)*, SS 4241418, 2003.

[39] *Power system protection - principles and components*, 2nd ed. P. Peregrinus Ltd., Stevenage, UK and New York, 1990, vol. 1.

[40] *3RV1 Circuit Breaker/MSP*, [online] Available: http://cache.automation.siemens.com /dnl/TY1Nzg1NwAA_6009084_HB/02sirius_en.pdf (last accessed on 2005-05-09).

[41] G. Gregory, "Applying low-voltage circuit breakers in direct current systems," *IEEE Trans. Ind. Applicat.*, vol. 31, no. 4, pp. 650–657, July/Aug. 1995.

[42] C. Kimblin and R. William, "Low-voltage power circuit breakers and molded case circuit breakers-a comparison of test requirements," in *Proc. IEEE Industrial and Commercial Power Systems Technical Conference*, Pitsburgh, PA, May 2–6 1999.

[43] *Eaton Arc Twister HVDC Contactors*, Sarasota, FL.

[44] P. McEwan and S. Tennakoon, "A two-stage dc thyristor circuit breaker," *IEEE Trans. Power Electron.*, vol. 12, no. 4, pp. 597–607, July 1997.

[45] R. Erickson and D. Maksimovic, *Fundamentals of power electronics*. Kluwer Academic Publishers, Norwell, MA, 2002.

[46] W. R. N. Mohan, T. Undeland, *Power electronics converter, applications, and design*, 2nd ed. New York, NY: John Wiley & Sons, Inc., 1996.

[47] K. D. Gusseme, D. V. de Sype, and J. Melkebeek, "Design issues for digital control of boost power factor correction converters," in *Proc. IEEE International Symposium on Industrial Electronics (ISIE'02)*, vol. 3, Ghent, Belgium, May 26–29 2002, pp. 731–736.

[48] M. Lindgren, "Modeling and control of voltage source converters connected to the grid," Ph.D. dissertation, Chalmers University of Technology, Gothenburg, Sweden, 1998.

[49] J. Svensson, "Grid-connected voltage source converters," Ph.D. dissertation, Chalmers University of Technology, Gothenburg, Sweden, 1998.

[50] L. Hongtao, X. Zheng, and G. Zhi, "A control strategy for three-level VSC-HVDC system," in *Proc. IEEE Power Engineering Soc. Summer Meeting*, vol. 1, Chicago, IL, July 21–25 2002, pp. 480–485.

[51] E. Einarsson and B.-O. Wickbom, "Load modelling for steady-state and transient analysis of low-voltage dc systems," Master's thesis, Chalmers Universisty of Technology, Gothenburg, Sweden, 2004.

[52] D. Nilsson and A. Sannino, "Load modelling for steady-state and transient analysis of low-voltage dc systems," in *Conf. Rec. IEEE-IAS Annu. Meeting*, vol. 2, Seattle, WA, Oct. 3–8 2003, pp. 774–780.

[53] *IEEE Recommended practice for industrial and commercial power system analysis*, IEEE Std. 399, 1997.

[54] K. Lindén and I. Segerqvist, "Modelling of load devices and studying load/system characteristics," Chalmers University of Technology, Gothenburg, Sweden, Tech. Rep. 131L, 1992.

[55] P. Cen, *Principles of electric machines and power electronics*, 2nd ed. New York, NY: John Wiley & Sons, Inc., 1996.

[56] H. Cheng, C. Moo, H. Yen, T. Lin, and S. Huang, "Single-switch high-power-factor electronic ballast for compact fluorescent lamps," in *Proc. IEEE PEDS'01*, vol. 2, Indonesia, Oct. 22–25 2001, pp. 764–769.

[57] Y.-C. Wu, T.-F. Wu, and Y.-K. Chen, "A compact single-stage converter for emergency lighting applications," in *Proc. IEEE PESC'02*, vol. 2, Cairns, Australia, June 23–27 2002, pp. 779–784.

[58] S. Lee, H.-H. Chung, and S. Hui, "A novel electrode power profiler for dimmable ballasts using dc link voltage and switching frequency controls," *IEEE Trans. Power Electron.*, vol. 19, no. 3, pp. 847–853, May 2004.

[59] M. Kazmierkowski, R. Krishnan, and F. Blaabjerg, *Control in power electronics - selected problems*. Academic press, San Diego, CA, 2002.

[60] L. Harnefors, *Control of variable-speed drives*. Västerås, Sweden: Applied Signal Processing and Control, Dept. of Electronics, Mälardalen University, 2002.

[61] N. Hingorani and L. Gyugyi, *Understanding FACTS*. Piscataway, NJ: IEEE Press, 2000.

[62] M. Alaküla, *Power electronics control*. Lund University, Sweden, 2002.

[63] S. Bowes and P. Clark, "Regular-sampled harmonic-elimination PWM control of inverter drives," in *IEEE Trans. Power Electron.*, vol. 10, no. 5, Sept. 1995, pp. 521–531.

[64] M. Bongiorno, "Control of voltage source converters for voltage dip mitigation in shunt and series configurations," Chalmers University of Technology, Gothenburg, Sweden, Tech. Rep. 515L, 2004.

[65] R. Ottersten and J. Svensson, "Vector current controlled voltage source converter - deadbeat control and saturation strategies," *IEEE Trans. Power Electron.*, vol. 17, no. 2, pp. 279–285, Mar. 2002.

[66] R. Ottersten, "On control of back-to-back converters and sensorless induction machine drives," Ph.D. dissertation, Chalmers University of Technology, Gothenburg, 2003.

[67] Z. Zhou, Y. Liu, and P. Unsworth, "Design of dc link current observer for a 3-phase active rectifier with feedforward control," in *Conf. Rec. IEEE-IAS Annu. Meeting*, vol. 1, Seattle, WA, Oct. 3–7 2004, pp. 468–475.

[68] M. Bollen, *Understanding power quality*. Piscataway, NJ: IEEE Press, 2000.

[69] *dSPACE, Solutions for Control*, [online] Available: http://www.dspace.de/ww/en/pub/home.htm (last accessed on 2005-05-10).

[70] *Danfoss design guide for frequency converters VLT 5000*, [online] Available: http://www.danfoss.com (last accessed on 2005-05-10).

[71] *Ny Teknik "Gudruns härjningar kostar en halv miljard" (in Swedish)*, [online] Available: http://www.nyteknik.se/pub/ipsart.asp?art_id=38287 (last accessed on 2005-05-11).

[72] R. Lasseter and P.Paigi, "Microgrid: a conceptual solution," in *Proc. IEEE PESC'04*, vol. 6, Aachen, Germany, June 20–25 2004, pp. 4285–4290.

[73] R. Lasseter, "Microgrids," in *Proc. IEEE Power Engineering Soc. Winter Meeting*, vol. 1, New York, NY, Jan. 27–31 2002, pp. 305–308.

[74] C. Du, "The control of VSC-HVDC and its use for large industrial power systems," Chalmers University of Technology, Gothenburg, Sweden, Tech. Rep. 484L, 2003.

[75] S. Lundberg, "Configuration study of large wind parks," Chalmers University of Technology, Gothenburg, Sweden, Tech. Rep. 474L, 2003.